Summer 2017

Structural Characterization of Factor VIII C2 Domain Activated Platelet Membrane Binding

Serena W. Wo
Western Washington University, wos@wwu.edu

Structural Characterization of Factor VIII C2 Domain Activated Platelet Membrane Binding

By

Serena W. Wo

Accepted in Partial Completion
of the Requirements for the Degree
Masters of Science

Kathleen L. Kitto, Dean of the Graduate School

ADVISORY COMMITTEE

Chair, Dr. P. Clint Spiegel

Dr. Spencer Anthony-Cahill

Dr. Gerry Prody

MASTER'S THESIS

In presenting this thesis in partial fulfillment of the requirements for a master's degree at Western Washington University, I grant to Western Washington University the non-exclusive royalty-free right to archive, reproduce, distribute, and display the thesis in any and all forms, including electronic format, via any digital library mechanisms maintained by WWU.

I represent and warrant this is my original work, and does not infringe or violate any rights of others. I warrant that I have obtained written permissions from the owner of any third party copyrighted material included in these files.

I acknowledge that I retain ownership rights to the copyright of this work, including but not limited to the right to use all or part of this work in future works, such as articles or books.

Library users are granted permission for individual, research and non-commercial reproduction of this work for educational purposes only. Any further digital posting of this document requires specific permission from the author.

Any copying or publication of this thesis for commercial purposes, or for financial gain, is not allowed without my written permission.

Serena W. Wo

July 27th, 2017

Structural Characterization of Factor VIII C2 Domain Activated Platelet Membrane Binding

A Thesis
Presented to
The Faculty of
Western Washington University

In Partial Fulfillment
Of the Requirements for the Degree
Master of Science

By
Serena W. Wo
July 2017

Abstract

Hemophilia A is an X-linked blood disorder that results in the inability to form proper blood clots and may also cause spontaneous bleeding in the joints or muscles. This disorder is caused by mutations in the F8 gene that attenuate or abolish the activity of its protein product, factor VIII. Blood coagulation factor VIII (fVIII) is a glycoprotein that serves as a cofactor for the serine protease factor IXa on the surface of activated platelets to form the intrinsic tenase complex, which activates factor X during hemostasis to enable blood clot formation. Previous studies have shown that the C-terminal (C2) domain of fVIII is responsible for binding to phospholipids in platelet membranes. However, there are conflicting models for its structural binding mechanism. Elucidating the mechanism of factor VIII binding to phosphatidylserine-containing membranes in activated platelets is essential in the understanding and progress towards improving current hemophilia A therapeutics. Some mutations that occur in the C2 domain result in nonfunctional factor VIII possibly due to its inability to bind platelet membranes and form the tenase complex. This research helps to further describe this mechanism by analyzing the atomic interactions between the C2 domain of factor VIII and phosphatidylserine membranes by X-ray crystallography and biochemical assays. A 1.4 Å resolution X-ray crystal structure of the porcine C2 domain of factor VIII in complex with O-phospho-L-serine (OPLS), a soluble moiety of the headgroup of phosphatidylserine, revealed a favorable electrostatic interaction between Arg2320 and OPLS, implying the importance of the universally conserved arginine at residue 2320. Within the human hemophilia A population, two mutations at that residue in fVIII, Arg2320Thr/Ser, are of interest due to the ability of

these fVIII mutants to stay in circulation as non-functioning proteins. Characterizing these mutants with phosphatidylserine membrane-binding enzyme-linked immunosorbent assays (ELISAs), affinity pull-down assays, and intrinsic fluorescence has allowed for a more comprehensive understanding of the binding mechanism of fVIII. Because the C1 domain of fVIII is structurally homologous to the C2 domain, we attempted to study two naturally occurring mutations (Arg2163His and Arg2159His) in the C1 domain that likely interact with phosphatidylserine-containing membranes. Arg2163His is a mutation located in the same position structurally as Arg2320 in the C2 domain. However, we were unable to purify these C1 mutants to a level suitable for biochemical studies. Furthermore, phosphatidylserine lipid binding studies were conducted on an Arg2215Ala C2 domain mutant due to its proximity to the hydrophobic region of platelet membranes. We were able to express and purify all of the C2 domain mutants, and proper folding of these mutants was verified using affinity pull-down assays. Phosphatidylserine membrane binding ELISAs revealed that all the mutants studied were not able to bind to activated platelet phosphatidylserine-containing membranes in activated platelets. Preliminary intrinsic fluorescence analysis determined that Arg2320Ser was thermodynamically less stable than wild type, but was still predominantly folded. Our data further supported our activated platelet membrane binding mechanism that is centered on Arg2320, with two hydrophobic spikes docked within the hydrophobic lipid bilayer of platelet membranes, and nonspecific interactions between either the phosphate or carboxyl groups of phospholipids and the underlying basic residues of C2 (Arg2209, Arg2215, Lys2183, Arg2220, Arg2222, and Lys2249).

Acknowledgements

First and foremost, I would like to thank Dr. P. Clint Spiegel for accepting me into his lab and providing me guidance throughout this whole project. I have learned a lot these past two years because of him.

I would also like to thank my committee members, Dr. P. Clint Spiegel, Dr. Gerry Prody and Dr. Spencer Anthony-Cahill for their support on this project and for editing the early versions of this manuscript.

I owe a great deal of gratitude to former and present members of this lab. Specifically, Caileen Brison, Justin Walter, and Michelle Wuerth, who provided the groundwork for this project. Thank you to Alexis Neuman and Rachel Blazevic, who worked side-by-side with me to uncover the structural characteristics of C2 membrane binding. Lastly, Lily Konek, Chase Reynolds, and Martha Torujo, who helped me express and purify the mutant proteins used for functional studies.

Although these are acknowledgements for my graduate work, I would also like to thank Dr. Spencer Anthony-Cahill, my undergraduate principle investigator, who brought me into the research world, sparked my love for research, and inspired me to pursue this degree.

Table of Contents

List of Figures

List of Tables

List of Appendix Figures

List of Abbreviations

C2	Second carboxy-terminal domain of fVIII
FIX	Factor IX
FV	Factor V
FVII	Factor VII
FVIII	Factor VIII
FVIIIa	Activated Factor VIII
FX	Factor X
FXI	Factor XI
FXII	Factor XII
GPIb-IX-V	Glycoprotein GPIb-IX-V
OPLS	O-phospho-L-serine
PS	Phosphatidylserine
TF	Tissue Factor
TFPI	Tissue factor pathway inhibitor (or extrinsic pathway inhibitor)
trx	Thioredoxin
VWF	von Willebrand Factor
Xase complex	Tenase complex
Xq28	X chromosome at position 28

Introduction

The encompassing processes of hemostasis are maintaining blood in the fluid state, producing a blood clot confined to the area of vascular injury to prevent hemorrhage, and inhibiting blood clot formation once a stable clot is formed. Our area of interest is blood clot formation. Initially, the development of a hemostatic plug involves platelet adhesion and aggregation to the damaged vessel wall, resulting in the production of a soft clot during primary hemostasis. Immediately following the action of activated platelets, the crosslinking of insoluble fibrin within the area of damage provides mechanical strength to harden the clot during secondary hemostasis (Nemerson and Pitlick 1972). This study explicitly focuses on the second hemostatic process, the formation of a fibrin clot, which is dependent on protein blood coagulation factors (Davie and Ratnoff 1964). When the activity of these coagulation factors is impaired, it causes blood disorders, generally referred to as hemophilias. The disruption of hemostasis in patients with these disorders can result in potentially life-threatening bleeding. Specifically, hemophilia A is caused by a deficiency in coagulation factor VIII (fVIII). The activity of fVIII is dependent on its ability to bind activated platelet surfaces (Gilbert and Arena 1996). Although previous studies have shown that the second carboxy-terminal (C2) domain of fVIII is the primary domain that interacts with activated platelet membranes (Arai et al. 1989), the molecular basis of this interaction is poorly understood. We investigated this specific association between the C2 domain and the components of platelet membranes to explain its role in hemostasis and in causing hemophilia A.

Primary Hemostasis

Hemostasis describes the ability of an organism to prevent blood loss during injury. The two distinct events during hemostasis are primary and secondary hemostasis (Palta et al. 2014). During primary hemostasis, a soft hemostatic platelet plug is formed, which involves platelet adhesion and platelet aggregation (Nemerson and Pitlick 1972). This platelet-rich soft plug can then provide a surface for the assembly of blood coagulation factor proteins during secondary hemostasis, in which this soft clot is strengthened by a hard fibrin clot (Davie and Ratnoff 1964).

Platelet Adhesion—The initial event during primary hemostasis in forming a soft hemostatic plug is platelet adhesion onto damaged endothelial vessel walls (Nemerson and Pitlick 1972). Platelets are non-nucleated cells produced from megakaryocytes in bone marrow that have a pivotal role in primary hemostasis. This adhesion process is mediated by the large multimeric glycoprotein, von Willebrand factor (vWF), which contains three A domains, three B domains, two C domains, and four D domains (Zhou 2012). vWF provides the link between platelets and damaged vessels. Upon vascular damage, vWF is immobilized to the damaged collagen-containing vessel walls by its A1 and A3 domains. The A3 domain binds to fibrillary collagen type I and III (Huizinga et al. 1997), while the A1 domain binds collagen type VI of the subendothelial connective tissue (Pareti et al. 1987). Platelets can then adhere to the injured vessels indirectly by binding to the subendothelium-bound vWF. There are two receptors localized on platelet membranes that recognize vWF: the glycoprotein Ib-IX-V (GPIb-IX-V) receptor complex and integrin

$\alpha_{IIb}\beta_3$ (or also known as the glycoprotein IIb/IIa complex) (Hantgan et al. 1990). Glycoprotein GPIbα of the GPIb-IX-V complex binds to the vWF A1 domain, acting as the initial tethering of platelets to the subendothelium surface (Emsley et al. 1998). Integrin $\alpha_{IIb}\beta_3$ then recognizes an Arg-Gly-Asp sequence within the C1 domain of vWF (Beacham et al. 1992). Under the localized high shear stress of blood flow around sites of vascular damage, the globular conformation of vWF changes in a way that exposes available receptor binding sites and thereby increases the interactions between vWF and platelets.

Platelet Aggregation—Once platelets adhere to the subendothelium by means of vWF, they can then aggregate through platelet-platelet interactions to form a soft clot. The mechanism in which platelets aggregate is dynamic and complex, but the fundamental interaction is primarily mediated by integrin $\alpha_{IIb}\beta_3$, the transmembrane receptor that was also involved in vWF-mediated platelet adhesion (Jackson 2007). These receptors located on adjacent platelets can bind to fibrinogen, which allow the platelet-platelet interactions. ADP binding causes fibrinogen deposition, further encouraging these platelet-platelet interactions. During this process, platelets are also activated. The enzyme, scramblase, flips phosphatidylserine lipids nonspecifically between the two lipid bilayers of platelet membranes and this results in an increase in negatively charged phospholipids in the outer leaflet of the platelet membranes following platelet activation (Bevers et al. 1983, O'Donnell et al. 2014). These membranes can then provide a surface for secondary hemostasis in which a fibrin clot can formed to stabilize and strengthen this initial clot.

Secondary Hemostasis

Traditionally, the hemostatic process in forming a hard fibrin clot was explained by the blood coagulation cascade model, which described a series of protein interactions propagated by the proteolytic activation of clotting factors. These interactions distinctly lead to the formation of a stable blood clot through the covalent crosslinking of insoluble fibrin. This cascade model is composed of an extrinsic and intrinsic arm that converge at a common pathway (**Figure 1**; Macfarlane 1964, Davie and Ratnoff 1964). The extrinsic arm is stimulated by endothelial tissue damage, with the exposure of collagen to platelets, while the intrinsic arm was stimulated by trauma within the vasculature. However, this model was insufficient in explaining the entire blood clotting process, as each of these pathways cannot function independently to promote a stable blood clot. Instead, a cell-based model is now used to explain the existing coagulation cascade, which describes hemostasis in three distinct, but overlapping phases: initiation, amplification, and propagation (**Figures 2/3/4**; Monroe and Hoffman 2006).

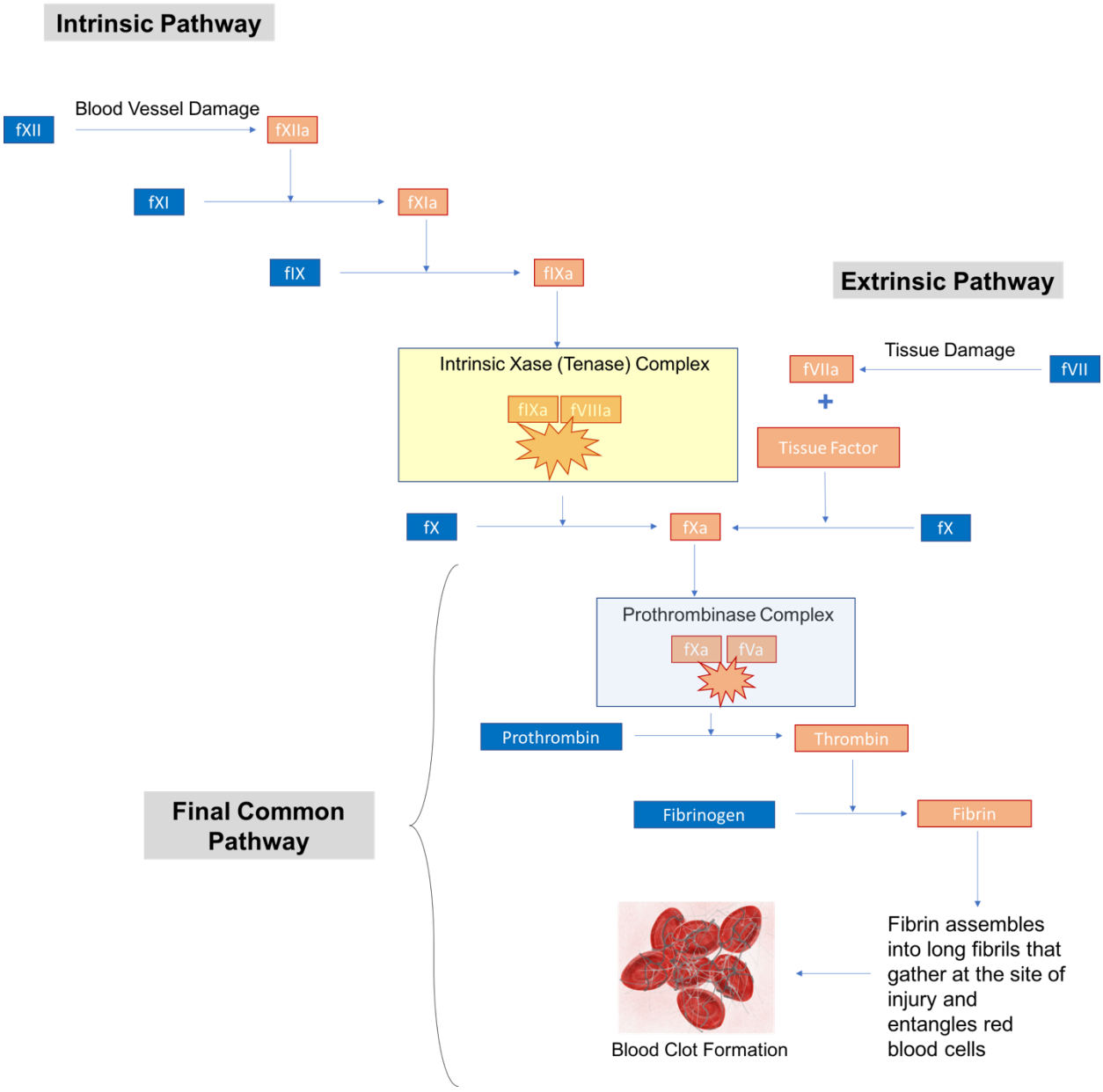

Figure 1. Blood coagulation cascade. The traditional model of blood coagulation is termed the blood coagulation cascade, composed of an intrinsic pathway and an extrinsic pathway that converge at the final common pathway to generate fibrin that enables the formation of a stable blood clot. The intrinsic pathway is stimulated by blood vessel damage, which activates fXII. Factor fXIIa then activates fXI, which activates fXI to form the intrinsic tenase complex. The extrinsic pathway is stimulated by tissue damage, which activates fVII. The tissue factor-fVIIa complex and the tenase complex both activate fX. In the final common pathway, fXa forms the prothrombinase complex with fVa and activated platelets to generate large burts of thrombin. Fibrinogen is then proteolytically converted to fibrin, which enable sthe formation of a stable blood clot.

Initiation—The first phase of hemostasis, initiation (or also traditionally known as the extrinsic pathway of the blood coagulation cascade), provides low amounts of activated coagulation factors and platelets (**Figure 2**). This phase is stimulated by tissue damage, which results in the expression of tissue factor (TF) on the surface of endothelial cells. Therefore, the initiation step is localized on TF-bearing cells, which are normally located outside the vasculature (Monroe et al. 1996).

During tissue damage, coagulation factor VII is activated (fVIIa) by trace active proteases circulating in the blood and TF is exposed to the bloodstream. Subsequently, fVIIa associates with its transmembrane receptor, TF, for the activation of factor IX (fIX) and factor X (fX) in small amounts (Lawson and Mann 1991; Monroe et al. 1996). Tissue damage additionally causes platelet adhesion to collagen and other extracellular matrix components of the damaged site, which promotes the secretion of partially activated factor V (fVa). Factor V (fV) can also be activated by fXa or thrombin to enable the formation of the prothrombinase complex, composed of fXa and fVa, on the surface of TF-bearing cells (Monkovic and Tracy 1990; Monroe et al. 1996; Briede et al. 2001). This complex is initially formed on TF-bearing cells to serve to convert sufficient amounts of prothrombin into thrombin, which functions as an initiating signal for platelet activation. In contrast, during the propagation phase, this complex is assembled on activated platelets to generate a burst of thrombin (Rosing et al. 1985) for a variety of procoagulant functions leading to the insoluble fibrin mesh.

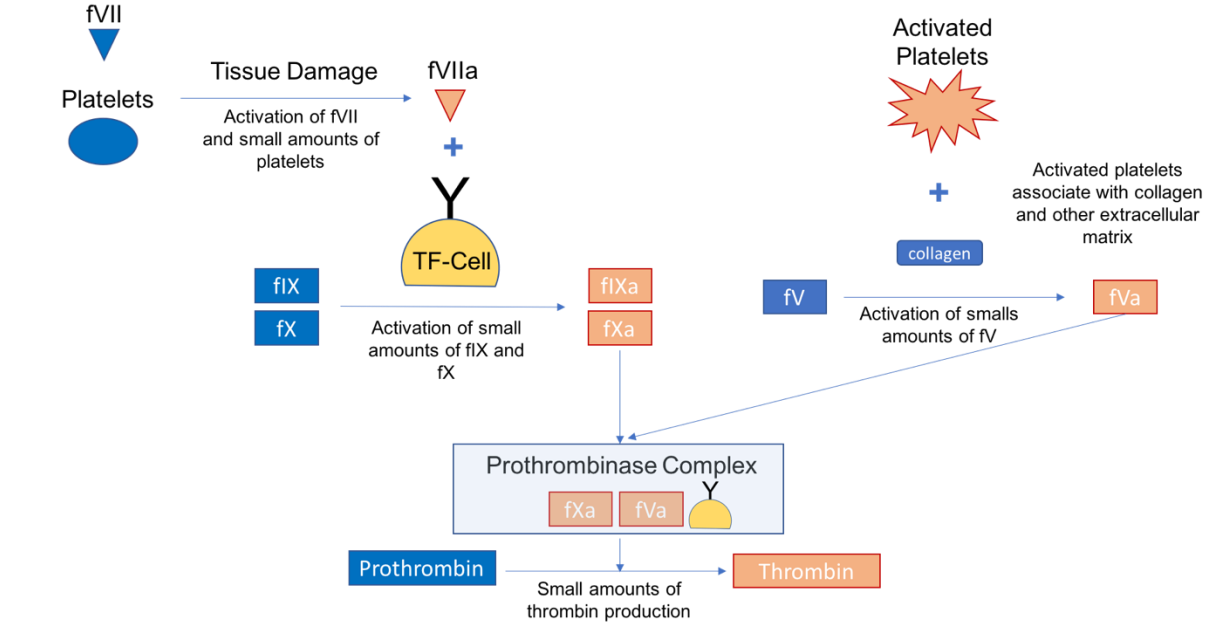

Figure 2. Phase 1 of hemostasis: initiation. The process of hemostasis has three distinct, but overlapping phases: initiation, amplification, and propagation. The first phase, initiation is stimulated by tissue damage, which activates fVII and platelets. Tissue factor exposed on the surface of cells binds to fVIIa, and activates small amounts of fIX and fX. Activated platelets bind to collagen and activates fV. The prothrombinase complex composed of fXa, fVa, and tissue factor, produces small amounts of thrombin on tissue factor-bearing cells for the use of the second phase of hemostasis.

Amplification—The second phase of hemostasis is amplification, which results in the increased level of activated coagulation factors (**Figure 3**). The small amounts of thrombin produced during initiation is then able to activate factors V, VIII, and XI on platelet surfaces during amplification (resulting in factors Va, VIIIa and XIa, respectively). Thrombin also activates platelets during this phase, resulting in an increased level of negatively charged phosphatidylserine headgroups exposed on the surface (or outer leaflet) of platelet membranes (Bevers et al. 1983, O'Donnell et al. 2014). Mainly, amplification sets the stage for large-scale thrombin production in the third phase, propagation.

Phase 2: Amplification

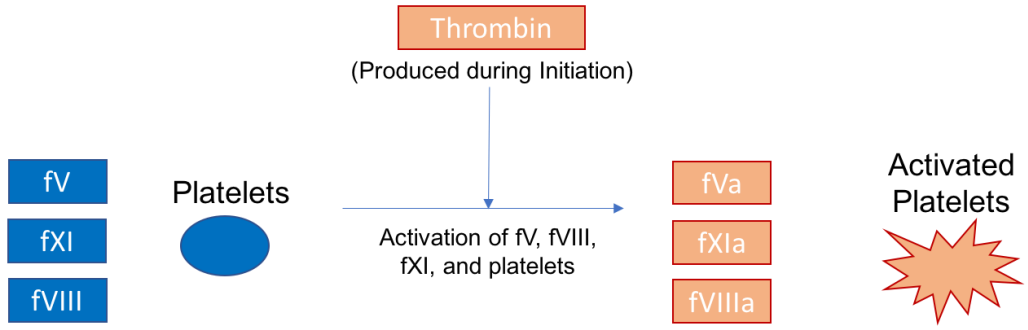

Figure 3. Phase 2 of hemostasis: amplification. The process of hemostasis has three distinct, but overlapping phases: initiation, amplification, and propagation. The second phase, amplification, elevates the levels of fVa, fXIa, fVIIIa, and activated platelets stimulated by sufficient amounts of thrombin generated during initiation. These activated factors and platelets are then used in third phase, propagation, for large-scale thrombin production.

Propagation—The third phase, propagation, takes place on the surface of these newly activated platelets. It is traditionally known as the intrinsic pathway of the blood coagulation cascade model. This phase contrasts with the initiation phase in that the protein interactions are localized on activated platelet surfaces instead of on TF-bearing cells (Rosing et al. 1985). At this stage, large bursts of thrombin are produced. Thrombin then converts the soluble plasma protein, fibrinogen, into insoluble fibrin after a series of protein interactions. The crosslinking of fibrin gathered at the site of injury entangles red blood cells, leading to the formation of blood clots (**Figure 4**; Kanaide and Shainoff 1975).

The specific protein interactions of the propagation phase begin with the stimulation of damaged blood vessels. The contact of factor XII to negatively charged surfaces spontaneously causes fXII activation (to fXIIa) (Cochrane et al. 1973; Griffin 1978), which

then activates factor XI. Factor XI can also be self-activated or activated by thrombin in the presence of negatively charged surfaces (Naito and Fujikawa 1991). Following fXI activation, fXIa converts fIX to fIXa (Fujikawa et al. 1974; Lindquist et al. 1978). The thrombin-activated fVIIIa then acts as a cofactor to serine protease fIXa and binds to phosphatidylserine exposed on the extracellular surface of activated platelets, forming an important complex termed the intrinsic Xase (tenase) complex due to its role in the activation of factor X (Bergsagsel and Hougie 1956; Dieijen et al. 1981). Subsequently, fXa associates with fVa on activated platelet membranes to form the prothrombinase complex, which causes large-scale thrombin production by activating prothombin (Rosing et al. 1985). Thrombin proteolytically converts the soluble precursor, fibrinogen, to insoluble fibrin. This insoluble fibrin is then able to assemble into long fibrils that gather at the site of injury, leading to the formation of a stable, hard blood clot (Kanaide and Shainoff 1975). Due to the importance of the Xase complex (fVIIIa/fIXa/platelets) in promoting hemostasis, the structural characterization of fVIIIa lipid binding is an important concern.

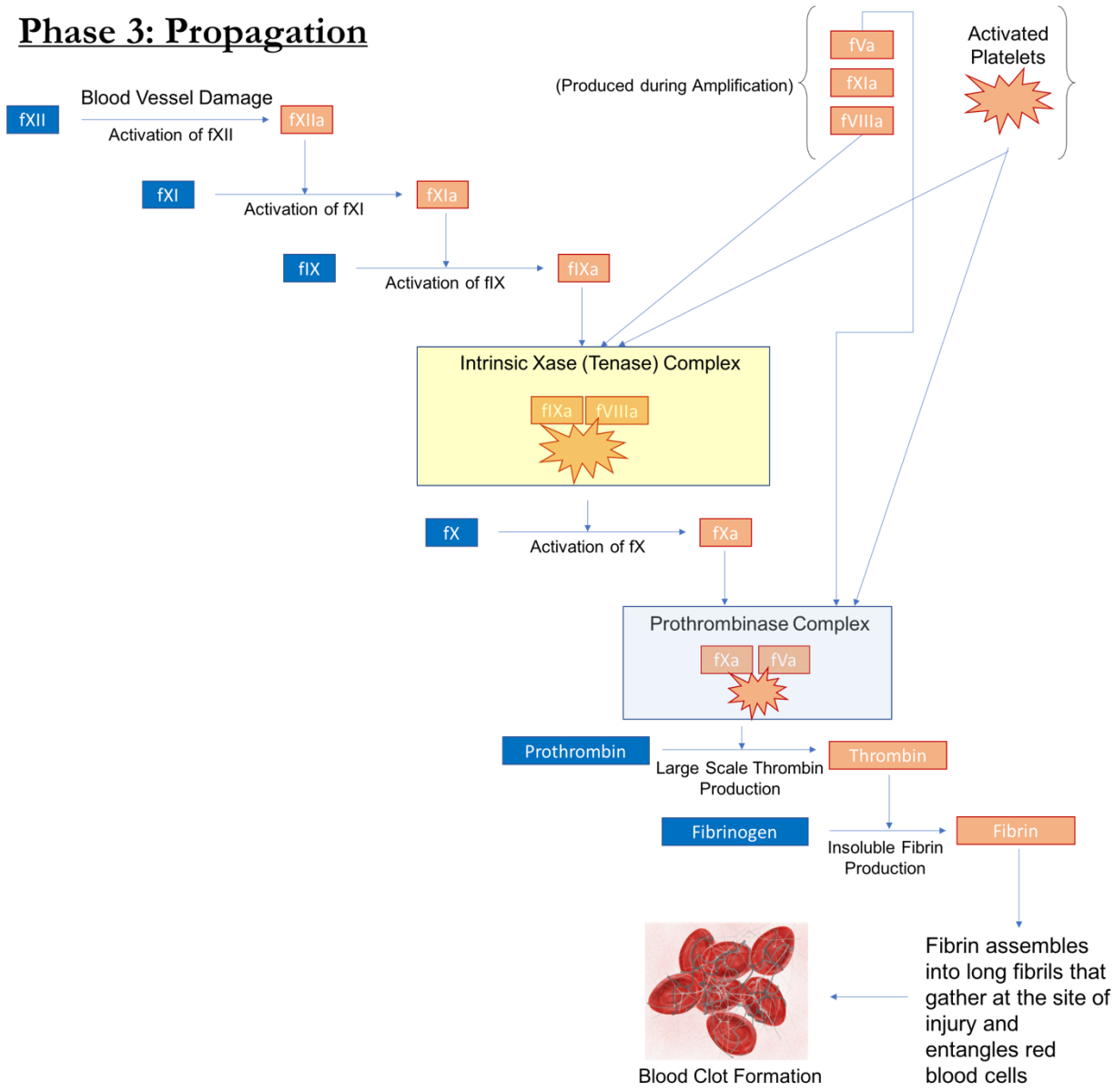

Figure 4. Phase 3 of hemostasis: propagation. The process of hemostasis has three distinct, but overlapping phases: initiation, amplification, and propagation. The third phase, propagation, is also traditionally known as the intrinsic pathway of blood coagulation. Propagation is stimulated by vascular damage, which activates fXII. Activated fXIIa then activates fXIa, which activates fIXa, allowing for the formation of the intrinsic tenase complex composed of fVIIIa/fIXa/ activated platelets. The tenase complex activates fXa that is used for the formation of the prothrombinase complex on the surface of activated platelets. The prothrombinase complex generates large-scale thrombin production, which then proteolytically converts soluble fibrinogen to insoluble fibrin that assemble into long fibrils that gather at the site of injury to form a stable, hard blood clot.

Inhibition of the Blood Coagulation Process

Once a stable blood clot is formed, the blood coagulation process needs to be inhibited to prevent thrombosis. Inhibition of the blood coagulation process is modulated by (1) activated Protein C, (2) antithrombin III, and/or (3) tissue factor pathway inhibitor.

Activated Protein C—The Protein C anticoagulant pathway inactivates the glycoproteins (fVa and fVIIIa) of the coagulation process and is mediated by thrombomodulin, a thrombin-binding protein present on cell surfaces (Esmon and Owen 1981). The thrombomodulin-thrombin complex serves to activate Protein C, a serine protease that inactivates fVa and fVIIIa upon binding phospholipid vesicles (Walker et al. 1979). Protein S acts a cofactor to Protein C to enhance Protein C phospholipid binding, resulting in the increased rate of glycoprotein inactivation (Walker 1981). Factor V can also serve to enhance inactivation rates of fVIIIa in the presence of Protein S (Varadi et al. 1996). The inactivation of fVIIIa can additionally be mediated by fXa, which can cleave at the same site as activated Protein C (Eaton et al. 1986).

Antithrombin III—Another method of inhibition is through antithrombin III, a plasma glycoprotein that serves as a cofactor to heparin to inhibit serine proteases such as thrombin (Abildgaard 1968), fIXa, fXa (Kurachi et al. 1976), fXIa (Damus et al. 1973), and fXIIa (Stead et al. 1976) by forming a covalent carboxylic ester bond with the active site serine residue in the catalytic site of these proteases (Owen, 1975).

Tissue Factor Pathway Inhibitor—A more recently discovered method of inhibition is through the tissue factor pathway inhibitor (TFPI or also known as the extrinsic pathway inhibitor), which inhibits the initiation of blood coagulation by preventing the TF-fVIIa complex from activating factors fIX and fX (Sanders et al. 1985; Rao and Rapaport 1987; Broze et al. 1988; Wun et al. 1988). This pathway starts with TFPI binding fXa (Sanders et al. 1985; Rao and Rapaport 1987; Broze et al. 1988; Wun et al. 1988). This TFPI-fXa complex then inhibits the TF-fVIIa complex by the formation of a larger TFPI-fXa-TF-fVIIa complex (Broze et al. 1988).

The complete process of hemostasis is complex and involves several different components. The focus of this study, however, is on the glycoprotein, blood coagulation factor VIII. Its central role is involved in forming of the important intrinsic tenase complex during propagation, which is essential in promoting the formation of a stable fibrin blood clot during hemostasis.

Blood Coagulation Factor VIII

Factor VIII (fVIII) is a glycoprotein that is essential in promoting proper hemostasis. It is primarily synthesized in liver sinusoidal cells (Webster 1971), but has been shown to be synthesized in other tissues as well, such as in the spleen, lymph nodes, and kidney (Wion 1985). Mature fVIII is initially synthesized as a single polypeptide with the domain structure A1-a1-A2-a2-B-a3-A3-C1-C2 and consists of 2332 residues (**Figure 5**; Vehar et

al. 1984; Toole et al. 1984). The A domains have short spacers (a1, a2, and a3) containing acidic regions, harboring clusters of Asp and Glu residues.

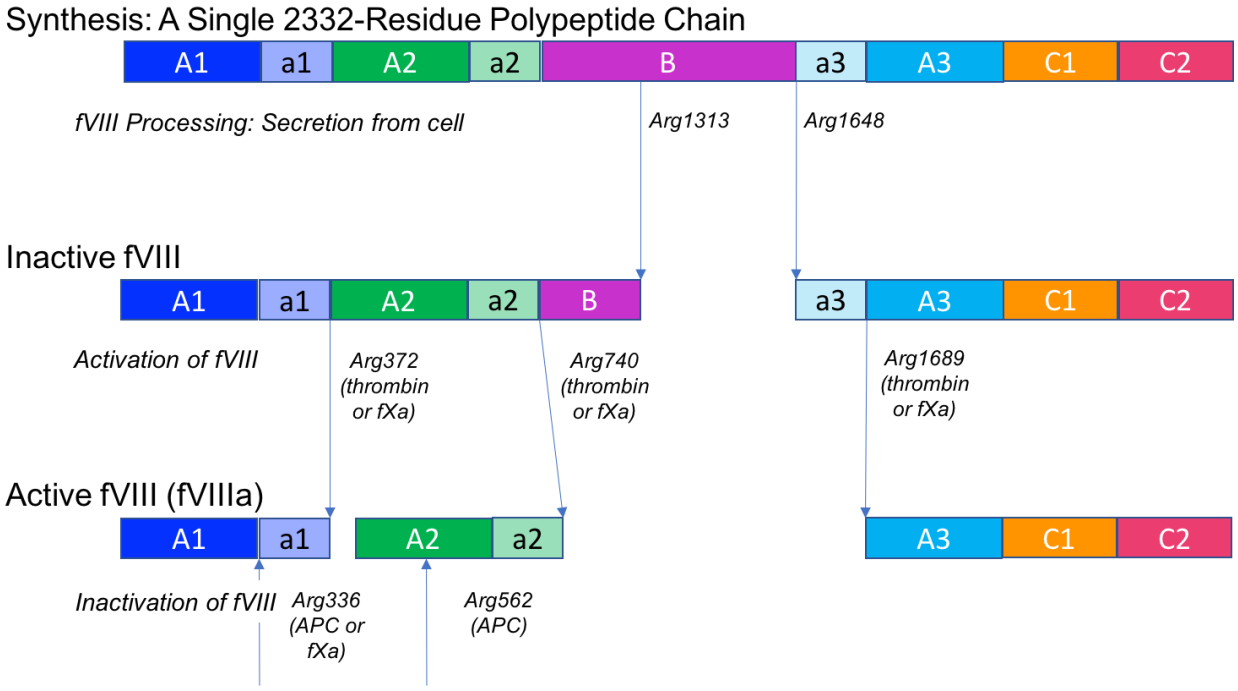

Figure 5. A schematic view of the fVIII construct. First, fVIII is synthesized as a single 2332-residue polypeptide chain with domains A1-a1-A2-a2-B-a3-A3-C1-C2. The lower-cased domains are acidic linker regions. Cleavage at Arg1313 and Arg1648 result in fVIII processing, which is secreted from the cell as an inactive heterodimer A1-a1-A2-a2-B/a3-A3-C1-C2. Factor VIII is then activated by thrombin cleavage at Arg372, Arg740, and Arg1689, which results in fVIIIa. Sites for fVIIIa inactivation are Arg336 and Arg562.

Upon secretion from the cell, fVIII is processed by cleavage occurring at the Arg1313 and Arg1648 residues within the B domain of fVIII, resulting in a heterodimer consisting of a heavy chain (A1-a1-A2-a2-B) and a light chain (a3-A3-C1-C2) that is held together by a metal ion bridge (**Figure 5**; Vehar, et al, 1984; Kaufman et al. 1988). The light chain of this inactive heterodimer is bound tightly in a noncovalent complex with the glycoprotein, von Willebrand factor (vWF). The fVIII/vWF complex maintains fVIII stability in

circulation by preventing premature inactivation by activated Protein C and blocking phospholipid interactions (Fay et al. 1991). During vascular injury, fVIII becomes proteolytically activated into a heterotrimer (A1-a1/A2-a1/A3-C1-C2) either by thrombin or fXa, which leads to the dissociation of fVIIIa from vWF upon removal of the acidic a3 region of fVIII (residues 1649-1689) (Eaton et al. 1986; Lollar et al. 1988). Thrombin activates fVIII by cleaving at Arg372 and Arg740 in the heavy chain and Arg1689 in the light chain (Eaton et al. 1986; Pittman and Kaufman 1988; Nogami et al. 2000). Factor Xa can also activate fVIII by cleaving at the same sites as thrombin, but additionally, it can cleave at Arg1721 (Eaton et al. 1986). However, the main activator of fVIII is thrombin because vWF inhibits fXa proteolysis of fVIII, whereas vWF does not affect thrombin cleavage of fVIII (Koedam et al. 1990).

An X-ray crystal structure of a B domain-deleted fVIII has been reported to a resolution of 3.7 Å to demonstrate the unambiguous placement of the domains (**Figure 6**; Shen et al. 2008). The function of fVIIIa is to act as a cofactor for serine protease fIXa on the surface of activated platelets, which forms the intrinsic tenase complex during the propagation phase of hemostasis to promote the formation of a stable blood clot (Dieijen et al. 1981). Previous findings from various labs have shown that the C2 domain of fVIIIa is the central domain involved in activated platelet membrane binding (Arai et al. 1989; Foster et al. 1990).

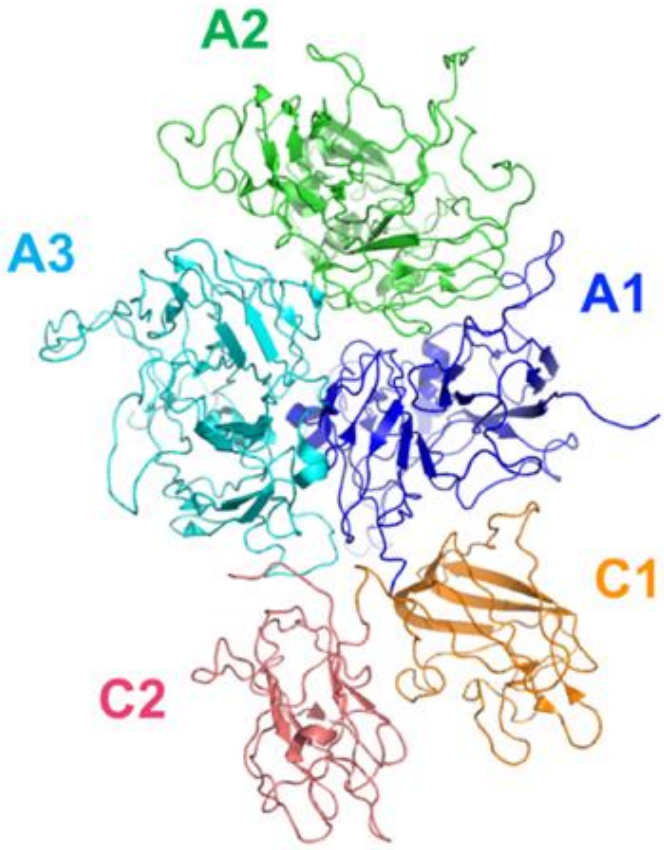

Figure 6. Factor VIII X-ray crystal structure. A 3.7 Å resolution X-ray crystal structure of a B domain-deleted fVIII heterodimer composed of a heavy chain (A1-A2) and a light chain (A3-C1-C2). The structure showed unambiguous modeling of domains A1 (blue), A2 (green), A3 (blue), C1 (orange), and C2 (pink) (PDB ID 2R7E; Shen et al. 2008).

C2 Domain of fVIII

Although fVIIIa contains five domains, the main domain of interest is the second carboxy-terminal (C2) domain of fVIII. The C2 domain has been shown to have binding sites for vWF (Saeneko et al. 1994), but the focus of this study will be on the structural basis for C2 domain binding to activated platelet membranes (Aria et al. 1989; Foster et al. 1990). Currently, there is controversy in the phospholipid binding mechanism of fVIII C2

domain. Previous studies have shown that residues 2303-2332 within the C2 domain are important for phosphatidylserine (PS) lipid membrane binding due to the ability of the 2302-2332 peptide to inhibit fVIII PS membrane binding (Foster et al. 1990). In 1999, a 1.5 Å resolution X-ray crystal structure of human fVIII C2 domain revealed two hydrophobic beta-hairpin loops that protrude from a ring of basic residues (**Figure 7A/B**; Pratt et al. 1999). From this crystal structure, it was suggested that the C2 domain-phospholipid binding interface was centered on Arg2220 (**Figure 7C**). This model had the hydrophobic beta hairpin loops (Leu2251-Leu2252 and Met2199-Phe2200) and residue Val2223 embedded within the lipid membrane. The model also included electrostatic interactions between the underlying basic residues (Lys2227, Arg2220, Lys2249, and Arg2215) and negatively charged phospholipid head groups of activated platelet membranes (**Figure 7C**). In support of this binding mechanism, an electron crystallographic structure of fVIII in its membrane-bound state was resolved to 1.5 nm and revealed that a loop containing residues Trp2313-His2315 was involved in membrane binding (Stoilova-McPhie et al. 2002). This binding mechanism, however, did not agree with recent ELISA binding studies from our lab, which will be explained later in the "Binding Analysis of Porcine C2 with 3E6 F_{AB} and G99 F_{AB}" section (Walter et al. 2013; Brison et al. 2015). Due to the large number of basic residues underlying the hydrophobic beta-hairpin loops, it is difficult to pinpoint the specific phospholipid binding site. Our goal is to define this mechanism with less ambiguity. The relevance of focusing on this mechanism is that when fVIIIa is unable to bind to activated platelet membranes, it causes the blood disorder, hemophilia A.

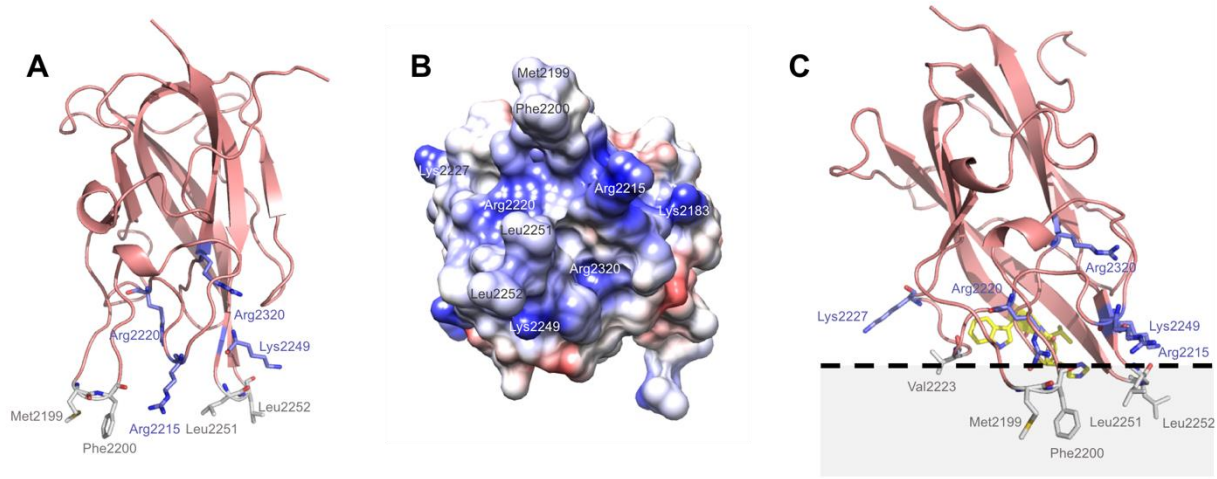

Figure 7. Factor VIII C2 domain X-ray crystal structure. A 1.5 Å resolution X-ray crystal structure of human fVIII C2 domain (PDB ID 1D7P; Pratt et al. 1999). (A) A ribbon diagram displaying the hydrophobic beta hairpin loops of hC2 include residues Met2199-Phe220 and Leu2251-Leu2252 (light gray). The ring of underlying basic residues consists of Arg2200, Arg2215, Arg2320, and Lys2249 (blue). (B) Coulombic surface coloring (generated in Chimera) shows the positively charged basic residues (blue) and the hydrophobic residues (light gray). Negatively charged residues are red. (C) The previously proposed model of C2 domain lipid binding centered on Arg2220. A loop containing residues Trp2313-His2315 (yellow) was hypothesized to be involved in lipid binding (Stoilova-McPhie et al. 2002). The dotted line and gray tinted area represents the phospholipid membrane of activated platelets.

Hemophilia A

Deficiency in fVIII clotting activity causes hemophilia A, an X-linked blood disorder that prevents proper blood clot formation. It is estimated that 1 in 5,000 male births is affected by hemophilia A worldwide (Soucie 1998). The other types of hemophilias are caused by deficiencies in factor I (fibrinogen), factor II (prothrombin), factor V, factor VII (proconvertin), factor X (Stuart-Prower factor), factor XI (which causes hemophilia C), factor XII (Hageman factor), factor XIII (fibrin stabilizing factor), and factor IX (which

causes hemophilia B) (Bolton-Maggs et al. 2004). Von Willebrand disease, caused by deficiency in vWF, is another bleeding disorder that results in a similar phenotype as hemophilias (Ginsburg et al. 1985). Hemophilia A, however, is the most common type of hemophilia, representing 80% to 85% of the total hemophilia population (Srivastava et al. 2013). Individuals with this disorder are characterized as having severe, moderate, or mild hemophilia, with fVIII activity levels of less than 1% of normal, 1% to 5% of normal, and 5% to less than 40% of normal, respectively. Phenotypes of patients with severe hemophilia include two to three spontaneous bleeding incidents into joins or muscles each month, while moderate and mild hemophilia only have seldom or none, respectively. Abnormal and prolonged bleeding with trauma or surgery are overlapping characteristics of all three types (Srivastava et al. 2013).

Hemophilia A is inherited in an X-linked recessive pattern, passed down by a pathogenic variant of the fVIII gene (F8) located on the long arm of the X chromosome at position 28 (Xq28; Gitschier et al. 1984). There are many different possible mutations within the fVIII gene that can affect protein clotting activity listed on the Factor VIII Gene Variant Database provided by the European Association for Haemophilia and Allied Disorders and the Structural Immunology Group from the University College London (Rallapalli et al. 2014). The four types of DNA mutations that may occur are deletions, insertions (including duplication), inversions, and substitutions (Tuddenham et al. 1994). These types of mutations can either be caused by nonsense (a point mutation in which the codon is changed to a stop codon), missense (a point mutation in which the amino acid is changed),

splice site change, frameshift, large structural change (>50 bp), or small structural change (<50 bp), mutations. Nonsense and missense mutations are point mutations that cause substitution mutations, with missense mutations being the most common in hemophilia. Splice site change mutations also primarily cause substitutions, but can additionally cause deletion, duplication, and insertion. Frameshift, large structural change, and small structural change mutations can cause deletion, duplication, or insertion. Large structural changes can additionally cause inversion. Mild hemophilia A is predominantly caused by substitution point mutations in the form of missense DNA mutations, while moderate hemophilia A can be caused by a large mix of different mutation types. Severe hemophilia A is primarily caused by debilitating substitution and deletion mutations in the form of nonsense, missense, splice site change, frameshift, large and small structural change mutations.

On rare occasions, hemophilia A can also be acquired through autoimmune processes in which there is a spontaneous development of inhibitory antibodies against endogenous fVIII (Lottenberg et al. 1987). Cases of acquired hemophilia A have occurred mostly in postpartum women and in patients aged 62 years and beyond. These antibodies inhibit the function of endogenous fVIII within the patient, causing the attenuation of hemostasis. To mediate the effects of hemophilia A, replacement therapies have been developed.

Hemophilia A Therapeutics

Therapeutics of hemophilia A include direct infusions of either plasma-derived or recombinant human fVIII (hfVIII) concentrates for replacement therapy (Coppola et al. 2010). These can be either be used on-demand as episodic infusions, or be used to treat severe hemophilia A prophylactically, i.e., receiving regular infusions of fVIII concentrates for hemorrhage prevention. The advantage of prophylactic treatment over episodic infusions is the reduction in the number of bleeding episodes, thereby improving patient quality of life (Smith et al. 1996; Konkle et al. 2015). Plasma-derived human fVIII is prepared by extracting and purifying the glycoprotein from cryoprecipitate prepared from human plasma (Addiego et al. 1992). Complications associated with this are the transmission of viral contaminations and diseases. Current technology has eradicated this possibility by treating the plasma with viral inactivation methods and improved disease detection (Centers for Disease Control 1988). Treatment with recombinant hfVIII for replacement therapy is more common in the United States than the use of plasma-derived hfVIII. These proteins are primarily produced by Chinese hamster ovary (CHO) or baby hamster kidney (BHK) cells transfected with the human fVIII gene (Kaufman et al. 1988). To ensure safety, the concentrated proteins are then subjected to viral inactivation methods, even though they are considered free of viruses.

There are currently many recombinant fVIII products available. Common recombinant fVIII therapeutic products include Advate (Baxter), Xyntha (Pfizer) and Kogenate FS (Bayer Pharmaceuticals). Their doses are based on a person's deficiency of fVIII activity,

their weight, and the circumstance of bleeding. They are administered through intravenous infusion via IV bolus as soon as the bleeding episode occurs to promote proper hemostasis (McDaniel 2013). Recently in 2015, Adynovate (BAX 855), a PEGylated full-length recombinant fVIII based on Advate, was approved for on-demand and prophylactic treatment of hemophilia A (Konkle et al. 2015; Horling et al. 2016). Adynovate has an extended half-life due to PEGylation of the recombinant fVIII and thus is an improvement in hemophilia A therapeutics. In patients with mild or moderate hemophilia A, prophylactic treatment may not be required. Treatment with desmopressin (or also known as DDAVP), which increases the levels of fVIII in plasma by inducing secretion from endothelial cells, instead of direct infusions of hfVIII is a viable alternative in this patient population (Rose and Aledort 1991).

Inhibitory Antibody Development: Hemophilia A Treatment Complications and Management of Inhibitor Development

Although these transfusions are highly effective, approximately 30% of the patients who receive these direct infusions of human fVIII (hfVIII) eventually develop inhibitory antibodies that attenuate or abolish the function of the newly infused hfVIII (Bray et al. 1994; Lusher et al. 2003). This complication leaves the individual with the inability to form stable blood clots due to nonfunctional hfVIII being cleared from circulation. In these cases, and in cases of acquired hemophilia A, several options for treatment are available. Immune tolerance induction can be employed as an attempt to eradicate inhibitors and normalize pharmacokinetic parameters by means of frequent administration of

concentrates long-term, with success rates between 60% and 80% (DiMichele and Kroner 2002). Often, immune tolerance induction is accommodated by immunosuppression of either the T- or B-cell pathways to prevent the production of these inhibitory antibodies by the use of immunosuppression agents such as corticosteroids (Miao 2010). Although the mechanism of action is not well known, desmopressin (DDAVP) has been clinically used as an immunosuppressant as well (Franchini and Lippi 2011). Bypassing agents, such as activated prothrombin complex concentrates and recombinant fVIIa replacements, are also commonly used as first-line therapies to treat patients with inhibitory anti-hfVIII antibodies (Hoffman and Dargaud 2012). Adynovate (the PEGylated recombinant fVIII), and rfVIIIFc (a fusion protein composed of a recombinant fVIII covalently attached to the Fc domain of human IgG) may also be used in lieu of traditional recombinant fVIII concentrates, as they have been shown to have an extended half-life in circulation (van der Flier et al. 2015; Horling et al. 2016). Adynovate is also able to evade the immune response, making it a better alternative for fVIII infusions (Horling et al. 2016). Porcine fVIII (pfVIII) as a second-line therapeutic is another option due its low cross-reactivity to anti-hfVIII antibodies, especially inhibitory antibodies that prevent proteolytic activation of fVIII, relative to hfVIII (Hay et al. 1996; Barrow and Lollar 2006; Brison et al. 2015). Other reasons pfVIII is an appropriate fVIII replacement is that pfVIII is more stable and more active due to the A2 domain being in a tighter complex within the active form of pfVIII (Lollar et al. 1992).

The antibodies developed against fVIII can either be completely or incompletely inhibitory, which corresponds to either type I or type II inhibition behavior, respectively (Gawryl and Hoyer 1982). The epitopes of inhibitory antibodies are primarily located in the A2, A3, and C2 domains of fVIII (Fulcher et al. 1985; Scandella et al. 1989). Within the C2 domain, there are 5 different structural epitopes to which these inhibitory antibodies can bind, and display two main mechanisms of inhibition (Meeks et al. 2007). Classical (e.g. 3E6 and BO2C11) antibodies bind at either group A, AB, or B epitopes and inhibit the function of fVIIIa by blocking phospholipid and/or vWF binding (**Figure 8**; Arai et al. 1989; Barrow et al. 2001). The other, "nonclassical", mechanism of inhibition prevents thrombin or fXa activation of fVIII, by antibodies (e.g. G99) that bind at either group BC or C epitopes of C2 (Meeks et al. 2008).

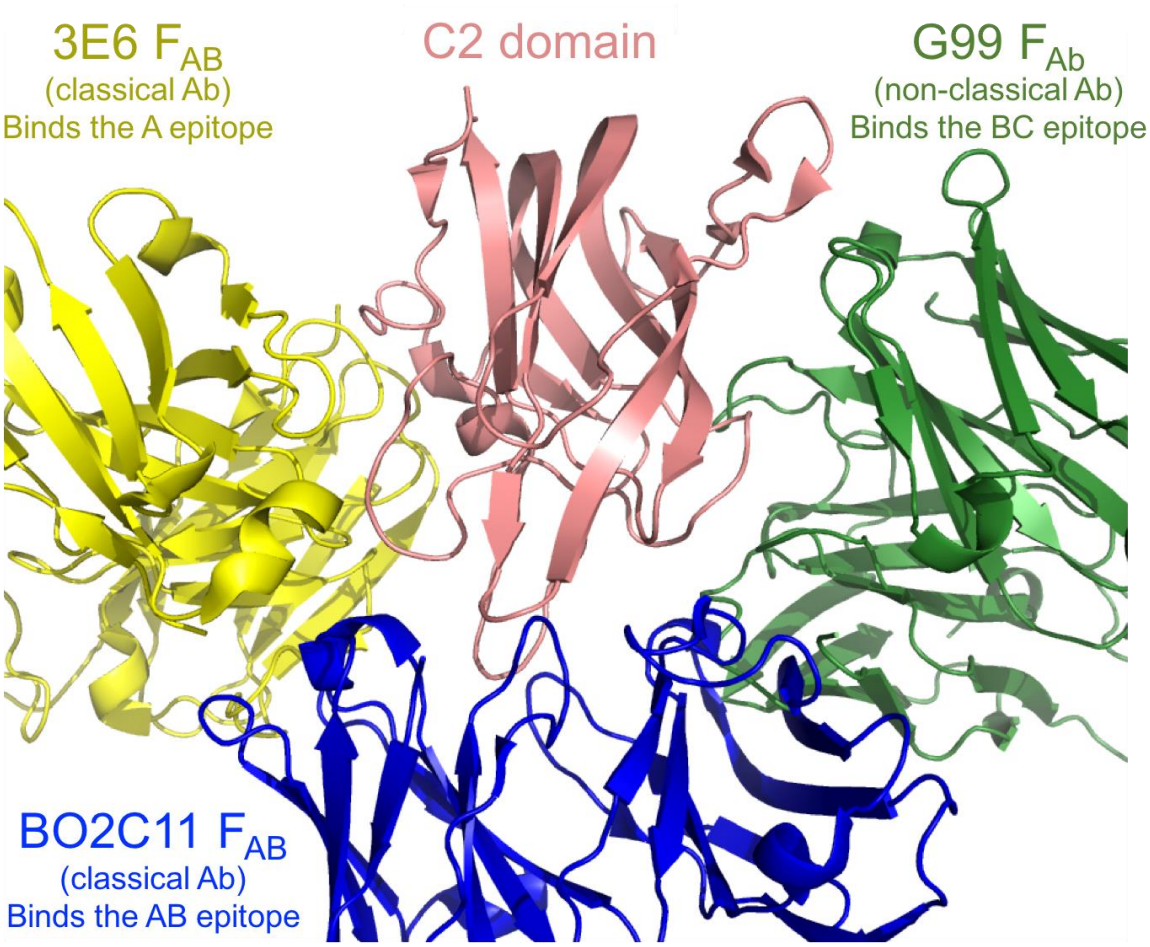

Figure 8. Examples of the inhibitory binding epitopes of the C2 domain. A 2.47 Å resolution X-ray Crystal ternary structure of hC2 (pink)/G99 F_{AB} (yellow)/3E6 F_{AB} (dark green) (pdb ID 4KI5; Walter et al. 2013) superimposed with a 2.0 Å crystal structure of hC2/BO2C11 F_{AB} (blue) (pdb ID 1IQD; Spiegel et al. 2001). 3E6 and BO2C11 are both classical antibodies that bind at either the A or AB epitope of C2, while the nonclassical antibody, G99, binds to the BC epitope of C2.

Structural Characterization of Human fVIII C2 Domain Interactions with Antibodies 3E6 F_{AB} and G99 F_{AB}

Specific residue interactions between the two classes of anti-C2 inhibitory antibodies and human fVIII C2 domain were elucidated in a 2.47 Å resolution crystal structure of a ternary complex (C2 domain/3E6 F_{AB}/G99 F_{AB}), which was solved in our lab (**Figure 9**, Walter et al. 2013).

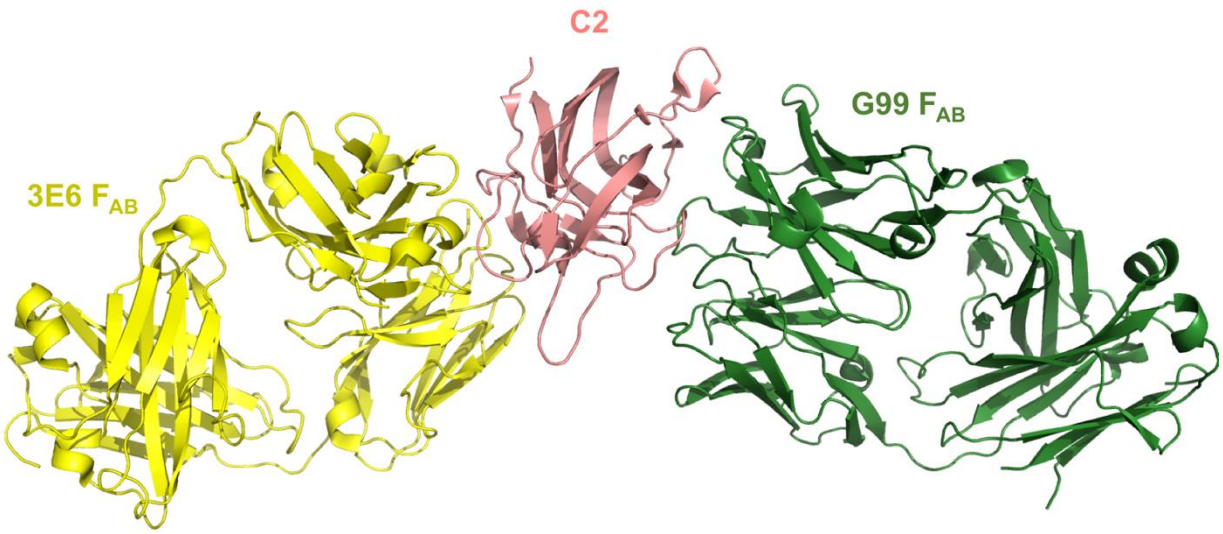

Figure 9. An X-ray Crystal structure of a ternary complex (hC2 domain (pink)/ 3E6 F_{AB} (yellow)/ G99 F_{AB} (dark green)) determined to 2.47 Å resolution (pdb ID 4KI5; Walter et al. 2013).

This revealed that the classical epitope face of C2, where 3E6 binds, has a positively charged surface potential (**Figure 10A**) that interacts electrostatically with the oppositely charged surface of the 3E6 variable region (**Figure 10B**; Walter et al. 20013). Residues Lys2183 and Gln2213 in C2 are 80% buried upon binding 3E6 F_{AB}, based on analysis using NACCESS (S. Hubbard and J. Thornton 1992-6), which divides the measured buried surface area by the free accessible surface area (Walter et al. 2013). Lys2183 has a possible cation-π interaction with Trp90 of 3E6 F_{AB} (**Figure 10C**).

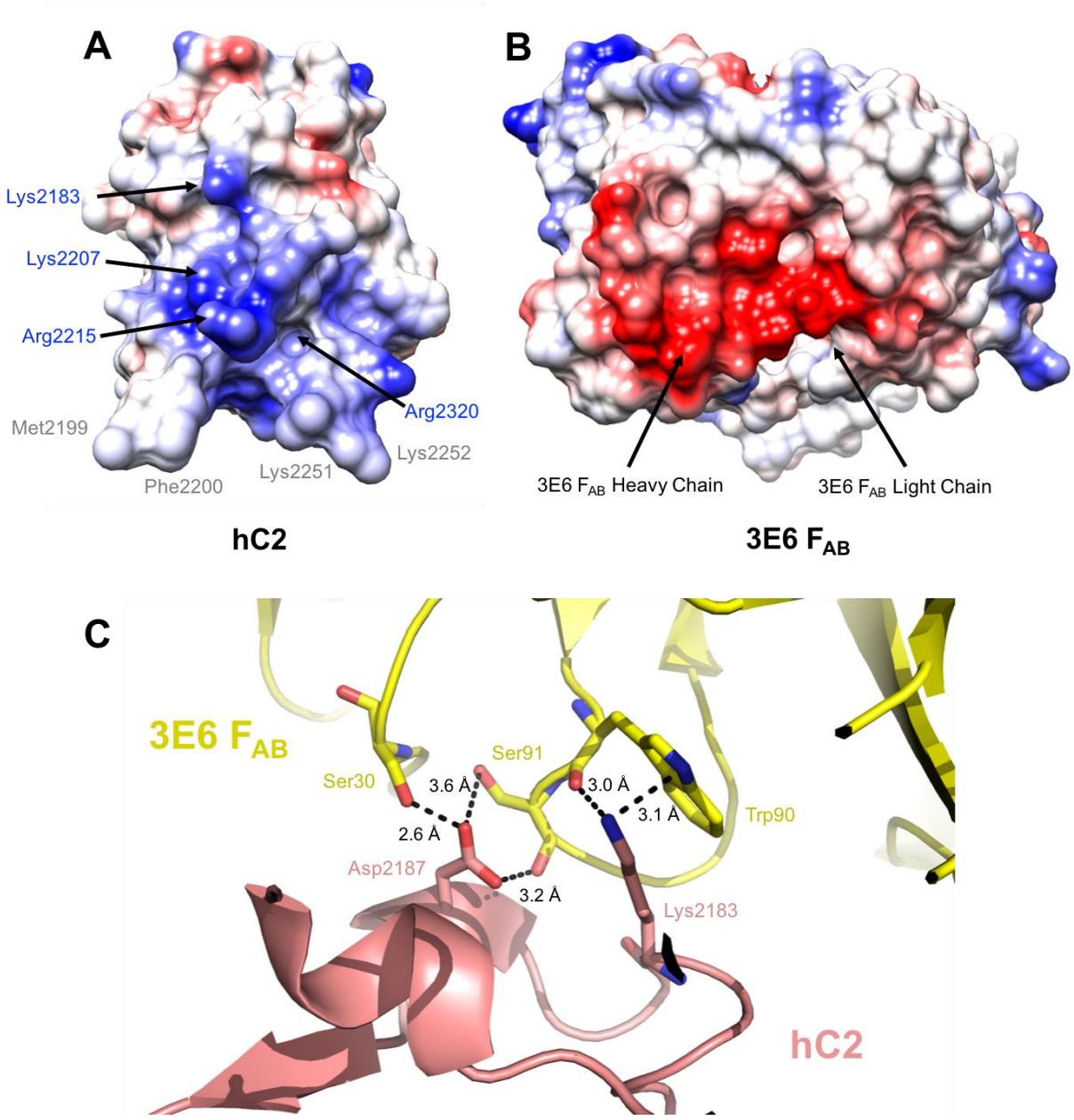

Figure 10. A coulombic surface coloring (generated in Chimera) of a 2.47 Å resolution X-ray crystal structure of the 3 E6 F_{AB} epitope in human C2 domain and of the 3E6 F_{AB} surface where human C2 binds. (A) The classical epitope face of hC2 where 3E6 F_{AB} binds is predominantly negatively charged (blue) and (B) the variable region of 3E6 F_{AB} has a positively charged surface (red) that interacts with hC2. White colors represent hydrophobic residues. (C) Specific residue interactions of 3E6 F_{AB} (yellow) and hC2 (pink) involve Asp2187 and Lys2183 of hC2 and Ser30, Ser91, and Trp90 of 3E6 F_{AB} (PDB ID 4KI5; Walter et al. 2013).

Similarly, the nonclassical epitope face where G99 F_{AB} binds showed an electrostatic interaction where the nonclassical G99 F_{AB} has a negatively charged anionic pocket (**Figure 11A**) that allowed for the basic Lys2227 residue within the nonclassical epitope face of C2 to bind (**Figure 11B**).

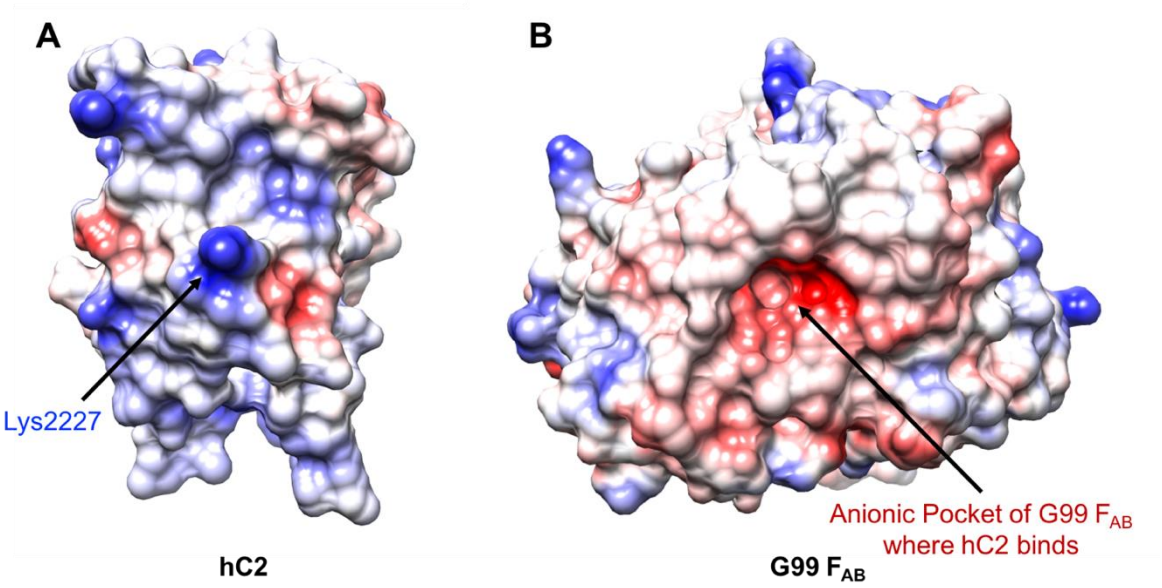

Figure 11. A coulombic surface coloring (generated in Chimera) of a 2.47 Å resolution X-ray Crystal structure of the G99 F_{AB} epitope in human C2 domain and of the G99 F_{AB} surface where human C2 binds. (A) The nonclassical epitope face of hC2 is predominantly positively charged (blue), (B) while the surface potential for the G99 pocket where hC2 binds is negatively charged (PDB ID 4KI5; Walter et al. 2013).

To understand the lowered cross-reactivity of pfVIII, a crystal structure of pfVIII C2 domain was determined to a resolution of 1.7 Å by a former member of our lab (Brison et al. 2015). This structure was superimposed with the ternary hC2/3E6 F_{AB}/G99 F_{AB} complex, revealing the specific differences between hC2 and pC2 in terms of the classical and nonclassical epitope faces. Overall, the tertiary structures are similar with a root-mean-square deviation (RMSD) value of 0.282 Å (**Figure 12**) and have a sequence identity of 80%.

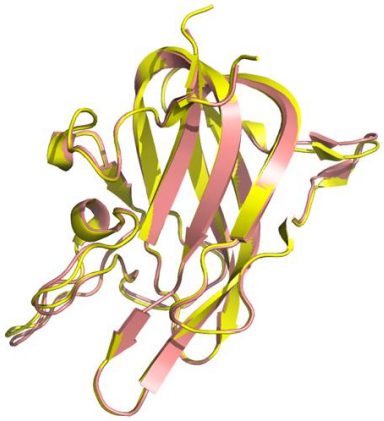

Figure 12. The crystal structures of human C2 (pink, PDB ID 4KI5) and porcine C2 (yellow, PDB ID 4MO3) superimposed with an RMSD of 0.842 Å (Walter et al. 2013; Brison et al. 2015).

The electrostatic surface potentials of hC2 and pC2 reveal that the differences between the 3E6 classical epitope faces are not as striking as the differences between hC2 and pC2 G99 nonclassical epitope faces. Sequence alignment shows that the differences between the human and porcine classical epitope faces are functionally minimal, with the most drastic change being the basic Lys2207 residue to a polar, uncharged Gln2207. This is further supported by observing that the electrostatic surface potentials of the classical epitope faces in the human and porcine structures are both primarily positive (**Figure 13A/B**). However, the surface potential of the nonclassical epitope face is primarily negatively charged in pC2 due to the acidic Glu2227 residue, whereas in hC2, the same residue is a basic Lys2227 (**Figure 13C/D**). Functional studies agreed with the observed differences between the two epitope faces between human and porcine C2 domains, providing a structural rationale for the observation that porcine fVIII is an effective alternative to human fVIII for replacement therapy in patients with nonclassical anti-human fVIII C2 inhibitory antibodies.

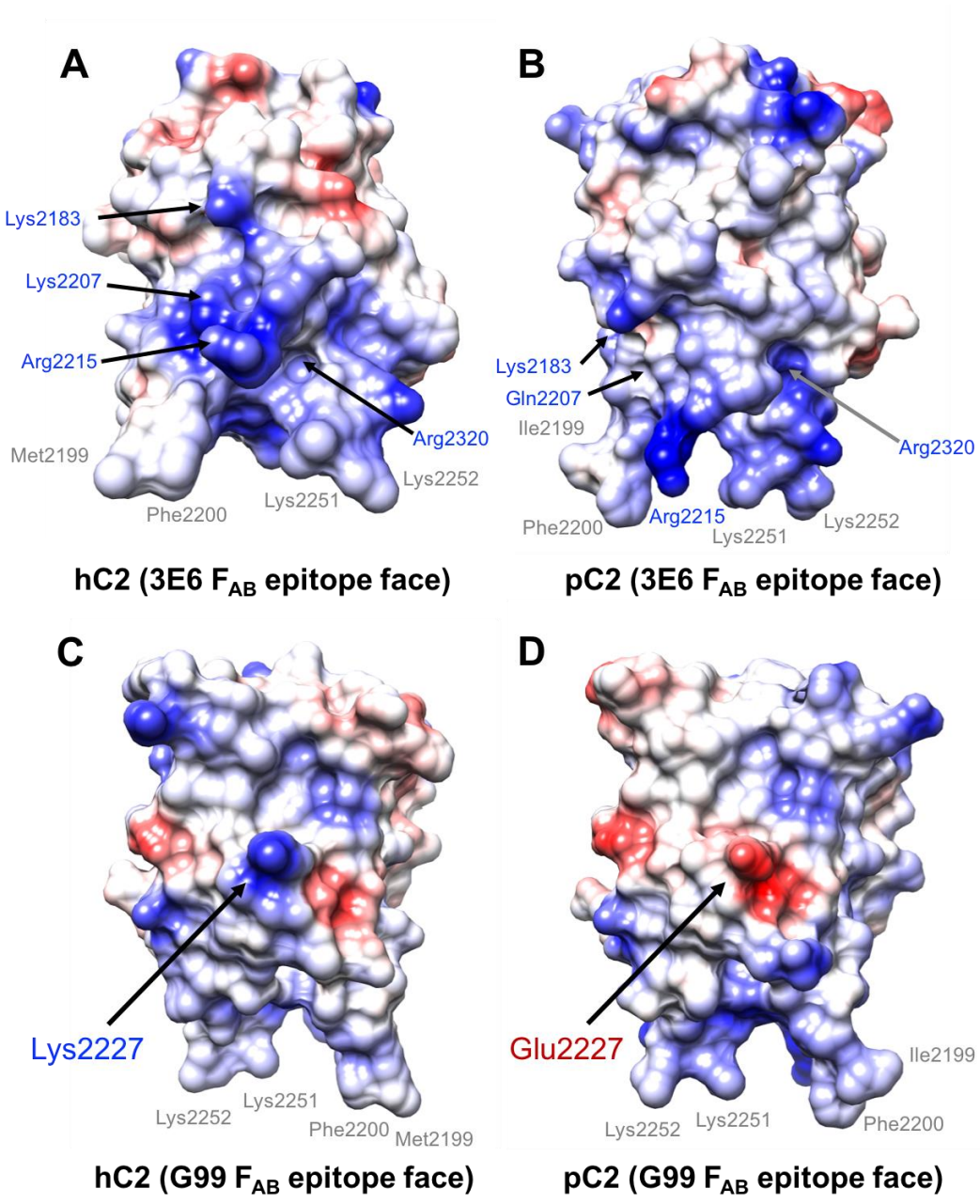

Figure 13. A coulombic surface coloring (generated in Chimera) of a 2.47 Å resolution X-ray Crystal structure of fVIII human C2 domain (PDB ID 4KI5, Walter et al. 2013) and a 1.4 Å resolution X-ray Crystal structure of fVIII porcine C2 domain (PDB ID 4MO3, Brison et al. 2015) visualized in Chimera. The differences between the 3E6 F_{AB} epitope faces of hC2 (A) and pC2 (B) are electrostatically similar. In contrast, the G99 F_{AB} epitope faces of hC2 (C) and pC2 (D) are oppositely charged, which demonstrates the structural reasoning as to why the human C2 antibody, G99 F_{AB}, has a high affinity for hC2, but does not bind pC2.

Binding Analysis of Porcine C2 with 3E6 F_{AB} and G99 F_{AB}

Inhibitory antibody binding analyses employing enzyme-linked immunosorbent assays (ELISA) showed that the binding affinities between human and porcine C2 with 3E6 mAb are more similar than with G99 mAb (Brison et al. 2015). Human and porcine C2 3E6 mAb binding had approximate K_D values of 2.2 and 4.3 nM, respectively (**Figure 14A)**. In contrast, hC2 bound G99 mAb with high affinity, while porcine C2 was unable to bind G99 mAb (**Figure 14B**). Although 3E6 mAb binding was similar in both human and porcine C2, 3E6 mAb inhibits human fVIII activity significantly more than that of porcine fVIII, revealed in a Bethesda assay, with inhibitory titers of 0.8 BU/mg IgG and 41 BU/mg IgG, respectively (**Figure 14C**; Brison et al. 2015). Porcine fVIII activity was not affected by G99 mAb, which is consistent with its inability to bind G99 F_{AB} (Brison et al. 2015).

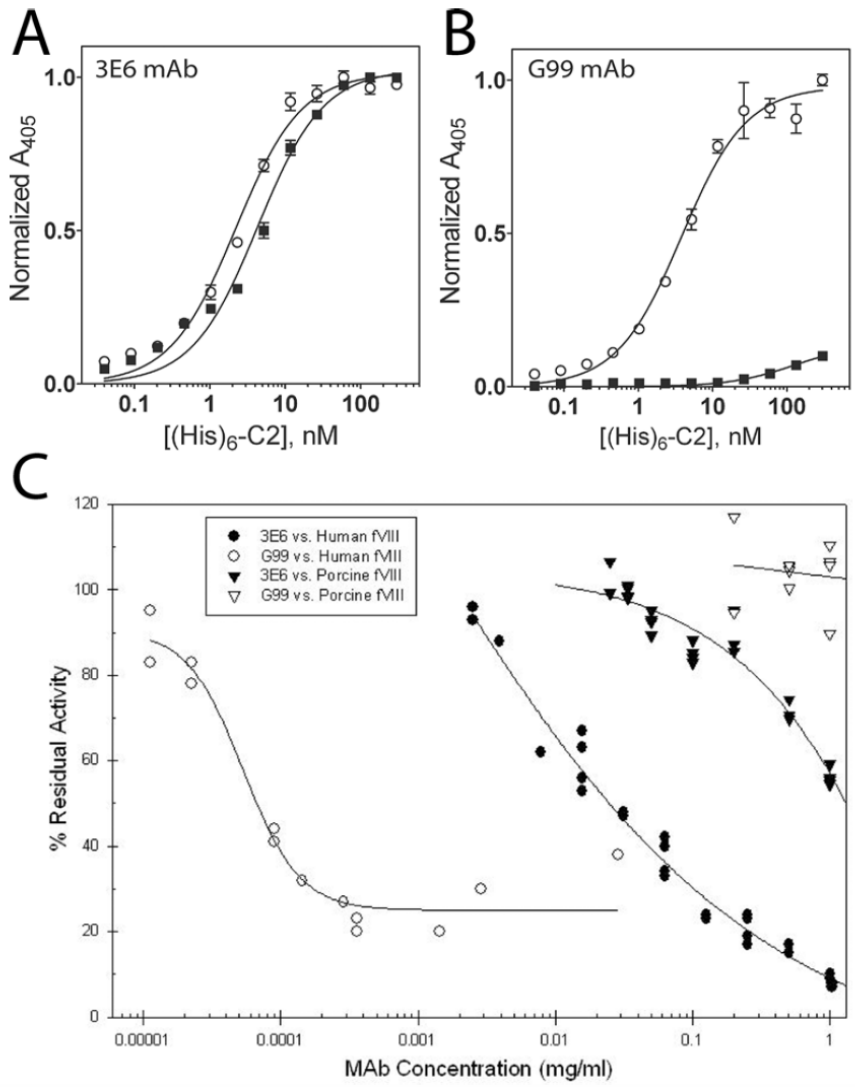

Figure 14. Inhibitory antibody binding analyses using ELISAs showed (A) 3E6 mAb binding was not significantly different between porcine (closed squares) and human (open circles) C2, (B) while G99 mAb was only able to bind human C2 (open circles). (C) Factor VIII inhibition studies through a Bethesda assay showed G99 mAb did not decrease porcine fVIII activity (open triangles), but it did significantly inhibit human fVIII activity (open circles). 3E6 mAb inhibited human fVIII activity (closed circles) significantly more than porcine fVIII activity (closed triangles) (Brison et al. 2015).

To examine which epitope of C2 binds PS-containing membranes, an ELISA detecting antibody binding of phosphatidylserine-bound fVIII C2 was employed by Brison et al. in 2015. This assay revealed which epitope was more solvent accessible when C2 is

immobilized on a membrane. Membrane-bound C2 was able to bind G99 mAb (with an affinity of 15.5 mM), but not 3E6 F_{AB} (**Figure 15**). This led to the conclusion that C2 binds membranes at the classical epitope face, where 3E6 binds, and not the nonclassical epitope face, where G99 binds. Because the C2 classical epitope face is centered on Arg2320, further studies were focused on this residue in C2.

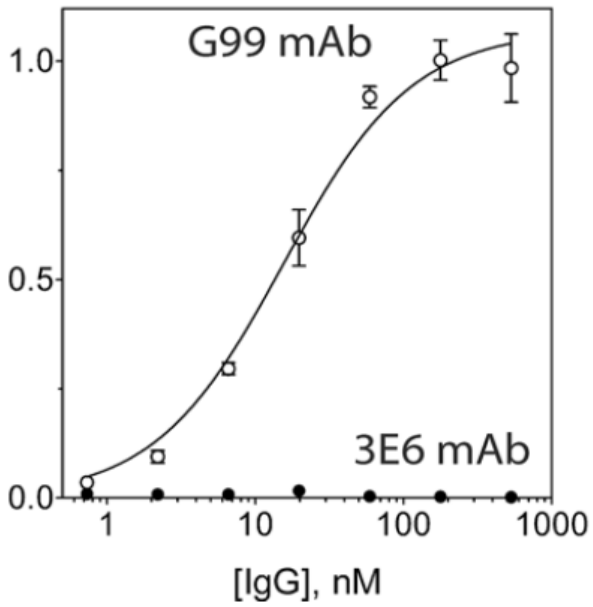

Figure 15. ELISA studies for phosphatidylserine (PS)-bound C2 and the two antibodies showed that the G99 epitope face was more solvent accessible than the 3E6 epitope face of C2. PS-bound C2 was able to bind G99 mAb, but not 3E6 mAb indicating that the PS binding occurs at the 3E6 epitope face (Brison et al. 2015).

Goals of this Study

Currently, the fVIII C2 domain binding mechanism of phosphatidylserine-containing activated platelet membranes remains controversial. The docking of the hydrophobic beta hairpin loops in C2 to platelet membranes is universally accepted, however the controversy lies within which epitope face docking occurs and with that, which underlying basic

residues interact with the negatively charged phospholipids of the activated platelet membranes (**Figure 7A/B**). Our previous research supports a new binding model that is centered on Arg2320 within the classical epitope face. Therefore, we studied the two naturally occurring hC2 mutants Arg2320Ser and Arg2320Thr that cause mild and moderate hemophilia A, respectively (Rallapalli et al. 2014). It is plausible that these mutations yield non-functional fVIII due to the inability of these mutants to bind membranes based on the concept that Arg2320 is one of the underlying basic residues that stabilize the membrane-C2 interaction. There are two other mutations, Arg2320Trp and Arg2320Met that occur naturally at this residue, but they were not examined. Arg2320Trp causes severe hemophilia A and likely does not fold correctly. Expression of the methionine mutation was attempted; however, the protein was unstable and could not be isolated in pure form. We also studied was an unnatural mutation, Arg2215Ala, because Arg2215 appears to be a positively charged residue that is positioned within the hydrophobic lipid bilayer during lipid binding and likely causes an unfavorable interaction. This observation led us to hypothesize that this C2 mutant would have a greater binding affinity to phospholipid membranes due to the removal of the positive charge. Because the fVIII C1 domain has also been shown to aid in the binding of factor VIII to phospholipid membranes (Meems et al. 2009; Lu et al. 2011), we extended two naturally occurring Arg mutations (Arg2159H and Arg2163H) to the isolated C2 domain of human fVIII. The C1 and C2 domains have a 40% sequence identity and a high structural homology, with an RMSD value of 3.08 Å (Figure 16). Studies with the Arg2163H mutant would be complementary to our hC2 mutant studies due to this mutation being at the same structural

location as the Arg2320 residue within the C2 domain (**Figure 16**). However, these hC1 mutants were difficult to purify and no further studies could be carried out. With these hC2 domain mutants, we analyzed (1) hC2 protein stability of Arg2320Ser and Arg2320Thr, and (2) hC2 membrane binding of Arg2320S, Arg2320Thr, and Arg2215Ala. In addition to studying these mutants, we also determined the X-ray crystal structure of wild type pC2 in complex with the soluble headgroup of phosphatidylserine, O-phospho-L-serine (OPLS).

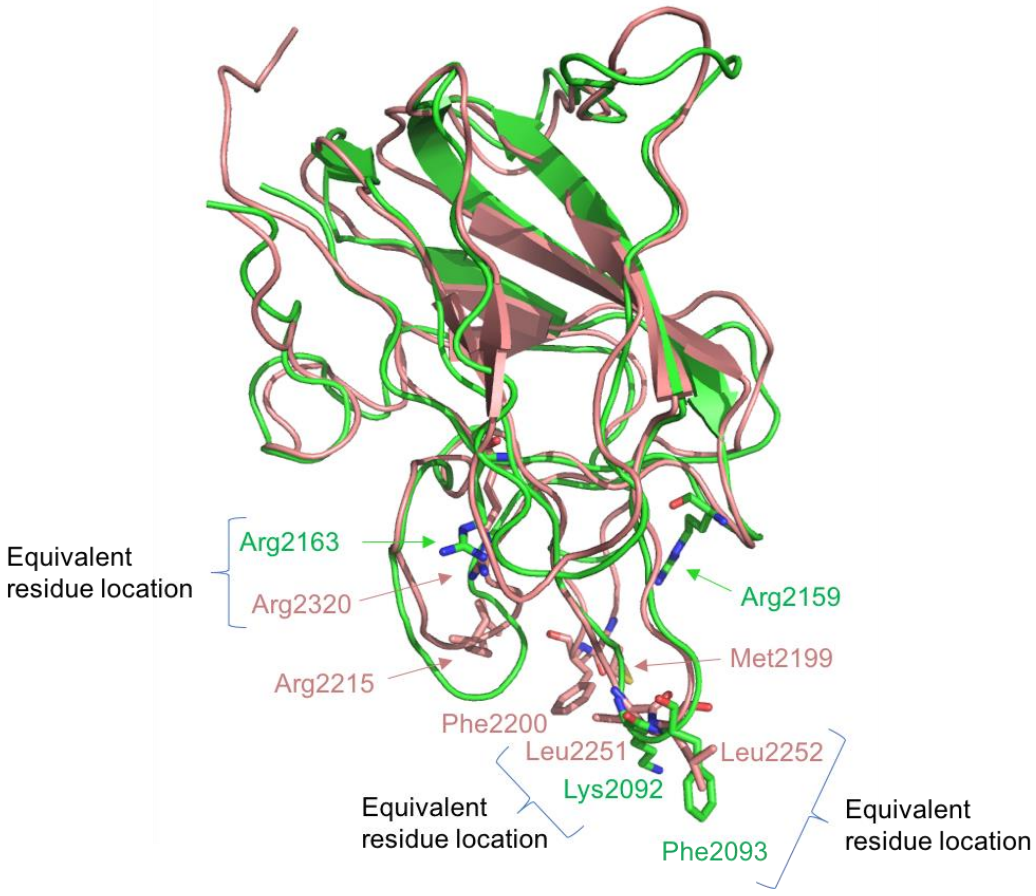

Figure 16. Structural alignment of the C1 (green) and C2 (pink) domains of human fVIII, with an RMSD value of 3.08 Å. Arg2320 within the C2 domain is in the same residue location as Arg2163 in the C1 domain. Arg2215 in the C2 domain and Arg2159 in the C1 domain were also of interest. These arginines were mutated to Arg2320Ser, Arg2320Thr, Arg2215Ala, Arg2163His, and Arg2159His for further analysis of C2 phospholipid membrane binding. (PDB ID 2R7E; Shen et al. 2008)

(1) Evaluation of Mutant Protein Stability—Functional studies of C2 Arg2320Ser and Arg2320Thr mutants were investigated to ensure proper folding and to analyze protein stability compared to wild type. These studies included (1) affinity pull-down assays and (2) intrinsic fluorescence. Pull-down assays showed whether mutants bound to anti-C2 antibodies. The nonclassical G99 antibody was used to assess proper protein folding, while the classical 3E6 antibodies determined whether the mutation in the classical epitope affected antibody binding. Intrinsic fluorescence evaluated tertiary structure stability, by measuring protein unfolding upon chemical denaturation.

(2) Membrane Binding Analysis—Analysis of platelet membrane binding employed (1) X-ray crystallography and (2) ELISAs. X-ray crystallographic analysis of the structure of wild type porcine C2 bound to the headgroup of phosphatidylserine, OPLS, allowed for elucidation of the structural interactions between fVIII pC2 and phosphatidylserine. This method first required the production of a high-quality protein crystal. Soaking the crystal in a solution of a small molecule allows for the molecule to diffuse into the crystal lattices if the interactions are favorable. The crystal is then exposed to X-rays, resulting in diffraction patterns based on the placements of atoms within the protein crystal. These diffraction patterns are then integrated and transformed using XYZ software to produce an electron density map. The locations of each atom within a protein can then be modeled into the electron density. As a result, an atomic resolution structural model of a protein is constructed. The main descriptors for evaluating the agreement between the protein model and the X-ray diffraction data are the R values. These R values measure how well the

crystallographic model predicts the experimental electron density map. The lower the R values, the better the fit between the model and the density map. R_{free} specifically describes the fit following removal of 10% of the reflections data to verify unbiased fitting (Brunger 1992). Therefore, R_{free} should always be larger in value than R_{work}. In cases when R_{free} is lower than R_{work}, the model had been biasedly over-fitted into the density map. An R value of approximately 0.6 or higher indicates random fitting of a model, while R values below 0.2 infer high quality fitting (Brunger 1992). Next, the analysis of membrane binding in the Arg2320Ser, Arg2320Thr, and Arg2215Ala hC2 mutants were determined using ELISAs. This is a colorimetric method that detects the amount of proteins bound to lipid-coated plates as a function of increasing protein concentration.

The main goal of this study was to elucidate the binding mechanism of fVIII to the phosphatidylserine-containing activated platelet membranes. Comprehension of the binding mechanism of fVIII allows for us to contribute to the advancement of hemophilia A therapeutics. With this information, we can help to improve recombinant fVIII replacement therapies by identifying potentially beneficial mutations that will cause an increase in coagulant activity.

Materials and Methods

Human C2 Cloning and Expression

The gene for wild type human fVIII C2 domain (residues 2171-2332) in a pET15b plasmid was prepared previously (Spiegel et al. 2004). Subsequently, former group members cloned this gene into a pSV plasmid. The human C2 (hC2) gene was excised from plasmid pSV in a 30 µl double digestion reaction containing 1 µg of hC2 pSV, 1x Cutsmart Buffer, 10 U BamHI, and 10 U XhoI. The restriction enzymes were purchased from New England Biolabs Inc. Vector pET32a(+) purchased from GenScript was also double digested using the same protocol. These reactions were incubated for four hours at 37°C. A 2% (w/v) agarose gel was used to verify cleavage. The cleaved pET32a (+) plasmid and hC2 gene were extracted from the gel using the Qiagen QIAquick Gel Extraction Kit. Cleaved hC2 and pET32a(+) was ligated with a 3:1 ratio of insert to vector using T4 DNA ligase and 1x T4 DNA ligase buffer. This reaction was incubated at 24°C for 10 minutes and ligase was heat-inactivated at 65°C for 10 minutes. The pET32a(+) vector allows for the expression with an N-terminal thioredoxin/$(His)_6$/S tag, and an enterokinase cleavage site (**Figure 17**). The sequence of the ligated vector was then verified by the Nevada Genomics Lab and transformed into New England Biolabs SHuffle B-line cells. Colonies were selected from Luria Bertani (LB) broth, ampicillin 50 µg/ml (amp^{50}) selection plates. One single colony was chosen and grown in 10 mL of LB amp^{50} media for 16 hours at 30°C to produce a seed stock for large-scale protein expression.

pET-32a(+) sequence landmarks	
T7 promoter	764-780
T7 transcription start	763
Trx•Tag coding sequence	366-692
His•Tag coding sequence	327-344
S•Tag coding sequence	249-293
Multiple cloning sites	
(*Nco* I - *Xho* I)	158-217
His•Tag coding sequence	140-157
T7 terminator	26-72
lacI coding sequence	1171-2250
pBR322 origin	3684
bla coding sequence	4445-5302
f1 origin	5434-5889

The maps for pET-32b(+) and pET-32c(+) are the same as pET-32a(+) (shown) with the following exceptions: pET-32b(+) is a 5899bp plasmid; subtract 1bp from each site beyond *Bam*H I at 198. pET-32c(+) is a 5901bp plasmid; add 1bp to each site beyond *Bam*H I at 198 except for *Eco*R V, which cuts at 209.

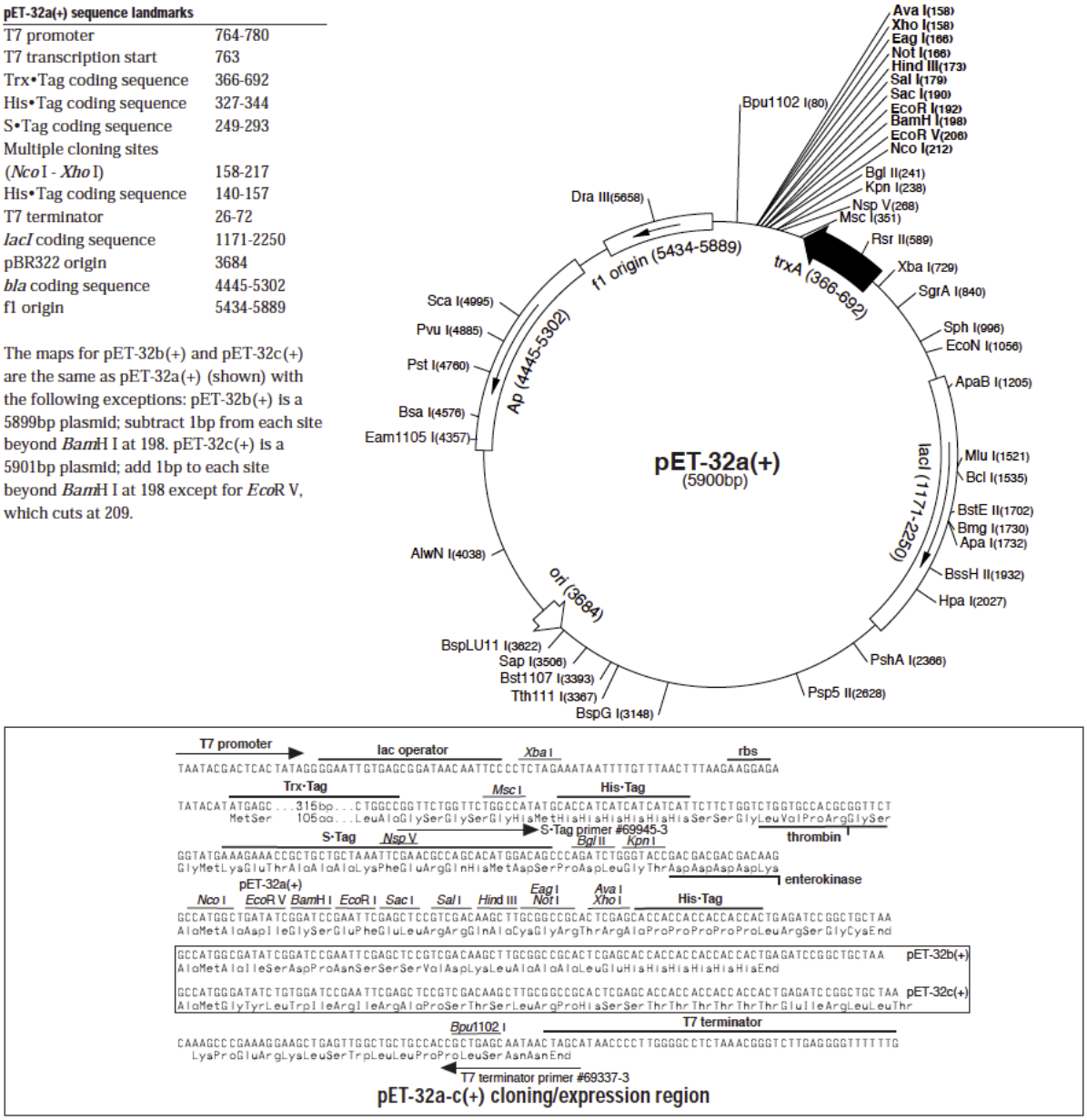

Figure 17. pET32a (+) vector construct (LaVallie et al. 1993; Novagen). The human fVIII C2 domain gene was inserted between XhoI and BamHI. Expression of C2 included thioredoxin/6 His/S tags. Enterokinase cleavage separates the thioredoxin/6 His/S tags from C2.

Site Directed Mutagenesis of Human C2 and C1 Domain Genes

Human C2 (R2320S, R2320T, and R2215A) and C1 (R2159H and R2163H) domains were constructed using the Agilent Technologies QuikChange Lightning Site-Directed Mutagenesis Kit with pET32a(+)/6His-thioredoxin-S-fVIII C2 and C1 plasmid templates, respectively. Primers for the mutations were designed based on recommendations from the Agilent Technologies website and were purchased from Integrated DNA Technologies.

Mutagenesis of wild type genes of human C2 and C1 isolated domains was performed using a QuikChange Lightning Site-Directed Mutagenesis Kit from Agilent Technologies. The temperatures for denaturation, annealing, and extension were 95°C, 60°C, and 68°C, respectively, with 18 total cycles.

DNA Extraction

To extract the plasmids containing the hC2 mutants from the XL10-Ultracompetent cells, the QIAquick PCR purification kit purchased from Qiagen was used. The overnight cells suspended in 950 µl of LB-Amp[50] were pelleted at 4969 x *g* and resuspended in 500 µl of P1 buffer. P2 and N3 buffers were added at 500 µl and 700 µl, respectively, and mixed by inversion. The solutions were centrifuged for 10 minutes at 17,000 x *g* and the supernatant was transferred to a spin column that contained resin that bound DNA. The column was washed with 500 µl of PB and 750 µl of PE buffer. The plasmids were eluted with 50 µl of nanopure water.

DNA Sequencing

Sequencing at Nevada Genomics allowed for verification of the DNA mutations. Each DNA mutation had two samples prepared with either T7 promoters or T7 terminators due to the average reliable sequencing results extending to approximately 500 to 600 base pairs. From the T7 promoter, the thioredoxin/His/S tags alone contained 560 base pairs prior to our gene inserts. T7 terminators were closer to our insert and used to verify our mutations more reliably. Samples were prepared with 880 to 3500 ng of DNA and 10 picomoles of primer.

Transformation of Competent SHuffle® T7 B Cells with Mutated Plasmids

Subsequently, chemically competent SHuffle® T7 B *E. coli* cells purchased from New England Biolabs Inc. were transformed with pET32a(+) plasmids encoding each hC2 and hC1 mutant. Approximately 100 ng of DNA were incubated with the competent cells for 30 minutes on ice. They were then heat shocked at 42°C for 30 seconds, with a 5-minute recovery time on ice. Room temp LB medium was added up to 1 mL in the mixture and shaken at 200 rpm at 30°C for 60 minutes. The cells were spread onto LB/ampicillin^{50} plates. A single colony was chosen to prepare a seed stock for subsequent overexpression of the mutant proteins.

Overexpression and Purification of hC2 and hC1 Mutants

Overexpression of each hC2 and hC1 mutant was carried out in 1 L of LB-amp^{50} broth with 10 g dextrose incubated at 30°C. Cells were inoculated with saturated 10 mL

overnights and induced with 0.4 μM isopropyl-β-D-thiogalactopyranoside (IPTG) when OD_{600} readings reached 0.5-0.6 AU. The temperature was adjusted to 16°C following induction. After approximately 20 hours of expression at 16°C, the cells were harvested at 6000 rpm in an F12-6x500 LEX rotor from Thermo Scientific for 10 minutes. The cells were resuspended in lysis buffer (300 mM NaCl, 20 mM Tris-HCl pH 7.5, 10 mM imidazole pH 8.0, 10.0% (v/v) glycerol, and 0.5% (v/v) Triton X-100) and lysed by sonication using a Branson Sonifier 450 probe at power output five and duty cycle 50% for 90s. To remove cell debris, the lysed cells were centrifuged at 17,500 rpm in an F20-12x50 LEX Thermo Scientific rotor for 35 minutes at 4°C. The high-speed supernatant was filtered through a 5 μm, then a 0.45 μm filter before purifying with 1 mL of settled TALON® cobalt immobilized metal affinity chromatography resin per 2 L of *E. coli* cell growth. Wash steps included 30 column volumes (CV) of lysis buffer and 30 CV of wash II buffer (150 mM NaCl, 20 mM Tris-HCl pH 7.5, 10 mM imididazole pH 8.0, and 10% (v/v) glycerol). The protein was eluted with elution buffer (150 mM NaCl, 20 mM Tris-HCl pH 8.0, 150 mM imidazole pH 8.0, and 10% (v/v) glycerol) following a 10-minute incubation time and dialyzed with 500 mL of storage buffer (150 mM NaCl, 25 mM Tris-HCl pH 8.0, and 10% (v/v) glycerol) for every 15-20 mL of eluted protein sample. The resin was cleaned with recharge buffer (3 mM NaCl and 20 mM MES pH 5.0) and stored in 20% (v/v) ethanol.

Recombinant Enterokinase Cleavage

The hC2 mutants were cleaved with recombinant enterokinase to remove the thioredoxin/His_6/S tag. Four units of enterokinase were used to cleave every 1 mg of hC2 protein. For every 1 unit of enterokinase, 25 µl of rEKapture agarose resin were used to remove the enzyme. Removing the tags from the cleaved protein required 500 µl of TALON resin. Both resins allowed for hC2 to be collected in the initial flow through due to its inability to bind either resin.

HiTrap Capto S Column Purification

When necessary, impure protein samples were purified on a 5 mL HiTrap Capto S strong cation exchanger column (GE Healthcare Life Sciences) connected to a fast protein liquid chromatography (FPLC) device, AKTAprime Plus manufactured by GE Healthcare Life Sciences. The column was equilibrated in buffer A (50 mM MES pH 6.5). Protein samples were diluted 1:10 into buffer A to prevent premature elution and precipitation. The diluted samples were loaded onto the column with a 10 mL Superloop. Buffer B (50 mM MES pH 6.5 with 1 M NaCl) was used to elute the protein with a gradient setting of 50% Buffer B in 20 CV. Elution of the proteins typically occurred at approximately 18% (180 mM NaCl) buffer B. The column was cleaned with 5 CV 1 M NaCl and 5 CV of 1 M NaOH after each injection and stored in 200 mM sodium acetate in 20% (v/v) ethanol.

Mass Spectrometry

Protein samples were prepared by diluting the proteins to 10 μM with nanopure water. Either 1 or 3 μl of sample was injected into the Thermoscientific Ultimate 3000 UHPLC connected to a C18 column (Kinetex 2.6 μm 100 Å) in-line with an Expression LCMS mass spectrometer (Advion).

Affinity Pull-Down Assays

Thioredoxin fusion hC2 mutants were incubated in 50 μl of TALON resin for 15 minutes and washed four times with five CV of storage buffer (150 mM NaCl, 25 mM Tris-HCl pH 8.0, and 10% (v/v) glycerol). Antibodies were similarly incubated for 15 minutes and washed five times with five CV of storage buffer. The mass ratio of hC2 to antibody was 2:3 (50 μg of hC2 and 75 μg of antibody). The complex was eluted from the resin after a 5-minute incubation time with 2 CV of elution buffer (150 mM NaCl, 20 mM Tris-HCl pH 8.0, 150 mM imidazole pH 8.0, and 10% (v/v) glycerol). The elution step was repeated to ensure complete elution of the protein. Each elution fraction was analyzed with SDS-PAGE.

Enzyme-Linked Immunosorbent Assays (ELISAs)

Nunc-Immuno MicroWell PolySorp 96 well solid plates were coated with 80% 1,2-dioleoyl-sn-glycero-3-phosphocholine (DOPC), 5% 1,2-dioleoyl-sn-glycero-3-phosphoethanolamine (DOPE), and 15% 1,2-dioleoyl-sn-glycero-3-phospho-L-serine sodium salt (DOPS) at 10 μg/ml. These lipids were purchased from Avanti Polar Lipids

Inc. (Alabaster, AL) as a 10 mg/ml stock dissolved in chloroform and were diluted to 10 μg/ml with methanol before plate coating. Negative control wells were coated with 100% DOPC at 10 μg/ml. The wells were then blocked with a 1% (w/v) bovine serum albumin (BSA)/50 mM Tris-HCl pH 7.5/0 mM, 20 mM, 85 mM, or 150 mM NaCl solution with a 45 minute incubation time at 37°C and shaking at 75 rpm. Protein samples were prepared with serial dilutions of 1:2 in 1% (w/v) BSA/50 mM Tris-HCl pH 7.5/0 mM, 20 mM, 85 mM, or 150 mM NaCl solution with initial protein concentrations of either 2000 nM, or 4000 nM for 12 samples total. These samples were incubated for 90 minutes. Subsequently, Ni-NTA•HRP diluted to 1:1500 (in 1% (w/v) BSA/50 mM Tris-HCl pH 7.5/0 mM, 20 mM, 85 mM, or 150 mM NaCl solution) was incubated for 30 minutes. Lastly, 2,2'-Azino-bis(3-ethylbenzthiazoline-6-sulfonic acid) (ABTS) was the colorimetric reagent was used to detect binding at 405 nm after incubation times of 30 minutes, 45 minutes, 1 hour, 1.5 hours, and 2 hours. All incubation steps were at 37°C and shaken at 75 rpm. Between each incubation, the wells were washed with a 1% (w/v) BSA/ 50 mM Tris-HCl pH 7.5 solution.

Intrinsic Fluorescence

Chemical denaturation of mutants using a gradient of guanidine-HCl was monitored by intrinsic fluorescence. A 2 mL native sample was prepared with a protein concentration of 0.1 mg/ml and diluted with a buffer composed of 150 mM NaCl, 25 mM Tris-HCl pH 8.0, and 5% (v/v) glycerol. Additionally, a denatured sample was prepared with the same protein concentration and with the same buffer conditions, but with 6 M guanidine-HCl.

The native protein sample was titrated with the denatured sample by removing either 100 or 125 µl from the native sample and adding back the same amount removed with the prepared denatured sample for a total of either 23 (for 100 µl titrations) or 19 (for 125 µl titrations) samples. Each sample was excited at 280 nm and emission spectra were collected between 300-400 nm with a 1 nm step size and an integration time of 1 second. The slit widths for both excitation and emission were 0.69 mm in a Photon Technology International Fluorometer (Horiba Scientific).

X-Ray Crystallography

A porcine fVIII C2 domain crystal was prepared by a former group member, Caileen Brison, using the hanging drop vapor diffusion method with a 2:1 ratio of crystallization buffer (0.1 M CHES (pH 10.4), 0.1 M magnesium acetate, and 10% (v/v) ethanol) and 2 mg/mL porcine C2 domain. This porcine C2 domain crystal was soaked with a 5 mM solution of the headgroup of phosphatidylserine, OPLS. Diffraction data were collected at beamline 5.0.1 at the Advanced Light Source (Lawrence Berkeley National Labs, Berkeley, CA). These diffraction data were indexed, merged and scaled with HKL2000 (Otwinowski and Minor; HLK Research, Inc. Charlottesville, VA), and the phases were determined by molecular replacement using Phaser within the Phenix software package. The previously published structure of porcine C2 (PDB ID 4MO3; Brison et al. 2015) was used for Phaser molecular replacement. Initial refinement with Phenix.refine included settings: 3 cycles, rigid body, occupancies, and individual B-factors. The program, Coot (Crystallographic Object-Oriented Toolkit), provided a means to manually change the locations of the atoms

to fit the electron density map. After each set of manual refinements within Coot, an automatic refinement of the model was performed using Phenix.refine (Afonine et al. 2012) with the refinement parameter settings: 10 to 30 cycles, XYZ coordinates, real-space, TLS parameters, simulated annealing (torsion angles), occupancies, and individual B-factors. These settings were chosen based on several 3-cycle refinements with various combinations of settings. The TLS parameters setting is especially important in that it is a relatively new parameter that improves refinement (Zucker et al. 2010). For this structure, this parameter reduced R_{work} by 7.6%. The combination of parameter settings that provided the lowest R_{free} and R_{work} numbers were the parameters used for further refinements. Individual water molecules were added with the Phenix.refine program during the last few sets of refinements by including the 'update waters' setting. These waters were manually modeled in Coot and again, automatically refined in Phenix.refine. OPLS was manually added in Coot where there was positive density that was unaccounted for, then automatically refined in Phenix.refine. Secondary structure was predicted using the secondary structure assessment program STRIDE (Frishman and Argos 1995) and assigned manually in PyMol.

Results

Mutant hC2 Expression and Purification

Production and isolation of hC2 mutants with immobilized metal affinity chromatography (IMAC) TALON® cobalt resin were successful, albeit in low yields with low purity (**Table 1, Figure 18A**). Additional purification steps employing HiTrap Capto S cation strong exchanger columns improved the purity of the thioredoxin fusion and the enterokinase-cleaved proteins (**Figures 18B/C/D/E**).

Table 1. Approximate average protein yields per 6 L E. coli growths and percent recovery yields following recombinant enterokinase cleavages.

Protein	Average Yields for 6 L of Overexpression (Post IMAC)	% Recovery of Protein Following Enterokinase Cleavage
Wild Type hC2	~30 mg, ~90% pure	~13%
hC2 R2320S	~5 mg, ~60% pure	~20%
hC2 R2320T	~ 5 mg, ~50% pure	~20%

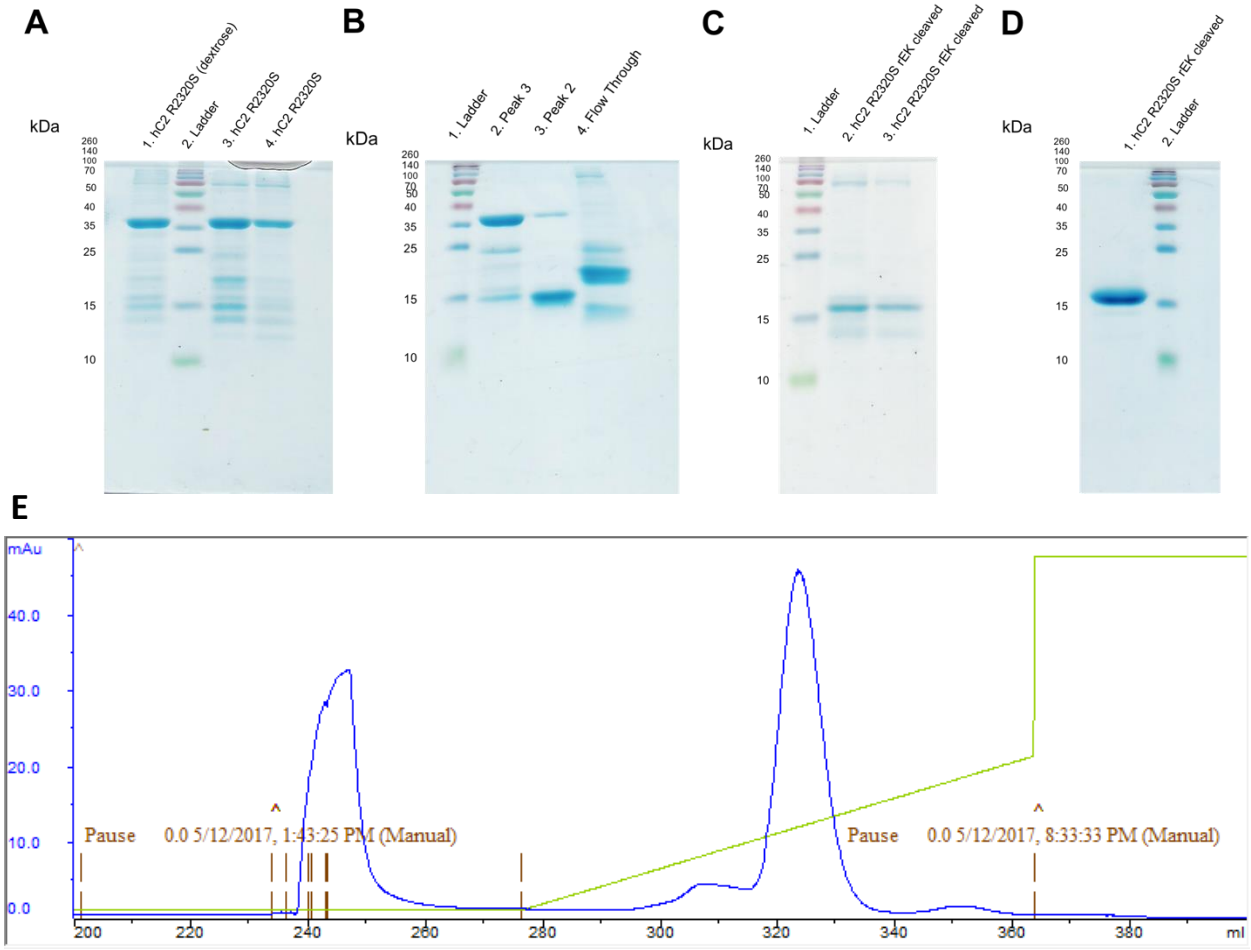

Figure 18. Purification and Analysis. SDS-PAGE results for hC2 Arg2320Ser following purification and cleavage with recombinant enterokinase. (A) Arg2320Ser hC2 thioredoxin fusion samples with a molecular weight of 35.8 kDa following immobilized metal affinity chromatography with TALON resin IMAC were visualized on SDS-PAGE. All lanes are of the post IMAC samples, but lane 1 was purified protein expressed with an addition of 10 g of dextrose. (B) Samples combined from lanes 3 and 4 of gel A were purified with a HiTrap Capto S column. Lane 2 shows the eluted peak number 3 that contained the purified Arg2320Ser hC2 thioredoxin fusion protein. Lanes 3 and 4 shows eluted peak 2 and the flow through, respectively, contained the contaminants in the post IMAC sample. (C) The hC2Arg2320Ser thioredoxin fusion protein was cleaved with recombinant enterokinase and had a molecular weight of 18.7 kDa following cleavage (lanes 2 and 3). (D) The two cleaved samples from gel C were combined and further purified using a HiTrap Capto S column. (E) The UV chromatogram (blue) profile of the Capto S column purification of recombinant enterokinase cleaved Arg2320Ser mutant shows the flow through peak (peak 1), removing unwanted contaminants and the elution peak (peak 2) containing the cleaved Arg2320Ser mutant. The elution gradient is indicated by the green graph. Peak 2 corresponds to lane 1 in D.

Mass Spectrometry

Mass spectrometry results indicated correct protein expression and cleavage at the correct site. DNA sequencing results also verified correct hC2 mutant sequences (**Appendix Figure 1**). The mass of cleaved wild type hC2 was 18.796 kDa. Masses of mutants hC2 Arg2320Ser and Arg2320Thr cleaved were 67 Da and 57 Da and below that of wild type, respectively (**Table 2**). This was expected since serine and threonine are 69 Da and 55 Da lower in mass, respectively, than arginine. Similarly, wild type thioredoxin (trx) fusion hC2 protein had a mass determined to 35.724 kDa, while hC2 Arg2320Thr-trx fusion had mass that was 56 Da lower. The purity of the hC2 Arg2320Ser-trx fusion sample for mass spectrometry was low compared to that of WT and Arg2320Thr, likely contributing to the discrepancy in mass. The mass spectrometry data are reported in the appendices.

Table 2. Mass spectrometry verification of correct protein expression and cleavage at the correct site. See appendix for the mass spectrometry spectra.

Protein	Expected Mass	Actual Mass	Difference
hC2 WT-trx fusion	35,859 Da	35,724 Da	135 Da
hC2 Arg2320Ser-trx fusion	35,790 Da	35,733 Da	57 Da
hC2 Arg2320Thr-trx fusion	35,804 Da	35,668 Da	136 Da
hC2 WT rEK cleaved	18,801 Da	18,798 Da	3 Da
hC2 Arg2320Ser rEK cleaved	18,731 Da	18,731 Da	0 Da
hC2 Arg2320Thr rEK cleaved	18,745 Da	18,741 Da	4 Da

Affinity Pull-Down Assays

To evaluate proper folding of the mutant proteins, pull-down assays were utilized. The antibodies were immobilized on TALON resin before incubation of the hC2 mutants. Binding of the mutant hC2 proteins to the antibodies was assessed by the presence of both the antibody and hC2 mutant in the elution lanes. The pull-down assays showed both G99 F_{AB} and hC2 mutants in the elution lanes, indicating that all the mutants bound the nonclassical G99 F_{AB} (**Figure 19A/C/E**). This suggests proper folding of the mutants. However, the hC2 Arg2320Ser mutant was unable to bind 3E6 F_{AB}, indicated by the lack of a 3E6 F_{AB} band in the elution lanes (**Figure 19B**). This implies that the serine residue caused a significant unfavorable electrostatic change for the binding of 3E6. Classical 3E6 was able to bind both hC2 Arg2215Ala and hC2 Arg2320Thr mutants (**Figure 19D/F**). Though, the 3E6 F_{AB} bands in the elution lanes appear to be less intense compared to the hC2 bands. These mutations likely attenuated the electrostatic interactions between the hC2 classical epitope in the mutants and 3E6 F_{AB} due to removal of the positive charge provided by arginine. Lastly, the Arg2320Ser mutant was not able to not bind 3E6 F_{AB} while the other mutants were able to likely because it caused the most significant electrostatic change.

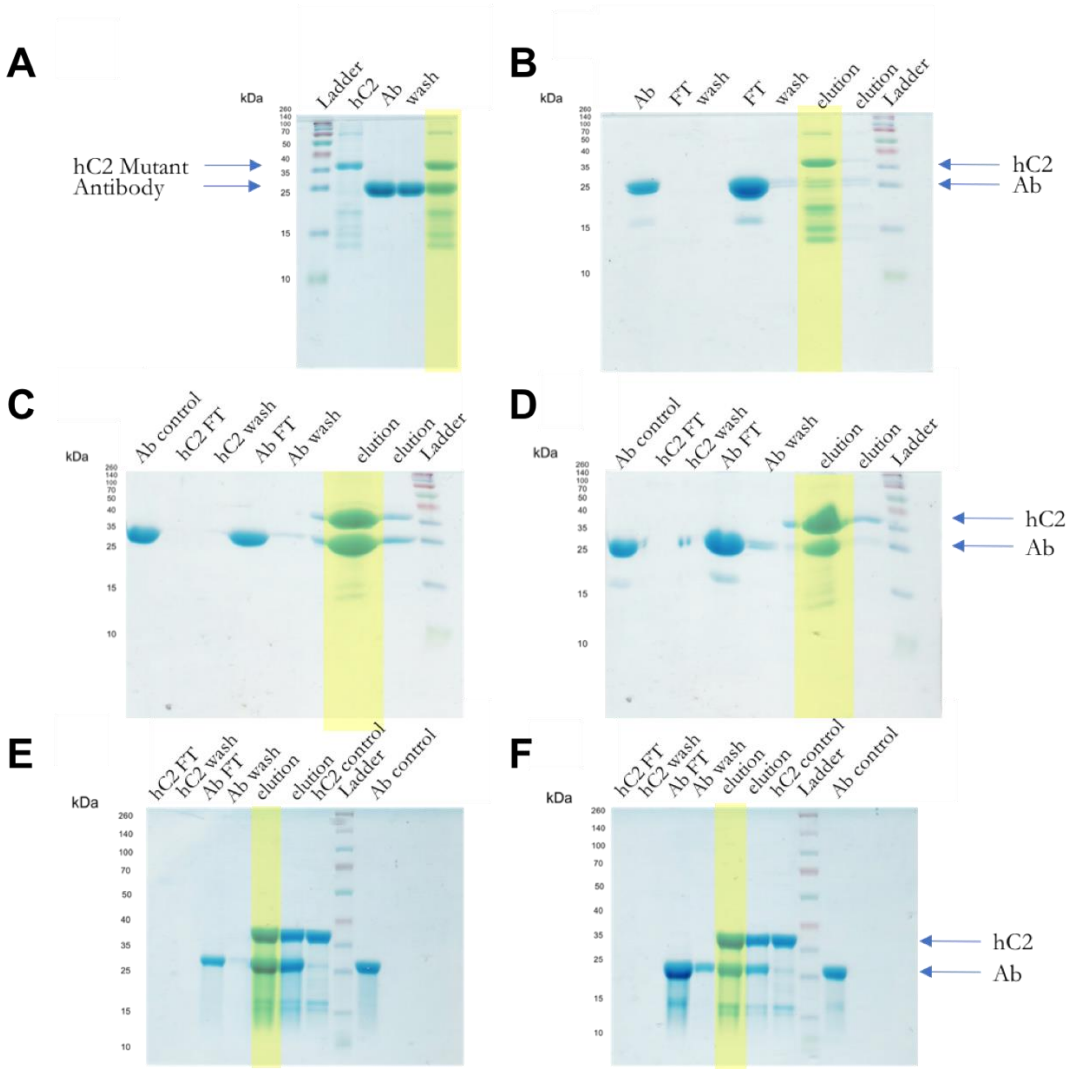

Figure 19. Affinity pulldown assay results of hC2 mutants with either G99 F_{AB} or 3E6 F_{AB}. The hC2 mutants were immobilized on TALON resin and washed several times with storage buffer to rinse non-bound hC2. Antibodies were then flowed through the column and was also washed several times with storage buffer. Flow through (FT) and the last wash steps were visualized on SDS-PAGE to verify non-bound proteins were washed out of the column. Elution steps 1 and 2 (first and second 10 mL of elution, respectively) were visualized to determine antibody binding of the hC2 mutants. Presence of both antibody and hC2 mutant bands in the elution lanes (highlighted) indicated antibody binding and proper folding of hC2 mutants. The molecular weights of the mutants were approximately 35.8 kDa and the molecular weights of the antibodies were approximately 25 kDa. (A) Pulldown assay of hC2 R2320S with G99 F_{AB} indicated antibody binding and proper folding. (B) Pulldown assay of hC2 R2320S with 3E6 F_{AB} indicated no antibody binding. (C) Pulldown assay of hC2 R2215A with G99 F_{AB} indicated antibody binding and proper folding. (D) Pulldown assay of hC2 R2215A with 3E6 F_{AB} indicated antibody binding and proper folding. (E) Pulldown assay of hC2 R2320T with G99 F_{AB} indicated antibody binding and proper folding. (F) Pulldown assay of hC2 R2320T with 3E6 F_{AB} indicated antibody binding and proper folding.

Intrinsic Fluorescence

Intrinsic fluorescence revealed the tertiary stability of the mutants relative to WT hC2 by monitoring the fluorescence emission of tryptophan residues following excitement at 280 nm during chemical denaturation. As buried tryptophan residues are exposed to solvent, water serves as an efficient quencher of tryptophan fluorescence. Gibbs free energy (ΔG_{H20}) of unfolding can be calculated from these denaturation curves (Walter et al. 2010). As predicted, the emission intensity at 335 nm decreased during the denaturation of WT hC2, indicative of protein unfolding (**Figure 20**; Munishkina and Fink 2007). In addition, an increase in fluorescence intensity was observed at around 355 nm due to the increase in solvent-accessible tryptophan (Munishkina and Fink 2007).

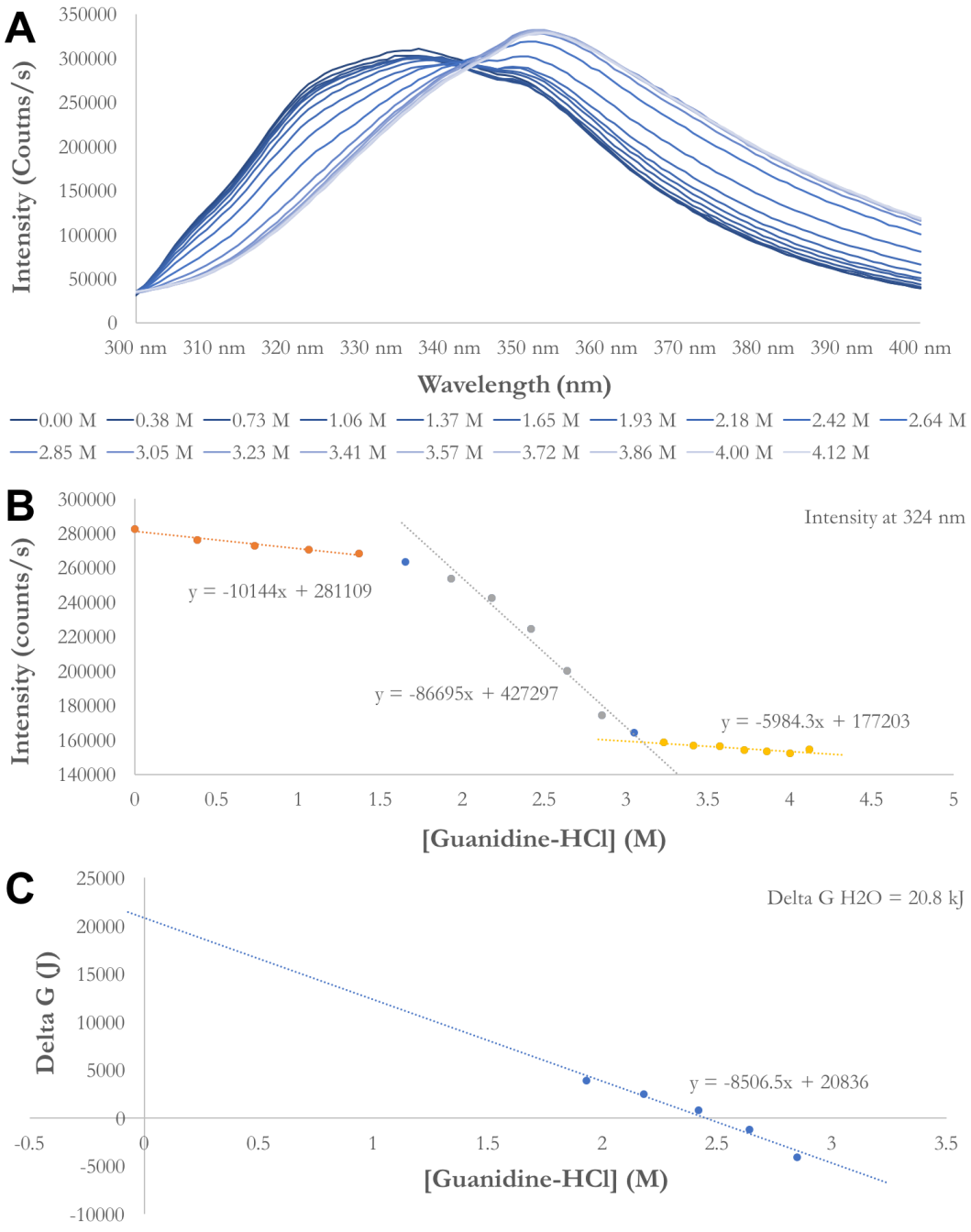

Figure 20. Intrinsic fluorescence of WT hC2. (A) Denaturation of WT hC2 with increased concentrations of guanidine-HCl showed a decrease in fluorescence around 335 nm indicative of fluorescence quenching from the exposure of buried tryptophan residues to solvent during unfolding. (B) Intensities at 324 nm were graphed with respect to increasing guanidine-HCl concentrations. (C) The most linear region of the denaturation curve was used to find the ΔG_{H2O} of unfolding.

Interestingly, the denaturation patterns of the hC2 Arg2320Ser mutant did not resemble that of WT hC2. From 0 to 1.36 M guanidine-HCl, the intensity trend was inconsistent, with decreasing intensity from 0 to 0.3 M and increasing in intensity from 0.30 to 1.36 M guanidine-HCl (**Figure 21**). This is possibly due to conformational changes that are quenching the fluorescence of a particular tryptophan residue. The thermodynamic calculations indicated that the Arg2320Ser mutant was slightly less stable than WT hC2, with ΔG_{H20} values of 18.5 kJ/mol and 20.8 kJ/mol, respectively. The 2.3 kJ/mol difference may not be significant and they may have similar tertiary stability.

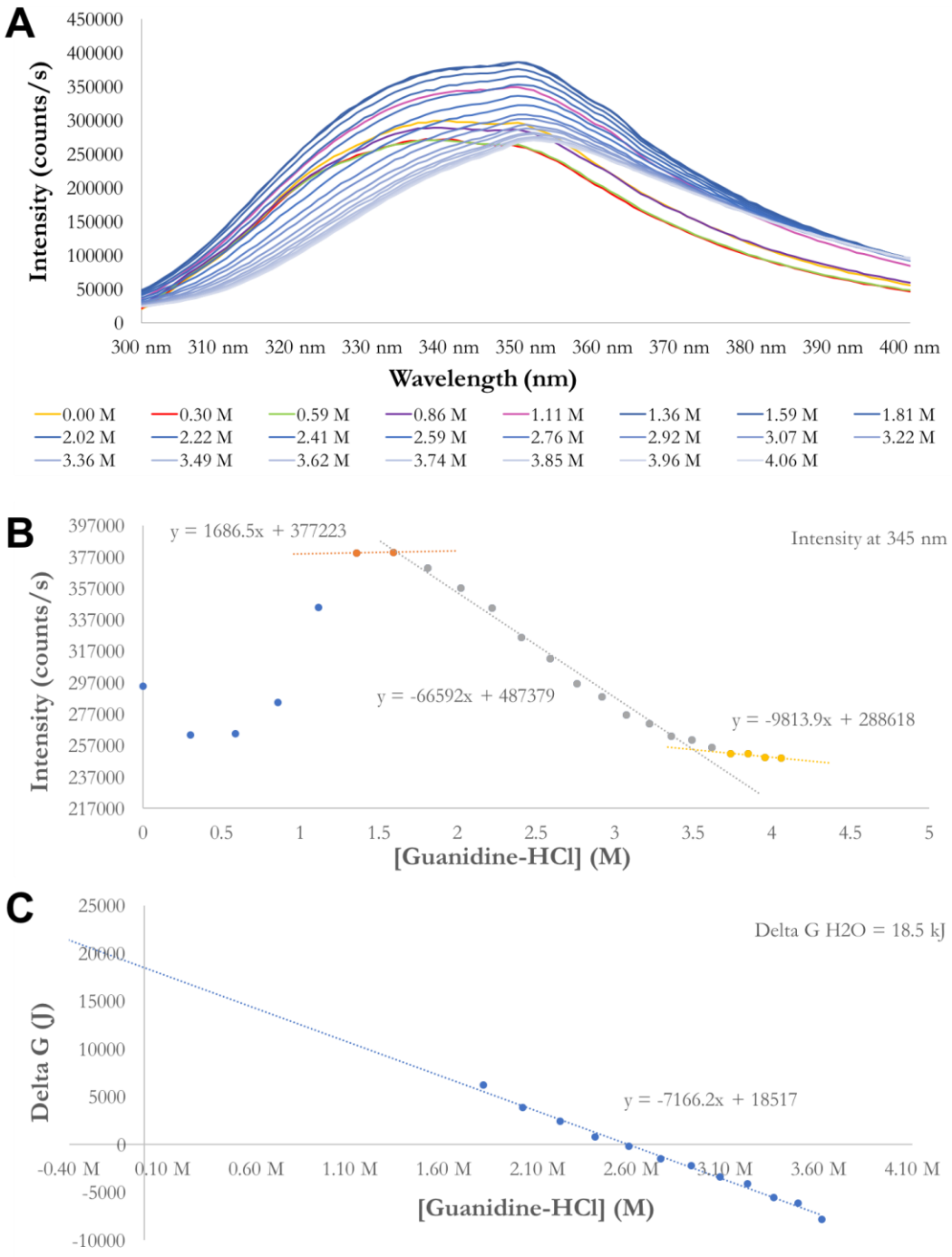

Figure 21. Intrinsic fluorescence of hC2 Arg232Ser mutant. (A) Denaturation of hC2Arg232Ser with increased concentrations of guanidine-HCl showed a general decrease in fluorescence indicative of fluorescence quenching from the exposure of buried tryptophan residues to solvent during unfolding. However, fluorescence of the mutant from 0 M to 1.11 M guanidine-HCl conditions showed erratic intensity curves. (B) Intensities at 345 nm were graphed with respect to increasing guanidine-HCl concentrations. (C) The most linear region of the denaturation curve was used to find the ΔG_{H2O} *of unfolding.*

Enzyme-Linked Immunosorbent Assays (ELISAs)

ELISAs were employed to assess PS phospholipid binding. A composition of the phospholipids, 25% phosphatidylserine (PS) and 75% phosphatidylcholine (PC), that mimicked the activated platelet membranes was initially immobilized to the walls of hydrophobic 96-well plates and incubated with wild type (WT) hC2 and our hC2 mutants Arg2320Thr, Arg2215Ala, and Arg2320Ser. Each assay was performed in triplicate. Every hC2 mutation studied had significantly attenuated phospholipid binding, presumably due to the loss of the positive charge of arginine. Dissociation constants (K_D) for hC2 WT and Arg2320Thr binding 25% PS/75% PC were 1600 nM and 9100 nM, respectively, in 0 mM NaCl conditions (**Figure 22A**). Human C2 Arg2215Ala and Arg2320Ser had binding affinities of 2400 nM (**Figure 22B**) and $4.8x10^{20}$ nM (**Figure 22C**), respectively which indicates these mutations inhibited binding compared to wild type. However, the large K_D for the Arg2320Ser mutant may have been inaccurately calculated due to the unsaturated PS-binding curve and can be interpreted as having no PS-binding characteristics.

Interestingly, NaCl inhibited WT hC2 binding to 25% PS/75% PC with K_D's of 1300 nM, 1300 nM, 4400 nM, and 5600 nM for 0 mM, 20 mM, 85 mM, and 150 mM concentrations of NaCl, respectively (**Figure 22D**). The dissociation constants between the 0 mM and 20 mM NaCl conditions were not significantly different. However, at 85 mM NaCl, the salt significantly inhibited C2 phospholipid binding. These results concur with the binding studies performed by Novakovic et al. in 2011, indicating that NaCl competes with the basic residues within the fVIII C2 domain for negatively charged PS binding.

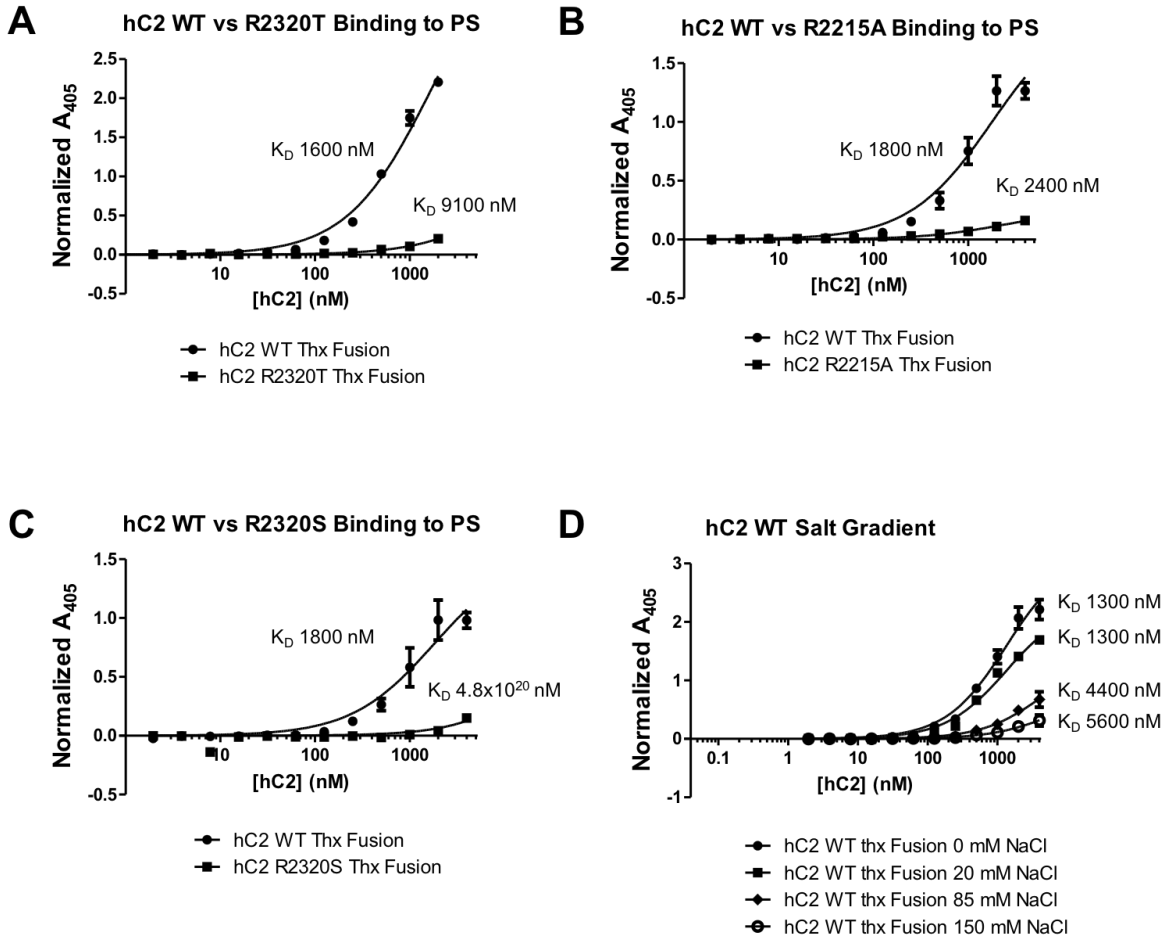

Figure 22. ELISA results of the hC2 mutants binding phospholipids compared to wild type hC2. The binding affinities of hC2 Arg2320Thr (A), Arg2215Ala (B), and Arg2320Ser (C) to phospholipids were lower than that of wild type hC2. (A) ELISA of Arg2320Thr vs WT hC2 binding to 25% phosphatidylserine (PS)/75% phosphatidylcholine (PC) in 0 mM NaCl conditions. (B) ELISA of Arg2215Ala vs WT hC2 binding to 25% PS/75% PC in 0 mM NaCl conditions. (C) ELISA of Arg2320Ser vs WT hC2 binding to 25% PS/75% PC in 0 mM NaCl conditions. (D) ELISA of WT hC2 binding to 25% PS/75% PC with varying amounts of NaCl. Increasing concentrations of NaCl inhibited hC2 binding.

Crystal Structure of Porcine C2 Interacting with O-Phospho-L-Serine

An X-ray crystal structure of pC2 soaked with the headgroup of phosphatidylserine, O-phospho-L-serine (OPLS), was determined to a resolution of 1.4 Å to identify which underlying basic residues behind the hydrophobic beta hairpin loops interact with the negatively charged headgroup of phosphatidylserine (**Table 3**). The three-dimensional model of pC2 was initially created by molecular replacement in Phenix.MR using a previously solved structure of pC2 (PDB ID: 4MO3; Brison et al. in 2015), which determines the phase of the X-ray diffraction data. Several iterations of manual modeling within the program, Coot, and automatic refinement in Phenix.refine resulted in a final pC2 crystal structure with model refinement statistics of R_{factor} (R_{work}) and R_{free} of 0.1522 and 0.1791, respectively. The R values of OPLS-soaked pC2 structure indicated that the model fits the diffraction data with high quality due to the values being below 0.2 (Brunger 1992). The R_{work} value was lower than that of R_{free}, which indicated non-biased model fitting into the X-ray diffraction data.

Table 3. X-Ray Data and Refinement Statistics of the pC2 OPLS structure.

X-Ray Data Statistics	Wavelength	1.00 Å
	Resolution Range	31.322 Å - 1.401 Å
	Space Group	Orthorhombic I 2 2 2
	Unit Cell	a = 48.99 Å b = 68.20 Å c = 105.78 Å α = 90° β = 90° γ = 90°
	Total Unique Reflections	35,055
	Redundancy	13.4 (12.2)
	Completeness	99.7 (99.9) %
	I/sigma(I)	45.1 (8.04)
	R_{pim}	0.019 (0.121)
Model Refinement Statistics	R_{factor} (R_{work})	0.1522
	R_{free}	0.1791
Number of atoms	Protein Atoms	1388
	Water Molecules	249
	Protein Residues	157
	Ligand	1 (OPLS)
	RMS Bond Length Restraints	0.007 Å
	RMS Angles Angle Restraints	1.283°
	Ramachandran Favored	95.1%
	Ramachandran Outliers	1.10%
	Rotamer Outliers	0.00%
	C-beta Outliers	0
	Clashscore	6.21
	Overall Score	1.68
Average B-factor	Protein	23.68 Å^2
	Solvent	35.94 Å^2
	Ligand	90.78 Å^2

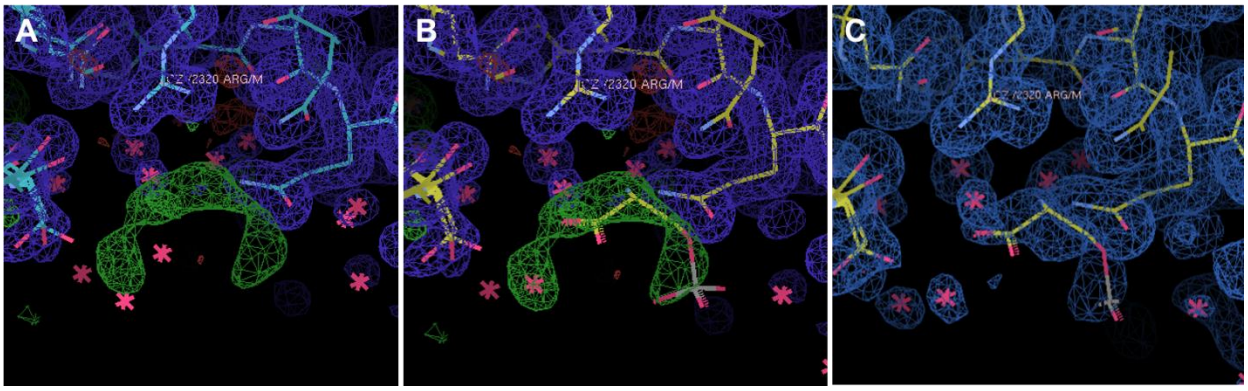

Figure 23. Manual molecular modeling and refinement of OPLS within the pC2/OPLS crystal structure using Coot. Blue density shows density that was accounted for during automatic refinement in Phenix. Red stars respresent individual water molecules. (A) Molecular modeling in the program, Coot, showed positive density (green) that was unaccounted for in the electron density map. (B) OPLS and a water molecule were manually added within the program to fit into this positive density. (C) Further refinement using the software, Phenix, showed an acceptable fit of OPLS.

The purpose of this crystal structure was to investigate which of the basic residues underlying the hydrophobic beta hairpin loops interact favorably with the negatively charged headgroup of phosphatidylserine. Modeling of OPLS placement was near Arg2320, because of the presence of a positive density within the electron density map (**Figure 23**). In this structure, we found that Arg2320 was the positive residue that directly interacted with the negatively charged OPLS, with a distance of 3.5 Å (**Figure 24**).

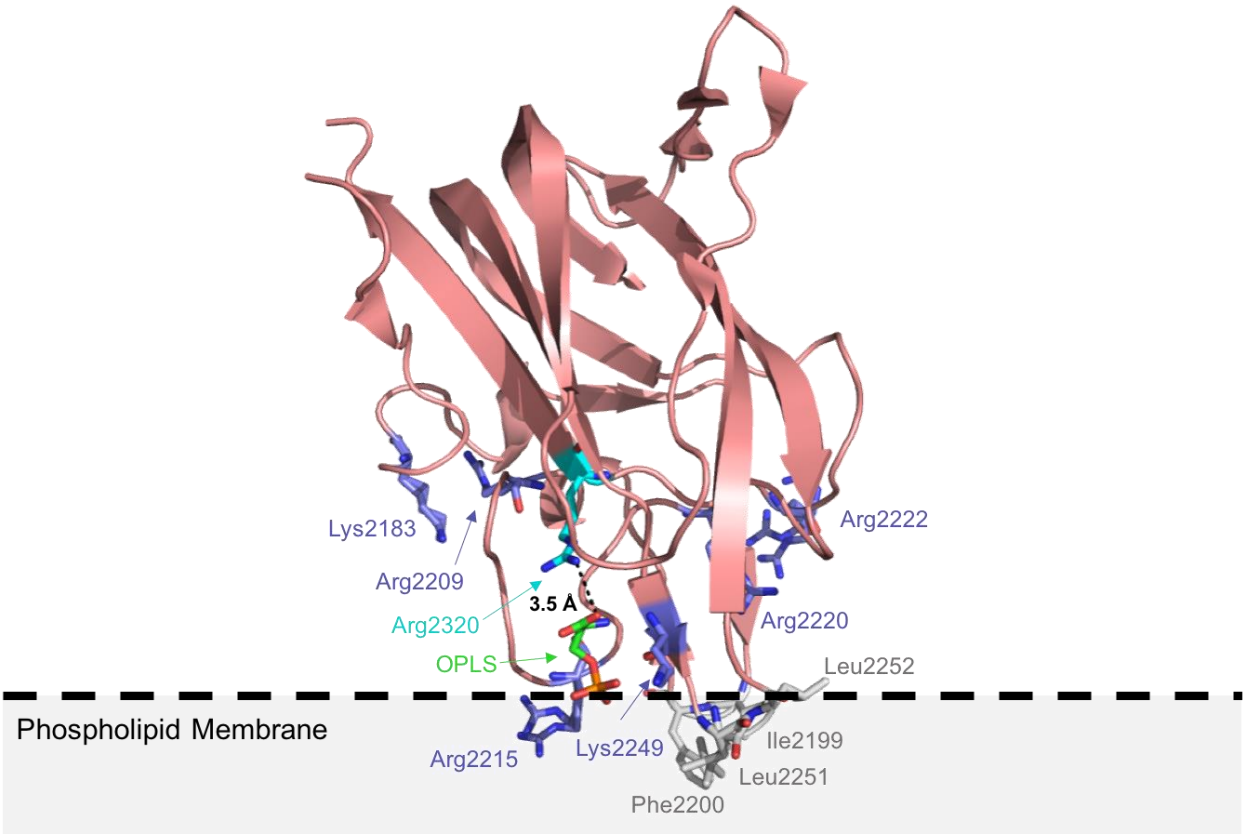

Figure 24. A 1.4 Å crystal structure of pC2 bound to O-phospho-L-serine (OPLS). In cyan is the Arg2320 residue that interacts with the OPLS (green), with a distance of 3.5 Å. The beta hairpin loops (gray) are embedded into the hydrophobic membrane (represented by the dashed line and gray-shaded area). A ring of basic residues (blue) possibly interact with negatively charged phospholipid headgroups during activated platelet membrane binding, but Arg2320 is likely the main contributor to phosphatidylserine membrane binding.

The placement of OPLS was in close proximity to the solvent-exposed hydrophobic beta-hairpin loops hypothesized to be embedded within lipid membranes during binding (Pratt, et al 1999; Gilbert et al. 2002). This provided structural evidence to support our 'new' classical epitope membrane binding model compared to the old model suggested in previous studies by other labs (Pratt, et al 1999; Stoilova-McPhie et al. 2002) because the old model appears to have OPLS floating well above the platelet membrane (**Figure 25**).

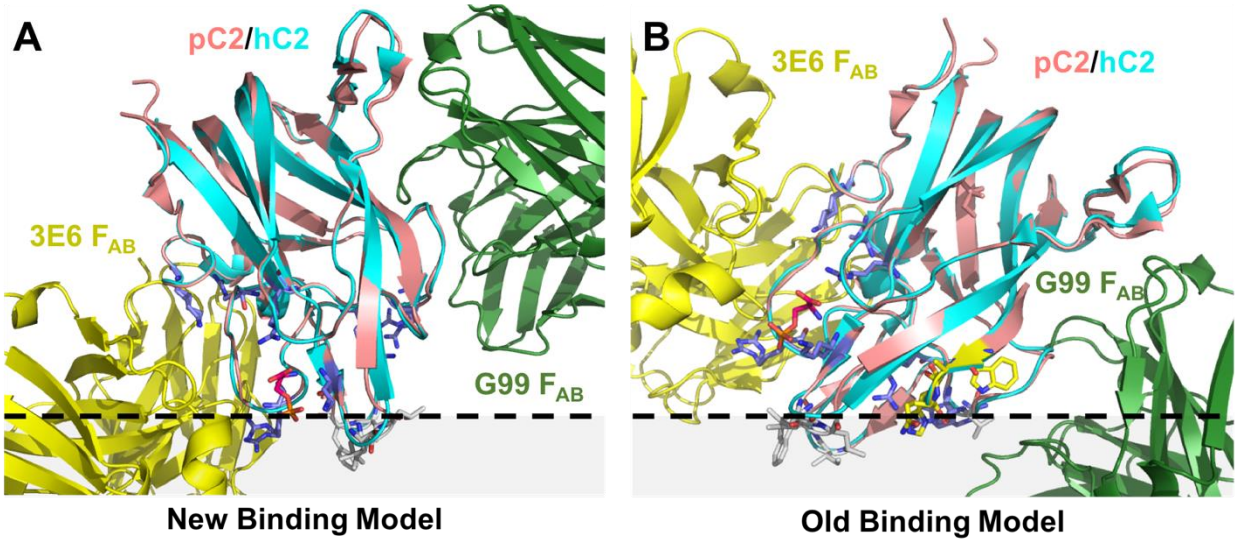

Figure 25. The ternary complex of fVIII/3E6 F_{AB}/G99 F_{AB} overlayed with the OPLS (red)/pC2 crystal structure to demonstrate the (A) new versus (B) old membrane binding models of C2 (PDB ID 4KI5; Walter et al. 2013).

In addition, it is possible that Arg2215 has favorable electrostatic interactions with the negatively charged phosphate group of OPLS, provided that this Arg2215-containing loop has high flexibility. A coulombic surface coloring showed the region of OPLS binding within pC2 is primarily positively charged (**Figure 26**). Our binding model revealed that Arg2209, Arg2215, Lys2183, Arg2220, Arg2222, Lys2249, and Arg2320 in pC2 are likely the basic underlying residues that form salt bridges with the exposed negatively charged phospholipids on the surface of activated platelet membranes, with Arg2320 being the main contributor to the direct interaction between OPLS and C2 (**Figure 24**).

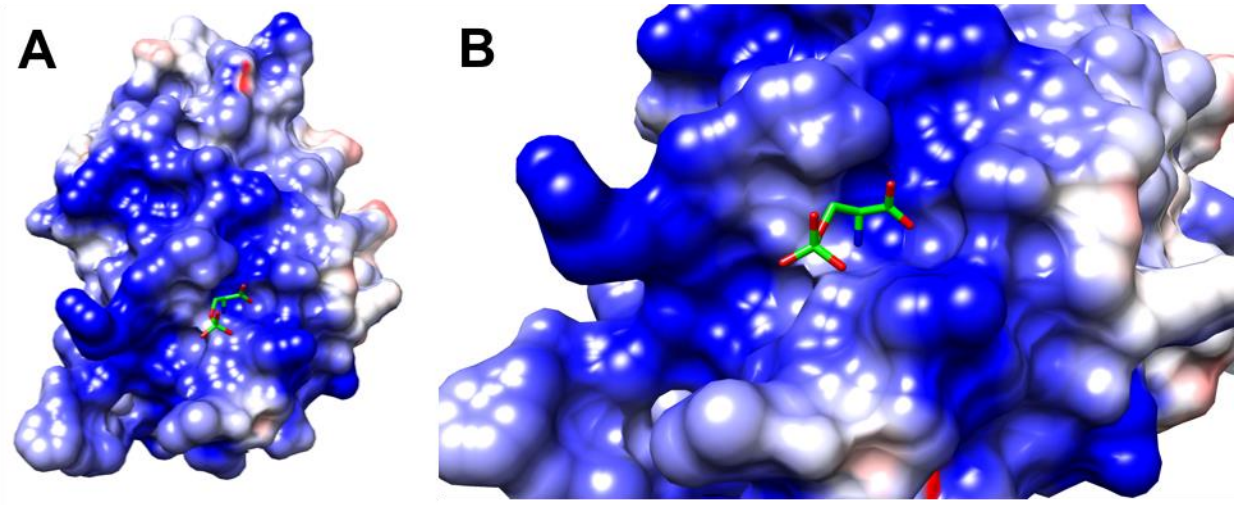

Figure 26. Coulombic surface coloring (generated in Chimera) of (A) pC2 domain of fVIII in complex with OPLS and (B) a zoomed-in image of the binding interface. The predominantly positively charged (blue) binding region of pC2 interacts favorably with the oppositely charged OPLS (green molecule).

Discussion

FVIII binds to PS-containing membranes primarily with its C2 domain. Within the C2 domain, the two hydrophobic beta hairpin loops penetrate the lipid layer of platelet membranes. This observation is supported by several different structural and functional studies from other labs (Pratt et al. 1999; Gilbert et al. 2002; Shen et al. 2008; Madsen et al. 2015). Several basic residues underlying the hydrophobic beta hairpin loops are hypothesized to form salt bridges with the negatively charged headgroups of PS on the surface of activated platelet membranes. However, the specific basic residues that form these interactions are currently not well defined.

Our research proposes a binding model that is distinct from the older binding model proposed by Pratt et al. 1999 and other labs (such as Stoilova-McPhie et al. 2002) at the non-classical epitope face. Previous studies performed in our lab have provided evidence of the new model at the classical epitope face of C2. Mainly, the C2-bound phosphatidylserine (PS) was able to bind the non-classical G99 mAb, but not the classical 3E6 mAb, revealing that PS blocks 3E6 mAb binding because they bind at the same C2 epitope (Brison et al. 2015). This indicates PS binds at the classical epitope face, and not the non-classical epitope face. This sparked our interest in elucidating the atomic-level details of C2 bound to OPLS for the purpose of providing structural evidence to identify which underlying basic residue directly interacts with the negatively charged phospholipid, PS.

Through this pC2-OPLS crystal structure, we found that the conserved Arg2320 residue is the main basic underlying residue that forms a salt bridge with PS, with a distance of 3.5 Å (**Figure 24**). This finding supports our new model in which the binding of phosphatidylserine-containing membranes occurs at the Arg2320-centered classical epitope face (**Figure 22**). In support of this Arg2320-OPLS interaction, molecular membrane binding simulations of the C2 domain completed by Madsen et al. in 2015 revealed that basic residues within C2 interact with the phosphate or carboxyl groups of PS lipids transiently and in a nonspecific manner, except for the two residues: Arg2220 and Arg2320. They found that these two residues can interact directly with the acidic headgroup of PS lipids. These two direct interactions, however, are mutually exclusive. For the orientation of C2 to form direct interactions between Arg2320 and PS, this direct interaction cannot occur for Arg2220. The differences between the old model centered on Arg2220 and the new C2 membrane binding model centered on Arg2320 exhibit this precise difference. Furthermore, they employed the same membrane binding simulation study on the C1 domain and discovered that Arg2163, the residue corresponding to the same location as Arg2320 within C2, was able to achieve a tight interaction with PS (Madsen et al. 2015). The equivalent residue of Arg2220 in C2 is Ser2063 in C1, indicating that the Arg2320 interaction may be more robust since it is conserved between both the C1 and C2 domains.

In support of the finding that Arg2320 is a central residue involved in PS membrane binding, the ELISA binding studies showed that the mutations at this residue, Arg2320Ser

and Arg2320Thr, inhibited phospholipid binding. This indicated the importance of the basic arginine at this residue location since the positive charge is lost with the serine and threonine mutations. In accordance with this, Arg2215Ala also caused a loss in C2 phospholipid binding activity. In the new binding model, Arg2215 appeared to be docked within the hydrophobic layer of the lipid membrane based on its proximity to the hydrophobic beta hairpin loops, which generated an interest in removing this positive charge to probe whether this increases C2 phospholipid binding activity. However, our data showed that Arg2215Ala attenuated binding to phospholipids. This result indicates that the basic Arg2215 residue also plays an important role in forming a salt bridge with phospholipid membranes. We now hypothesize that Arg2215 may form a favorable electrostatic interaction with the negatively charged phosphate group within OPLS, given that this Arg2215-containing loop is highly flexible.

From the pC2-OPLS crystal structure we also showed that there was no major conformation change upon OPLS binding. The difference in the pC2 and pC2-OPLS crystal structures were minimal, with an RMSD value of 0.810 Å, calculated in PyMol when outliers were not rejected (**Figure 27**). The main differences between the structures were in the highly dynamic regions of the beta hairpin loops, N-terminal, and C-terminal. Omission of these areas reduced the RMSD value to 0.532 Å (when calculated with residues 2173-2195, 2202-2249, and 2255-2329 and no outlier rejection).

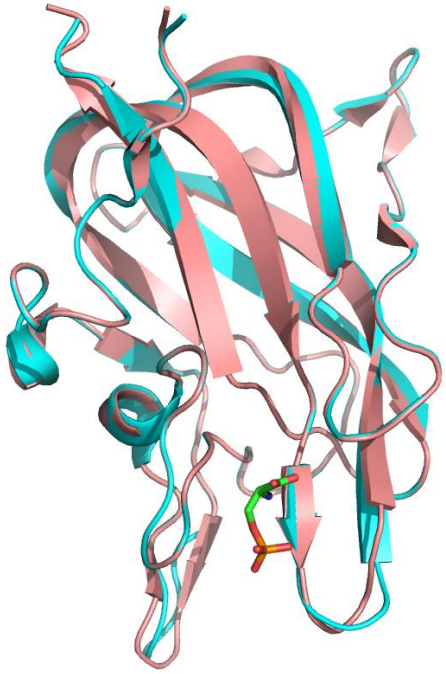

Figure 27. Superposition of the pC2/OPLS crystal structure (pink) and the previously solved pC2 structure (cyan) (PDB ID 4MO3; Brison et al. 2015), provided an RMSD of 0.810 Å. The RMSD value with the omission of the dynamic regions of the beta hairpin loops, N-terminal, and C-terminal is 0.532 Å.

A caveat to our studies is that the methods employed only probed membrane binding of the isolated C2 domain, and not of full-length fVIIIa. The C2 domain within full length fVIIIa is structurally near the C1 domain. The C1 domain has also been shown to contribute to binding membranes (Meems et al. 2009). It is possible that the C1 domain may play a role in orienting the C2 domain during membrane anchoring (Lu et al. 2011). If this is the case, the new model supports this idea more so than the old model. Superposition of the pC2-OPLS crystal structure to the human full length fVIII structure (Shen et al. 2008) show that the classical epitope face of C2 (which includes Arg2320 and OPLS) faces the C1 domain, whereas the non-classical epitope face does not (**Figure 28**). The yellow residues in the back of the image within the C2 domain are the residues

involved in the old membrane binding model, which shows that the old binding model would cause C2 to tilt away from the C1 domain during membrane binding, instead of towards it in the new binding model. Future binding studies should include ELISAs performed with a C1-C2 construct. Studies should also include ELISAs with C2 mutants that have mutations in the basic residues involved in the old membrane model such as Lys2227 and Arg2220 to probe whether they attenuate C2 binding and thus, determine the importance of these residues for C2 membrane binding.

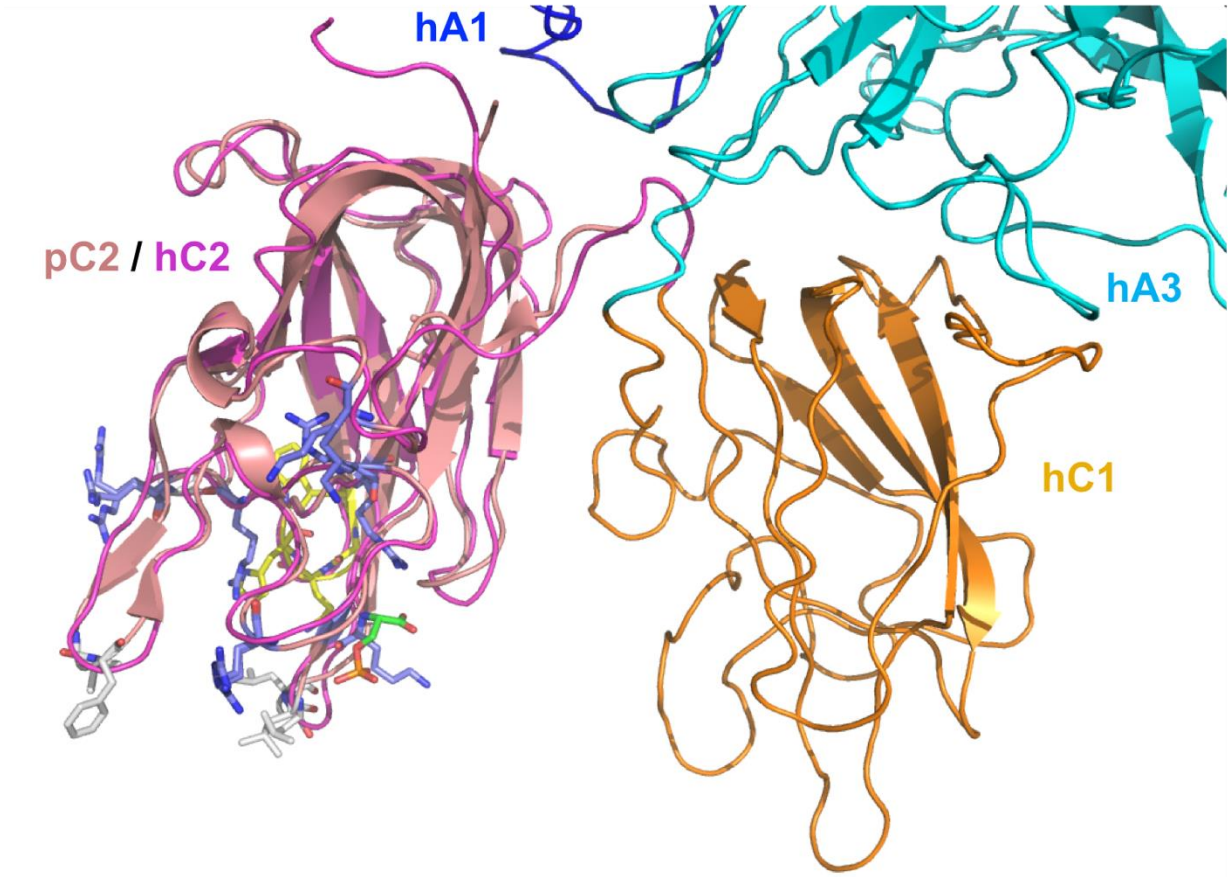

Figure 28. The pC2/OPLS crystal structure superimposed with a structure of human full length fVIII (PDB ID 2R7E; Shen et al. 2008). The green OPLS and Arg2320 faces the C1 domain while the yellow residues involved in the 'old' phospholipid binding model do not. This further supports our new binding model and coincides with the idea that the C1 domain likely orients the C2 domain during membrane binding.

The pull-down assays and intrinsic fluorescence studies validated our ELISAs by providing information about whether the proteins were folded and their structural stability, respectively. All the hC2 mutants were able to bind to the nonclassical G99 F_{AB}, which informed us that our hC2 mutant proteins were likely folded properly. The pull-down assays also showed that the Arg2320Ser mutation disrupted 3E6 binding, which further supports our hypothesis that hC2 binds membranes at the same site as 3E6, at the classical epitope. It is also possible that the classical epitope face of C2 was not properly folded. However, this is unlikely because of the similar protein stability between the Arg2320Ser mutant and wild type C2. Intrinsic fluorescence revealed that the Arg2320Ser mutation also decreased protein stability, but only by approximately 11%. This finding, along with the results from the pull-down assays, suggest that the decreased membrane binding of the arginine mutants determined by the ELISAs were not due to improper folding of the mutants. They were most likely due to the removal of the positive charge by mutating the arginine to residues that have no charge.

Interestingly, we also discovered that NaCl inhibited C2 phospholipid binding, even at the physiological salt concentration, 150 mM NaCl (**Figure 22D**). This finding has also been supported by a study from a different lab (Novakovic et al. 2011). The observed attenuation of phospholipid binding is likely due to NaCl competing with the basic residues of C2 for the negatively charged phosphatidylserine during binding. In the presence of 80 mM NaCl, the K_D increased by approximately 70% compared to binding with no salt

present. This leads to the conclusion that *in vivo*, C2 membrane binding is dependent on other factors, such as the proximity of the C1 domain. Thus, future lipid binding needs to be further investigated with intact fVIII to complement our isolated C2 domain studies. It has been found that the C2 domain binds membranes with a 40-fold lower affinity than intact fVIII (Novakovic et al. 2011), further indicating that fVIII membrane binding is complex and in order to understand the full mechanism, supplementary binding studies must be done. This observation, however, does not undermine our isolated C2 domain binding research as it still reveals the important basic residues within C2 that are involved in PS-containing membrane binding. Gilbert et al. in 2002 were unable to express an intact B-domain-deleted fVIII Arg2320Ala mutant. Because we were able to isolate the Arg2320 mutants in the C2 domain, our studies showed the importance of this residue during PS-membrane binding. This same group, nonetheless, was able to investigate an intact B-domain-deleted fVIII Arg2215Ala mutant. The clotting activity of this mutant was similar to wild type revealed by an activated partial thromboplastin time assay (Gilbert et al. 2002). In contrast, our hC2 Arg2215Ala mutant was unable to bind PS compared to wild type hC2. This further suggests that the full-length fVIII lipid binding mechanism is more complex than that of isolated C2.

Although this study was not all-encompassing, we have provided useful structural information about the phospholipid membrane binding mechanism of the isolated C2 domain within fVIII. Mainly, the orientation of the C2 domain during membrane binding is likely centered on Arg2320Ser, and occurs at the classical epitope face. Specific

interactions between activated platelet membranes include favorable interactions of the two hydrophobic beta hairpin loops (Met2199-Phe2200 and Leu2251-Lue2252) with the hydrophobic lipid bilayer of membranes. The underlying basic residues Arg2209, Arg2215, Lys2183, Arg2220, Arg2222, Lys2249, and Arg2320 in pC2 likely form nonspecific salt bridges with negatively charged phosphate or carboxyl groups of phospholipids on the surface of activated platelet membranes, with Arg2320 being the main contributor to the interaction between C2 and OPLS (**Figure 24**). In the future, other researchers may use this information to design novel fVIII replacement concentrates that have an increased activity in phospholipid binding for the improvement in current hemophilia A therapeutics.

References

1. **Abildgaard, U.** (1968) Inhibition of the Thrombin-Fibrinogen Reaction by Heparin and Purified Cofactor. *Scand. J. Haemat.* **5**: 440-453.
2. **Addiego, J. E. Jr, Gomperts, E., Liu, S. L., Bailey, P., Courter, S. G., Lee, M. L., Neslund, G. G., Kingdon, H. S. and Griffith, M. J.** (1992) Treatment of Hemophilia A with a Highly Purified Factor VIII Concentrate Prepared by Anti-FVIIIc Immunoaffinity Chromatography. *Thromb Haemost.* **67(1)**: 19-27.
3. **Afonine, P. V., Grosse-Kunstleve, R. W., Echols, N., Headd, J. J., Moriarty, N. W., Mustyakimov, M., Terwilliger, T. C., Urzhumtsev, A., Zwart, P. H. and Adams, P. D.** (2012) Towards Automated Crystallographic Structure Refinement with Phenix.Refine. **68(4)**: 352-367.
4. **Arai, M., Scandella, D. and Hoyer, L. W.** (1989) Molecular Basis of Factor VIII Inhibition by Human Antibodies: Antibodies that Bind to the Factor VIII Light Chain Prevent the Interaction of Factor VIII with Phospholipid.
5. **Barrow, R. T., Healey, J. F., Jacquemin, M. G., Saint-Remy, J. M. and Lollar, P.** (2001) Antigenicity of putative phospholipid membrane binding residues in factor VIII. *Blood.* **97**:169–174.
6. **Barrow, R. T. and Lollar, P.** (2006) Neutralization of antifactor VIII inhibitors by recombinant porcine factor VIII. *J Thromb Haemost.* **4**: 2223–2229.
7. **Beacham, D. A., Wise, R. J., Turci, S. M. and Handin, R. I.** (1992) Selective inactivation of the Arg-Gly-Asp-Ser (RGDS) binding site in von Willebrand factor by site-directed mutagenesis. *J. Biol. Chem.* **267**: 3409-3415
8. **Bergsagel, D. E. and Hougie, C.** (1956) Intermediate Stages in the Formation of Blood Thromboplastin. *Brit. J. Haemat.* **2**:113-129.
9. **Bevers, E. M., Comfurius, P. and Zwaal, R. F. A**. (1983) Changes in Membrane Phospholipid Distribution During Platelet Activation. *Biochimica et Biophysica Acta*. **736**: 57-66.
10. **Bolton-Maggs, P. H. B., Perry, D. J., Chalmers, E. A., Parapia, L. A, Wilde, J. T., Williams, M. D., Collins, P. W., Kitchen, S., Dolan, G. and Mumford, A. D.** (2004) The rare coagulation disorders-review with guidelines for management from the United Kingdom Haemophilia Centre Doctors' Organisation. *Haemophilia*. **10**: 593-628.
11. **Bray, G. L., Gomperts, E. D. Courter, S. et al.** (1994) A Multicenter Study of Recombinant Factor VI11 (Recombinate): Safety, Efficacy, and Inhibitor Risk in Previously Untreated Patients With Hemophilia A . *Blood.* **83(9)**: 2428-2435.
12. **Briede, J. J., Heemskerk, J. W., Van'T Veer, C. et al.** (2001) Contribution of Platelet-Derived Factor Va to Thrombin Generation on Immobilized Collagen- and fibrinogen-adherent platelets. *Thromb Haemost.* **85(3)**: 509-513.
13. **Brison, C. M., Mullen, S. M., Wuerth, M. E. et al.** (2015) The 1.7 Å X-Ray Crystal Structure of the Porcine Factor VIII C2 Domain and Binding Analysis to Anti-Human C2 Domain Antibodies and Phospholipid Surfaces. *PLOS One.* **0122447**: 1-17.

14. **Broze, G. J., Warren, L. A., Novotny, W. F., Higuchi, D. A., Girard, J. J. and Miletich, J. P.** (1988) The Lipoprotein-Associated Coagulation Inhibitor that Inhibits the Factor VII-Tissue Factor Complex also Inhibits Factor Xa: Insight into its Possible Mechanism of Action. *Blood*. **71(2)**: 335-343.
15. **Brunger, A. T.** (1992) Free R Value: A Novel Statistical Quantity for Assessing the Accuracy of Crystal Structures. *Nature*. **355(6359)**: 472-475.
16. **Centers for Disease Control.** (1988) Safety of Therapeutic Products for Hemophilia Patients. *MMWR Morb Mortal Wkly Rep*. **37 (29)**: 441-450.
17. **Cochrane, C. G., Revak, S. D. and Weupper, K. D.** (1973) Activation of Hageman Factor in Solid and Fluid Phases. *The Journal of Experimental Medicine*. **138**: 1564-1583.
18. **Coppola, A., Capua, M. D., Minno, D., Palo, M. D., Marrone, E., Lerano, P., Arturo, C., Tufano, A. and Cerbone, A. M.** (2010) Treatment of Hemophilia: A Review of Current Advances and Ongoing Issues. *Journal of Blood Medicine*. **I**: 183-195.
19. **Damus, P. S., Hicks, M. and Rosenberg, R. D.** (1973) Anticoagulant Action of Heparin. *Nature*. **246**: 355-357.
20. **Davie, E.W. and Ratnoff, O.D.** (1964) Waterfall sequence for intrinsic blood clotting. *Science*. **145(3638)**: 1310-1312.
21. **Dieijen, G. V., Tans, G., Rosing, J. and Hemker, C.** (1981) The Role of Phospholipid and Factor VIIIa in the Activation of Bovine Factor X. *The Journal of Biological Chemistry*. **256(7)**: 3433-3442.
22. **DiMichele, D. and Kroner, B. L.** (2002) The North American Immune Tolerance Resistry: Practices, Outcomes, Outcome Predictors. *Thromb Haemost*. **87(1)**: 52-57.
23. **Eaton, D., Rodriguez, H. and Vehar, G. A.** (1986) Proteolytic Processing of Human Factor VIII. Correlation of Specific Cleavages by Thrombin, Factor Xa, and Activated Protein C with Activation and Inactivation of Factor VI11 Coagulant Activity. *ACS Biochemistry*. **25(2)**: 505-512.
24. **Emsley, J., Cruz, M., Handin, R. and Liddington, R.** (1998) Crystal Structure of the von Willebrand Factor A1 Domain and Implications for the Binding of Platelet Glycoprotein Ib. *The Journal of Biological Chemistry*. **273**: 10396-10401.
25. **Esmon, C. T. and Owen, W. G.** (1981) Identification of an Endothelial Cell Cofactor for Thrombin-Catalyzed Activation of Protein C. *Proc. Natl. Acad. Sci.* **78(4)**: 2249-2252.
26. **Fay, P. J., Coumans, J. V. and Walker, F. J.** (1991) von Willebrand Factor Mediates Protection of Factor VIII from Activated Protein C-Catalyzed Inactivation. *The Journal of Biological Chemistry*. **266(4)**: 2172-2177.
27. **Foster, P. A., Fulcher, C. A., Houghten, R. A. and Zimmerman, T. S.** (1990) Synthetic Factor VIII Peptides With Amino Acid Sequences Contained Within the C2 Domain of Factor VIII Inhibit Factor VIII Binding to Phosphatidylserine. *Blood*. **75(10)**: 1999-2004.
28. **Franchini, M. and Lippi, G.** (2011) The Use of Desmopressin in Acquired Haemophilia A: A Systematic Review. *Blood Transfusion*. **9(4)**: 377-382.

29. **Frishman, D. and Argos, P.** (1995) Knowledge-Based Protein Secondary Structure Assignment. *Proteins: Structure, Function, and Genetics*. **23**: 566-579.
30. **Fujikawa, K., Legaz, M. E., Kato, H. and Davie, E. W.** (1974) The Mechanism of Activation of Bovine Factor IX (Christmas Factor) by Bovine Factor XIa (Activated Thromboplastin Antecedent). *Biochemistry*. **13(22)**: 4508-4516.
31. **Fulcher, C., de Graaf Mahoney, S., Roberts, J., Kasper, C. and Zimmerman, T.** (1985) Localization of Human Factor FVIII Inhibitor Epitopes to Two Polypeptide Fragments. *Proc Natl Acad Sci*. **82**: 7728–7732.
32. **Gawryl, M. S. and Hoyer, L. W.** (1982) Inactivation of Factor VIII Coagulant Activity by Two Different Types of Human Antibodies. *Blood*. **60**:1103–1109.
33. **Gilbert, G.E. and Arena, A. A.** (1996) Activated of the Factor VIIIa-Factor IXa Enzyme Complex of Blood Coagulation by Membranes Containing Phosphatidyl-L-serine. *The Journal of Biological Chemistry*. **271(19)**: 11120-11125
34. **Gilbert, G. E., Novakovic, V. A., Shi, J., Rasmussen, J. and Pipe, S. W.** (2015) Platelet binding sites for factor VIII in relation to fibrin and phosphatidylserine. *Blood*. **126(10)**: 1237-1244.
35. **Gilbert, G. E., Kaufman, R. J., Arena, A. A., Miao, H. and Pipe, S. W.** (2002) Four Hydrophobic Amino Acids of the Factor VIII C2 Domain Are Constituents of Both the Membrane-binding and von Willebrand Factor-binding Motifs. *The Journal of Biological Chemistry*. **277(8)**: 6374-6381.
36. **Ginsburg, D., Handin, R. I., Bonthron, D. T., Donlon, T. A., Bruns, G. A., Latt, S. A. and Orkin, S. H.** (1985) Human von Willebrand factor (vWF): Isolation of Complementary DNA (cDNA) clones and Chromosomal Localization. *Science*. **228(4706)**: 1401-1406.
37. **Gitchier, J., Wood, W. I., Goralka, T. M., Wion, K. L., Chen, E. Y., Eaton, D. H., Vehar, G. A., Capon, D. J. and Lawn, R. M.** (1984) Characterization of the Human Factor VIII Gene. *Nature*. **312**: 326-330.
38. **Griffin, J. H.** (1978) Role of Surface in Surface-Dependent Activation of Hageman Factor (Blood Coagulation Factor XII). *Proc. Natl. Acad. Sci*. **75(4)**: 1998-2002.
39. **Hantgan, R. R., Hindriks, G., Taylor, R. G., Sixma, J. J. and de Groot, P. G.** (1990) Glycoprotein Ib, von Willebrand factor, and glycoprotein IIb:IIIa are all involved in platelet adhesion to fibrin in flowing whole blood. *Blood*. **76**: 345-353.
40. **Hay, C. R., Lozier, J. N., Lffan, M., Tradati, F., Santagostino, E., Ciavarella, N., Schiavoni, M., Fukui, H., Yoshioka, A., Teitel, J., Mannucci, P. M. and Kasper, C. K.** (1996) Safety profile of porcine factor VIII and its use as hospital and home-therapy for patients with haemophilia-A and inhibitors: the results of an international survey. *Thromb Haemost*. **75(1)**: 25-29.
41. **Hoffman, M. and Dargaud, Y.** (2012) Mechanisms and Monitoring of Bypassing Agent Therapy. *Journal of Thrombosis and Haemostasis*. **10**: 1478-1485.
42. **Horling, F. M., Allacher, P., Koppensteiner, H., Engl, W., Scheiflinger, F., Abbuehl, B. E. and Reipert, B. M.** (2016) Immunogenicity of BAX 855 in Previously Treated Patients with Congenital Severe Hemophilia A. *Blood*. **128(22)**: 2594.

43. **Huizinga, E. G., van der Plas, R. M., Kroon, J., Sixma, J. and Gros, P.** (1997) Crystal Structure of the A3 Domain of Human von Willegrand Factor: Implications for Collagen Binding. *Structure*. **5(9)**: 1147-1156.
44. **Jackson, S. P.** (2007) The growing complexity of platelet aggregation. *Blood*. **109(12)**: 5087-5095.
45. **Kanaide, H. and Shainoff, J. R.** (1975) Cross-linking of fibrinogen and fibrin by fibrin-stabilizing factor (factor XIIIa). *J Lab Clin Med*. **85(4)**: 574-597.
46. **Kaufman, R. J., Wasley, L. C. and Dorner, A. J.** (1988) Synthesis, Processing, and Secretion of Recombinant Human Factor VIII Expressed in Mammalian Cells. *The Journal of Biological Chemistry*. **263(13)**: 6352-6362.
47. **Koedam, J. A., Hamer, R. J., Beeser-Visser, N. H., Bouma, B. N. and Sixma, J. J.** (1990) The Effect of von Willebrand Factor on Activation of Factor VIII by Factor Xa. *Eur. J. Biochem*. **189**: 229-234.
48. **Konkle, B. A., Stasyshyn, O., Chowdary, P., Bevan, D. H., Mant, T., Shima, M., Engl, W., Dyck-Jones, J., Fuerlinger, M., Patrone, L., Ewenstein, B. and Abbuehl.** (2015) Pegylated, Full-Length, Recombinant Factor VIII for Prophylactic and On-Demand Treatment of Severe Hemophilia A. *Blood*. **126(9)**: 1078-1085.
49. **Kurachi, K., Fujikawa, K., Schmer, G. and Davie, E. W.** (1976) Inhibition of Bovine Factor IXa and Factor Xaß by Antithrombin III. *Biochemistry*. **15(2)**: 373-377.
50. **LaVallie, E.R., DiBlasio, E.A., Kovacic, S., Grant, K.L., Schendel, P.F. and McCoy, J.M**. (1993) A Thioredoxin Gene Fusion Expression System that Circumvents Inclusion Body Formation in the *E. coli* Cytoplasm. *Bio/Technology*. **11**: 187–193.
51. **Lawson, J. H. and Mann, K. G.** (1991) Cooperative Activation of Human Factor IX by the Human Extrinsic Pathway of Blood Coagulation. *The Journal of Biological Chemistry*. **266(17)**: 11317-11327.
52. **Lollar, P., Hill-Eubanks, D. C. and Parker, C. G.** (1988) Association of the Factor VIII Light Chain with von Willebrand Factor. *The Journal of Biological Chemistry*. **263(21)**: 10451-10455.
53. **Lollar, P., Parker, E. T. and Fay, P. J.** (1992) Coagulant Properties of Hybrid Human/Porcine Factor VIII Molecules. *The Journal of Biological Chemistry*. **267(33)**: 23652-23657.
54. **Lottenberg, R., Kentro, T. B. and Kitchens, C. S.** (1987) Acquired Hemophilia: A Natural History Study of 16 Patients With Factor VIII Inhibitors Receiving Little or No Therapy. *Arch Intern Med*. **147(6)**: 1077-1081.
55. **Lindquist, P. A., Fujikawa, K. and Davie, E. W.** (1978) Activation of Bovine Factor IX (Christmas Factor) by Factor XIa (Activated Plasma Thromboplastin Antecedent) and a Protease from Russell's Viper Venom. *The Journal of Biological Chemistry*. **253(6)**: 1902-1909.
56. **Lu, J., Pipe, S. W., Miao, H. et al.** (2011) A membrane-interactive surface on the factor VIII C1 domain cooperates with the C2 domain for cofactor function. *Blood*. **117(11)**: 3181-3189.

57. **Lusher, J. M., Arkin, S. and Abildgaard, C. F.** (2003) Recombinant Factor VIII for the Treatment of Previously Untreated Patients with Hemophilia A. *The New England Journal of Medicine*. **328(7)**: 455-459.
58. **Lusher, J. M., Lee, C. A., Kessler, C. M. et al.** (2003) The safety and efficacy of B-domain deleted recombinant factor VIII concentrate in patients with severe haemophilia A. *Haemophilia*. **9(1)**: 38-49.
59. **Macfarlane, R.G.** (1964) An enzyme cascade in the blood clotting mechanism, and its function as a biochemical amplifier. *Nature* **202**: 498–499.
60. **Madsen, J. J., Ohkubo Y. Z., Peters, G. H. et al.** (2015) Membrane Interaction of the Factor VIIIa Discoidin Domains in Atomistic Detail. *Biochemistry*. **54**: 6123-6131.
61. **McDaniel, M.** (2013) Treatment of Hemophilia A and B. *National Hemophilia Foundation*. 1-9.
62. **Meems, H., Meijer, A. B., Cullinan, D. B., Mertens, K. and Gilbert, G. E.** (2009) Factor VIII C1 Domain Residues Lys 2092 and Phe 2093 Contribute to Membrane Binding and Cofactor Activity. *Blood*. **114**: 3938-3946.
63. **Miao C.** (2010) Immunomodulation for inhibitors in hemophilia A: the important role of Treg cells. *Expert Rev Hematol*. **3**: 469–483.
64. **Monkovic, D. D. and Tracy, P. B.** (1990) Activation of Human Factor V by Factor Xa and Thrombin. *Biochemistry*. **29**: 1118-1128.
65. **Monroe, D.** M**., Hoffman, M. and Roberts, H.** (1996) Transmission of a Procoagulant Signal from Tissue Factor-Bearing Cells to Platelets. *Blood Coagulation and Fibrinolysis*. **7(4)**: 459-464.
66. **Monroe, D.M. and Hoffman M.** (2006) What does it take to make the perfect clot? *Arterioscler Throm Vasc Biol*. **26**: 41-48.
67. **Meeks, S. L., Healey, J. F., Parker, E. T., Barrow, R. T. and Lollar, P.** (2007) Antihuman factor VIII C2 domain antibodies in hemophilia A mice recognize a functionally complex continuous spectrum of epitopes dominated by inhibitors of factor VIII activation. *Blood*. **110(13)**: 4234-4242.
68. **Meeks, S. L., Healey, J. F., Parker, E. T., Barrow, R. T. and Lollar, P.** (2008) Nonclassical anti-C2 domain antibodies are present in patients with factor VIII inhibitors. *Blood*. **112(4)**: 1151–1153.
69. **Munishkina, L. A. and Fink, A. L.** (2007) Fluorescence as a Method to Reveal Structures and Membrane-interactions of Amyloidogenic Proteins. *Biochemica et Biophysica Acta*. **1768**: 1862-1885.
70. **Naito, K. and Fujikawa, K.** (1991) Activation of Human Blood Coagulation Factor XI Independent of Factor XII. *The Journal of Biological Chemistry*. **266(12)**: 7353-7358.
71. **Nemerson, Y. and Pitlick, F. A.** (1972) The Tissue Factor Pathway of Blood Coagulation. *Progress in Hemostasis and Thrombosis*. **1**: 1-37.
72. **Nogami, K., Shima, M., Hosokawa, K., Nagata, M. Koide, T., Saenko, E. L., Tanaka, I., Shibata, M. and Yoshioka, A.** (2000) Factor VIII C2 domain contains the thrombin-binding site responsible for thrombin-catalyzed cleavage at Arg1689. *J Biol Chem*. **275**: 25774–25780.

73. **Novakovic, V. A., Cullinan, D. B., Wakabayashi, H., Fay, P. J., Baleja, J. D. and Gilbert, G. E.** (2011) Membrane-Binding Properties of the Factor VIII C2 Domain. *Biochem. J.* **435**: 187-196.
74. **O'Donnell, V. B., Murphy, R. C., and Watson, S. P.** (2014) Platelet Lipidomic: A Modern Day Perspective on Lipid Discovery and Characterization in Platelets. *Circ Res.* **114(7)**: 1185-1203.
75. **Owen, W. G.** (1975) Evidence for the Formation of an Ester Between Thrombin and Heparin Cofactor. *Biochemica et Biophysica Acta*. **405**: 380-387.
76. **Palta, S., Saroa, R. and Palta, A.** (2014) Overview of the Coagulation System. *Indian J. Anaesth*. **58(5)**: 515-523.
77. **Pareti, F., Niiya, K., McPherson, J. M. and Rugger, Z. M.** (1987) Isolation and Characterization of Two Domains of Human von Willebrand Factor That Interact with Fibrillar Collagen Types I and III. *The Journal of Biological Chemistry*. **262(28)**: 13835-13841.
78. **Pittman, D. D. and Kaufman, R. J.** (1988) Proteolytic Requirements for Thrombin Activation of Anti-Hemophilic Factor (Factor VIII). *Proc. Natl. Acad. Sci.* **85**: 2429-2433.
79. **Pratt, K. P., Shen, B W., Takeshima, K., Davie, E. W., Fujikawa, K. and Stoddard, B. L.** (1999) Structure of the C2 Domain of Human Factor VIII at 1.5 Angstrom Resolution. *Nature*. **402**: 439-442.
80. **Pratt, K. P.** (2015) fVIII binds platelets + fibrin: no PS! *Blood*. **3(10)**: 1158-1159.
81. **Rallapalli, P. M., Kemball-Cook, G., Tuddenham, E. G., Gomez, K. and Perkins, S. J.** (2014) - Manuscript in Preparation.
82. **Rao, L. V. M. and Rapaport, S. I.** (1987) Studies of a Mechanism Inhibiting the Initiation of the Extrinsic Pathway of Coagulation. *Blood*. **69(2)**: 645-651.
83. **Rose, E. H. and Aledort, L. M.** (1991) Nasal Spray Desmopressin (DDAVP) for mild hemophilia A and von Willebrand Disease. *Annals of Internal Medicine*. **114(7)**: 563-568.
84. **Rosing, J., van Rijn, J. M. L., Bevers, E. M., Dieijen, G., Confurius, P. and Zwaal, R. F. A.** (1985) The Role of Activated Human Platelets in Prothrombin and Factor X Activation. *Blood*. **65(2)**: 319-332.
85. **Saenko, E. L. and Scandella, D.** (1997) The acidic region of the factor VIII light chain and the C2 domain together form the high affinity binding site for von Willebrand factor. *J Biol Chem*. **272**: 18007–18014.
86. **Sanders, N. L., Bajaj, S. P., Zivelin, A. and Rapaport, S. I.** (1985) Inhibition of Tissue Factor/Factor VIIa Activity in Plasma Requires Factor X and an Additional Plasma Component. *Blood*. **66(1)**: 204-212.
87. **Scandella, D., Mattingly, M., de Graaf S. and Fulcher C.** (1989) Localization of Epitopes for Human Factor VIII Inhibitor Antibodies by Immunoblotting and Antibody Neutralization. *Blood*. **74**: 1618–1626
88. **Shen, B.W., Spiegel, P.C., Chang, C.H., Huh, J. W., Lee, J. S., Kim, Y. H. and Stoddard, B. L.** (2008) The tertiary structure and domain organization of coagulation factor VIII. *Blood*. **111(3)**: 1240-1247.

89. **Smith, P. S., Teutsch, S. M., Shaffer, P. A., Rolka, H. and Evatt, B.** (1996) Episodic Versus Prophylactic Infusions for Hemophilia A: A Cost-Effective Analysis. *The Journal of Pediatrics*. **129(3)**: 424-431.
90. **Soucie, J. M., Evatt, B. and Jackson, D.** (1998) Occurrence of hemophilia in the United States. The Hemophilia Surveillance System Project Investigators. *Am J Hematol*. **59:** 288–294.
91. **Spiegel, P. C., Jacquemin, M., Saint-Remy, J. R., Soddard, B. L. and Pratt, K. P.** (2001) Structure of a factor VIII C2 domain–immunoglobulin G4k Fab Complex: Identification of an Inhibitory Antibody Epitope on the Surface of Factor VIII. *Blood*. **98**: 13-19.
92. **Spiegel, P. C., Murphy, P. and Soddard, B. L.** (2004) Surface-Exposed Hemophilic Mutations Across the Factor VIII C2 Domain Have Variable Effects on Stability and Binding Activities. *The Journal of Biological Chemistry*. **279(51)**: 53691-53698.
93. **Srivastava, A., Brewer, A. K., Mauser-Bunschoten, E. P., Key, N. S., Kitchen, S., Llinas, A., Ludlam, C. A., Mahlangu, J. N., Mulder, K., Poon, M. C. and Street, A.** (2013) Guideliens for the Management of Hemophilia. *Haemophilia*. **19**: e1-e47.
94. **Stead, N., Kaplan, A. P. and Rosenberg, R. D.** (1976) Inhibition of Activated Factor XII by Antithrombin-Heparin Cofactor. *The Journal of Biological Chemistry*. **251(21)**: 6481-6488.
95. **Stoilova-McPhie, S., Villoutreix, B. O., Mertens, K., Kemball-Cook, G. and Holzenburg, A.** 3-Dimentional Structure of Membrane-Bound Coagulation Factor VIII: Modeling of Factor VIII Heterdimer Within a 3-Dimentional Density Map Derived by Electron Crystallography. *Blood*. **99(4)**: 1215-1223.
96. **Toole, J. J., K Knopf, J.L., Wozney, J.M., Sultzman, L.A., Buecker, J.L., Pittman, D.D., Kaufman, R.J., Broown, E., Shoemaker, C., Orr, E.C., Amphlett, G.W., Foster, W.B., Coe, M.L., Knutson, G.J., Fass, D.N. and Hewick, R.M.** (1984) Molecular Cloning of a cDNA Encoding Human Antihemophilic Factor. *Nature*. **312**: 342-347.
97. **Tuddenham, E. G. D., Schwaab, R., Seehafer, J., Millar, D. S., Gitschier, J., Higuchi, M., Bidichandani, S., Connor, J. M., Hoyer, L. W., Yoshioka, A., Peake, I. R., Olek, K., Kazazian, H. H., Lavergne, J. M., Giannelli, F., Antonarakis, S. E. and Cooper, D. N.** (1994) Haemophilia A: Database of Nucleotide Substitutions, Deletions, Insertions, and Rearrangements of the Factor VIII Gene, Second Edition. *Nucleic Acids Research*. **22(17)**: 3511-3533.
98. **van der Flier, A., Liu, Z., Tan, S., Chen, K., Drager, D., Liu, T. Patarroyo-White, S., Jiang, H. and Light, D. R.** (2015) FcRn Rescues Recombinant Factor VIII Fc Fusion Protein from a VWF Independent FVIII Clearance Pathway in Mouse Hepatocytes. *PLOS One*. **10(4)**: 1-23.
99. **Varadi, K., Rosing, J., Tans, G. et al.** (1996) Factor V Enhances the Cofactor Function of Protein S in the APC-Mediated Inactivation of Factor VIII: Influence of the Factor VR506Q Mutation. *Thromb Haemost*. **76(2)**: 208-214.

100. **Vehar, G. A., Keyt, B., Eaton, D., Rodriguez, H., O'Brien, D. P., Rotblat, F., Oppermann, H., Keck, R., Wood, W. I., Harkins, R. N., Tuddenham, E. G. D., Lawn, R. M. and Capon, D. J.** (1984) Structure of Human Factor VIII. *Nature*. **312(22)**: 337-342.
101. **Walker, F. J., Sexton, P. W. and Esmon, C. T.** (1979) The Inibition of Blood Coagulation by Activated Protein C Through the Selective Inactivation of Activated Factor V. *Biochimica et Biophysica Acta*. **571**: 333-342.
102. **Walker, F. J.** (1981) Regulation of Activated Protein C by Protein S: The role of phospholipid in factor Va inactivation. *The Journal of Biological Chemistry*. **256(21)**: 11128-11131.
103. **Walter, J. D., Littlefield, P., Delbecq, S., Prody, G. and Spiegel, P. C.** (2010) Expression, Purification, and Analysis of Unknown Translation Factors from *Escherichia coli*: A Synthesis Approach. *Biochemistry and Molecular Biology Education*. **38(1)**: 17-22.
104. **Walter, J. D., Werther, R. A., Brison, C. M., Cragerud, R. K., Healey, J. F., Meeks, S. L., Lollar, P. and Spiegel, P.** (2013) Structure of the factor VIII C2 domain in a ternary complex with 2 inhibitor antibodies reveals classical and nonclassical epitopes. **122(26)**: 4270-4278.
105. **Webster, W. P., Zukoski, C. F., Hutchin, P., Reddick, R. L., Mandel, S. R. and Penick, G. D.** (1971) Plasma Factor VIII Synthesis and Control as Revealed by Canine Organ Transplantation. *Am J Physiol*. **220(5)**: 1147-54.
106. **Wion, K. L., Kelly, D., Summerfield, J. A., Tuddenham, E. G. D. and Lawn, R. M.** (1985) Distribution of fVIII mRNA and Antigen in Human Liver and Other Tissues. *Nature*. **317**: 726-729.
107. **Wun, T. C., Kretzmer, K. K., Girard, T. J., Miletch, J. P. and Broze, G. J.** (1988) Cloning and Characterization of cDNA Coding for the Lipoprotein associated Coagulation Inhibitor Shows that it Consists of Three Tandem Kunitz-type Inhibitory Domains. **263(13)**: 6001-6004.
108. **Zhou, Y.F., Eng, E.T., Zhu, J., Lu, C., Walz, T. and Springer, T.A.** (2012) Sequence and structure relationships within von Willebrand factor. *Blood*. **120**: 449–458.
109. **Zucker, F., Champ, P. C. and Merritt, E. A.** (2010) Validation of Crystallographic Models Containing TLS or Other Descriptions of Anisotropy. *Acta Cryst*. **D66**: 889-900.

Appendix

>hC2 R2320M 1Term-T7Term 904 42 774 0.05
GTGGTGGTGGTGGTGCTCGAGTCACTGTGCCTCGCAGCCCAGAACCTCCATCATCAGGGCAATCTGGTGCACCCAACTCTGGGGGTGAATTCGAAG
GTAGCGAGTCAGTAACGGTGGGTCTAGAGAGTTCACCACAGGTGTGAAGGAGTCTTGATTTCCCTGAAAAACCTTTACTTTGCCATTCTGAAAAAAGA
GAGTCCACTGATGGCCATCTTGACTGCTGGAGATGAGGAACTCCTTCACATACATGCTGGTAAGCAGAGATTTTACTCCCTGAGTAGTTACTCCTGTGA
CTTTCATTGTCTTCTGGAAGTCCACTTGCAGCCACTCTTTTGGATTATTCACCTGAGGTCTCCAGGCATTACTCCTCCCTTGGAGGTGAAGTCGAGCTT
TTGAAGGAGACCAGGTGGCAAACATATTGGTAAAGTAGGATGAAGCAGTAATCTGTGCATCTGATATTGCTTTACTCTCCATTCCCAATGGCATGCTGCA
ACTATTTAACATGGATCCGATATCAGCCATGGCCTTGTCGTCGTCGTCGGTACCCAGATCTGGGCTGTCCATGTGCTGGCGTTCGAATTTAGCAGCAGC
GGGTTTCTTTCATACCAGAACCGCGTGGCACCAGACCAGAAGAATGATGATGATGATGGTGCATATGGGCCAGAACCAGAACCGGCCAGGTTAGCGT
CGAGGAACTCTTTCAACTGACCTTTAGACAGTGCACCCACTTTGGGTTGCCGGCCACTTCACCGTTTTTGGAACAGCAGCAGAGTC

>hC2 R2320S 1Term-T7Term 930 42 606 0.05
GTGGTGGTGGTGGTGCTCGAGTCACTGTGCCTCGCAGCCCAGAACCTCCATGCTCAGGGCAATCTGGTGCACCCAACTCTGGGGGTGAATTCGAAG
GTAGCGAGTCAGTAACGGTGGGTCTAGAGAGTTCACCACAGGTGTGAAGGAGTCTTGATTTCCCTGAAAAACCTTTACTTTGCCATTCTGAAAAAAGA
GAGTCCACTGATGGCCATCTTGACTGCTGGAGATGAGGAACTCCTTCACATACATGCTGGTAAGCAGAGATTTTACTCCCTGAGTAGTTACTCCTGTGA
CTTTCATTGTCTTCTGGAAGTCCACTTGCAGCCACTCTTTTGGATTATTCACCTGAGGTCTCCAGGCATTACTCCTCCCTTGGAGGTGAAGTCGAGCTT
TTGAAGGAGACCAGGTGGCAAACATATTGGTAAAGTAGGATGAAGCAGTAATCTGTGCATCTGATATTGCTTTACTCTCCATTCCCAATGGCATGCTGCA
ACTATTTAACATGGATCCGATATCAGCCATGGCCCTTGTCGTCGTCGTCGGTACCCAGATCTGGGCTGTCCATGTGCTGGCGTTCGAATTTAGCAGCAG
CGGTTTCTTTCATAC

>hC2 R2320T 3Term-T7Term 910 50 759 0.05
TGGTGGTGCTCGAGTCACTGCTGCCTCGCAGCCCAGAACCTCCATCGTCAGGGCAATCTGGTGCACCCAACTCTGGGGGTGAATTCGAAGGTAGCG
AGTCAGTAACGGTGGGTCTAGAGAGTTCACCACAGGTGTGAAGGAGTCTTGATTTCCCTGAAAAACCTTTACTTTGCCATTCTGAAAAAAGAGAGTCC
ACTGATGGCCATCTTGACTGCTGGAGATGAGGAACTCCTTCACATACATGCTGGTAAGCAGAGATTTTACTCCCTGAGTAGTTACTCCTGTGACTTTCA
TTGTCTTCTGGAAGTCCACTTGCAGCCACTCTTTTGGATTATTCACCTGAGGTCTCCAGGCATTACTCCTCCCTTGGAGGTGAAGTCGAGCTTTTGAAG
GAGACCAGGTGGCAAACATATTGGTAAAGTAGGATGAAGCAGTAATCTGTGCATCTGATATTGCTTTACTCTCCATTCCCAATGGCATGCTGCAACTATT
TAACATGGATCCGATATCAGCCATGGCCTTGTCGTCGTCGTCGGTACCCAGATCTGGGCTGTCCATGTGCTGGCGTTCGAATTTAGCAGCAGCGGTTT
CTTTCATACCAGAACCGCGTGGCACCAGACCAGGAAGAATGATGATGATGATGGTGCATATGGCCAGAACCAGAACCGGCCAGGTTAGCGTCGAGGA
ACTCTTTCAACTGACCTTTAGACAGTGCACCCACTTTGGTTGCCGCCACTTCACCGTTTTTGACAGCAGCAG

>hC2 R2215A-C-Term-T7Term 865 32 665 0.05
Reverse Compliment
CCATATGCACCATCATCATCATCATTCTTCTGGTCTGGTGCCACGCGGGTCTGGTATGAAAGAAACCGCTGCTGCTAAATTCGAACGCCAGCACATGGA
CAGCCCAGATCTGGGTACCGACGACGACGACAAGGCCATGGCTGATATCGGATCCATGTTAAATAGTTGCAGCATGCCATTGGGAATGGAGAGTAAAG
CAATATCAGATGCACAGATTACTGCTTCATCCTACTTTACCAATATGTTTGCCACCTGGTCTCCTTCAAAAGCTCGACTTCACCTCCAAGGGGCGAGTAA
TGCCTGGAGACCTCAGGTGAATAATCCAAAAGAGTGGCTGCAAGTGGACTTCCAGAAGACAATGAAAGTCACAGGAGTAACTACTCAGGGAGTAAAAT
CTCTGCTTACCAGCATGTATGTGAAGGAGTTCCTCATCTCCAGCAGTCAAGATGGCCATCAGTGGACTCTCTTTTTTCAGAATGGCAAAGTAAAGGTTT
TTCAGGGAAATCAAGACTCCTTCACACCTGTGGTGAACTCTCTAGACCCACCGTTACTGACTCGCTACCTTCGAATTCACCCCCAGAGTTGGGTGCAC
CAGATTGCCCTGAGGATGGAGGTTCTGGGCTGCGAGGCACAGTGACTCGAGCACCACCACCACCACCACTGAG

>hC1 R2163H-B-Term-T7Term 760 62 616 0.05
Reverse Compliment
CGCTGCTGCTAAATTCGAACGCCAGCACATGGACAGCCCAGATCTGGGTACCGACGACGACGACAAGGGCCATGGCTGATATCGGATCCAGCAATAA
GTGTCAAACCCCGCTGGGCATGGCTTCTGGTCACATCCGCGACTTCCAAATCACGGCTTCTGGTCAATACGGTCAATGGGCGCCGAAACTGGCCCGT
CTGCATTATTCCGGCTCAATTAATGCGTGGTCCACCAAAGAACCGTTTTCATGGATCAAGGTGGATCTGCTGGCTCCGATGATTATCCACGGCATTAAA
ACCCAGGGTGCGCGTCAAAAGTTTAGCTCTCTGTATATCTCGCAGTTCATTATCATGTACAGCCTGGATGGTAAAAAGTGGCAAACCTACCGCGGCAAT
TCTACCGGTACGCTGATGGTGTTTTTCGGCAACGTTGACAGTTCCGGTATCAAGCATAACATCTTCAATCCGCCGATTATCGCCCGTTATATTCGCCTGC
ATCCGACCCACTACTCCATCCGTTCAACGCTGCACATGGAACTGATGGGCCGTTCAACGCTGCACATGGAACTGATGGGCCGTTCAACGCTGCACAT
GGAACTGATGGGCTGCGATCTGAACTC

>hC1 R2159H-C-Term-T7Term 853 48 739 0.05
Reverse Compliment
CAAAAACGGTGAAGTGGCGGCACCCAAAGTGGGTGCACTGTCTAAAGGTCAGTTGAAAGAGTCCCTCGACGCTAACCTGGCCGGTTCTGGTTCTGG
CCATATGCACCATCATCATCATCATTCTTCTGGTCTGGTGCCACGCGGTTCTGGTATGAAAGAAACCGCTGCTGCTAAATTCGAACGCCAGCACATGGA
CAGCCCAGATCTGGGTACCGACGACGACGACAAGGCCATGGCTGATATCGGATCCAGCAATAAGTGTCAAACCCCGCTGGGCATGGCTTCTGGTCAC
ATCCGCGACTTCCAAATCACGGCTTCTGGTCAATACGGTCAATGGGCGCCGAAACTGGCCCGTCTGCATTATTCCGGCTCAATTAATGCGTGGTCCAC
CAAAGAACCGTTTTCATGGATCAAGGTGGATCTGCTGGCTCCGATGATTATCCACGGCATTAAAACCCAGGGTGCGCGTCAAAAGTTTAGCTCTCTGTA
TATCTCGCAGTTCATTATCATGTACAGCCTGGATGGTAAAAAGTGGCAAACCTACCGCGGCAATTCTACCGGTACGCTGATGGTGTTTTTCGGCAACGT
TGACAGTTCCGGTATCAAGCATAACATCTTCAATCCGCCGATTATCGCCCGTTATATTCGCCTGCATCCGACCCACTACTCCATCCATTCAACGCTGCGC
ATGGAACTGATGGGCTGCGATCTGAACTCGTAACTCGAGCACCACCACCAC

Appendix Figure 1. DNA sequencing results from Nevada Genomics. Highlighted yellow are the hC2 or hC1 gene sequences. Highlighted in green or cyan are the correct mutations.

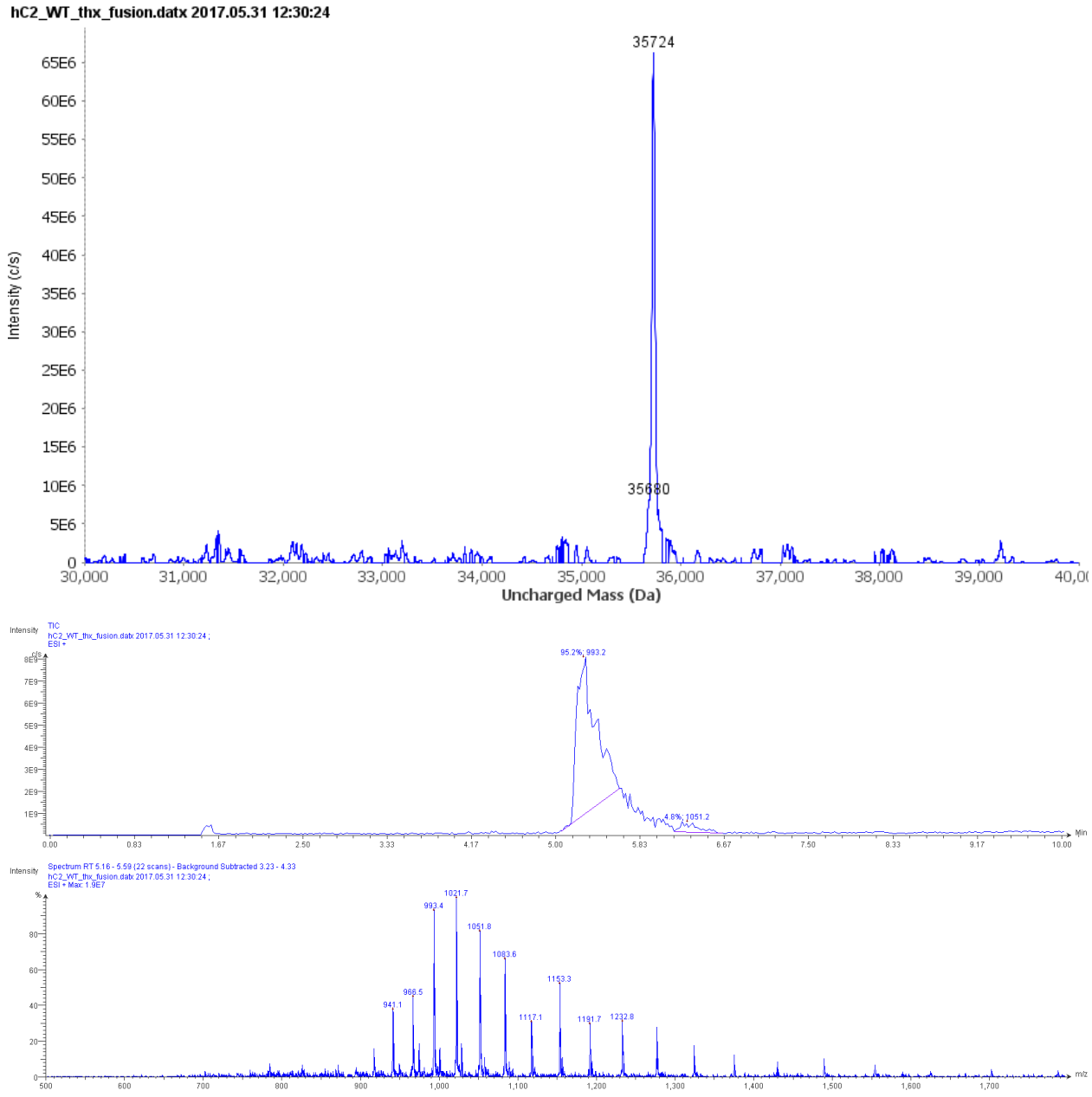

Appendix Figure 2. Human C2 wild type thioredoxin fusion mass spectrometry results.

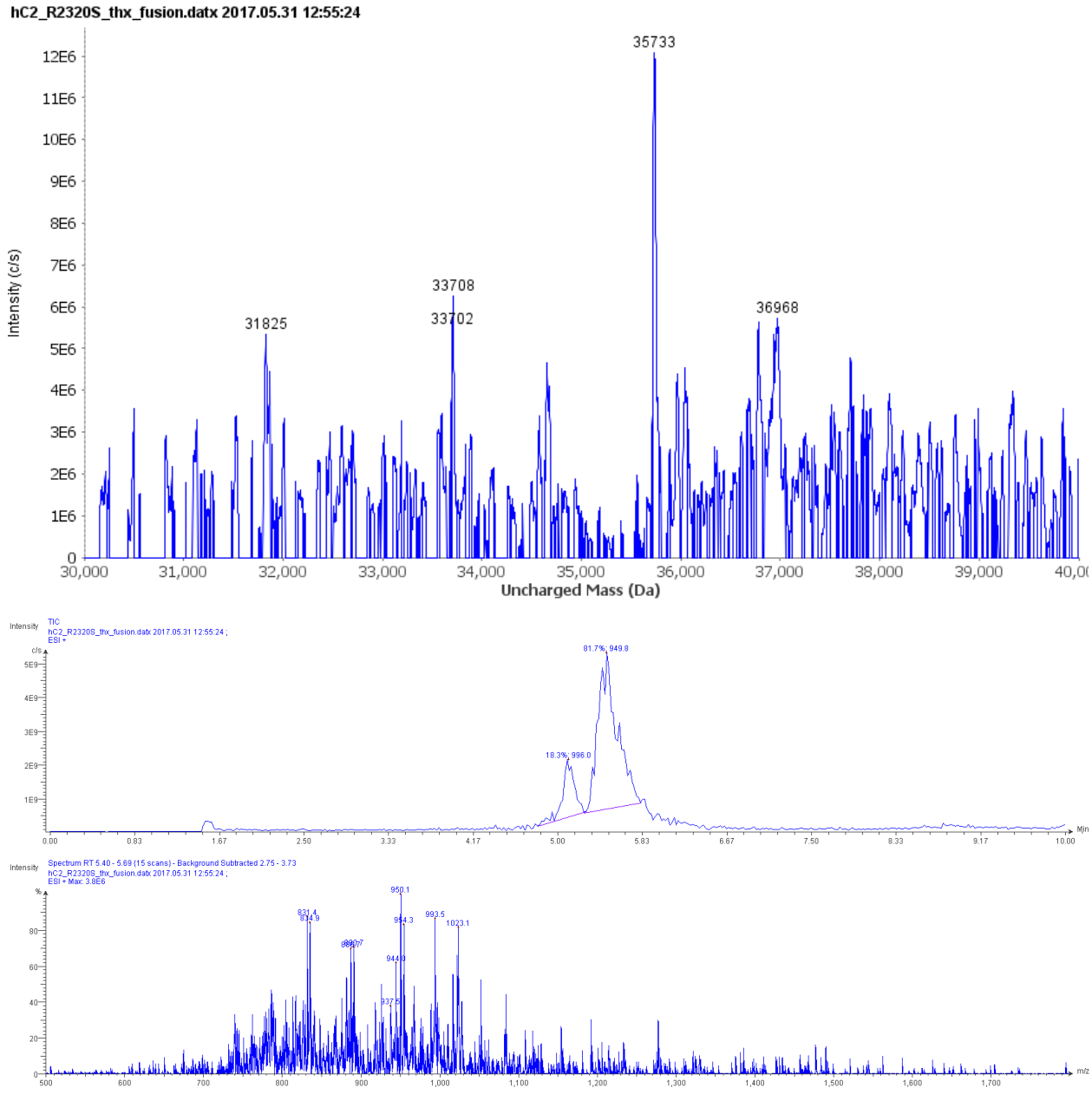

Appendix Figure 3. Human C2 R2320S thioredoxin fusion mass spectrometry results.

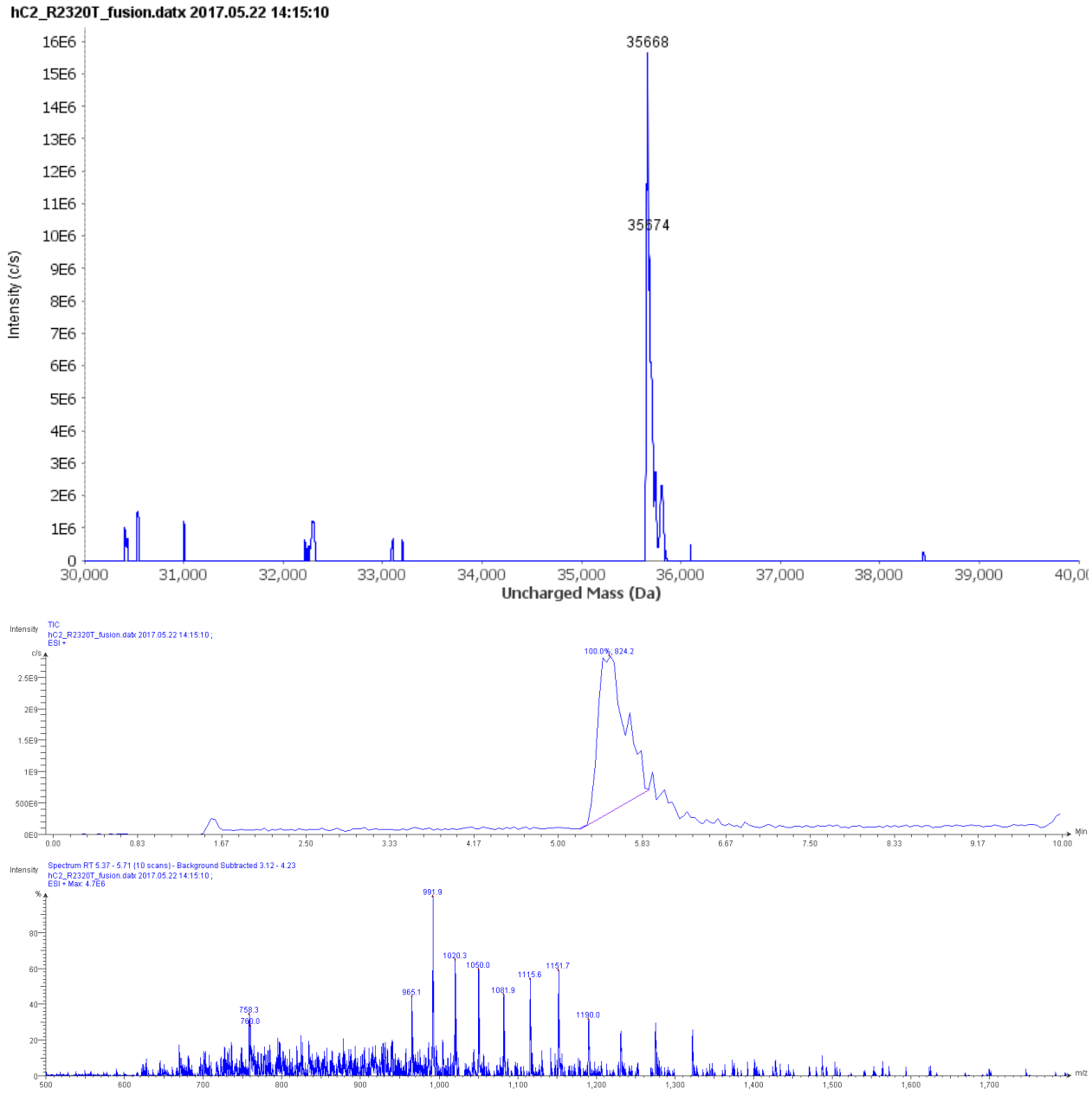

Appendix Figure 4. Human C2 R2320T thioredoxin fusion mass spectrometry results.

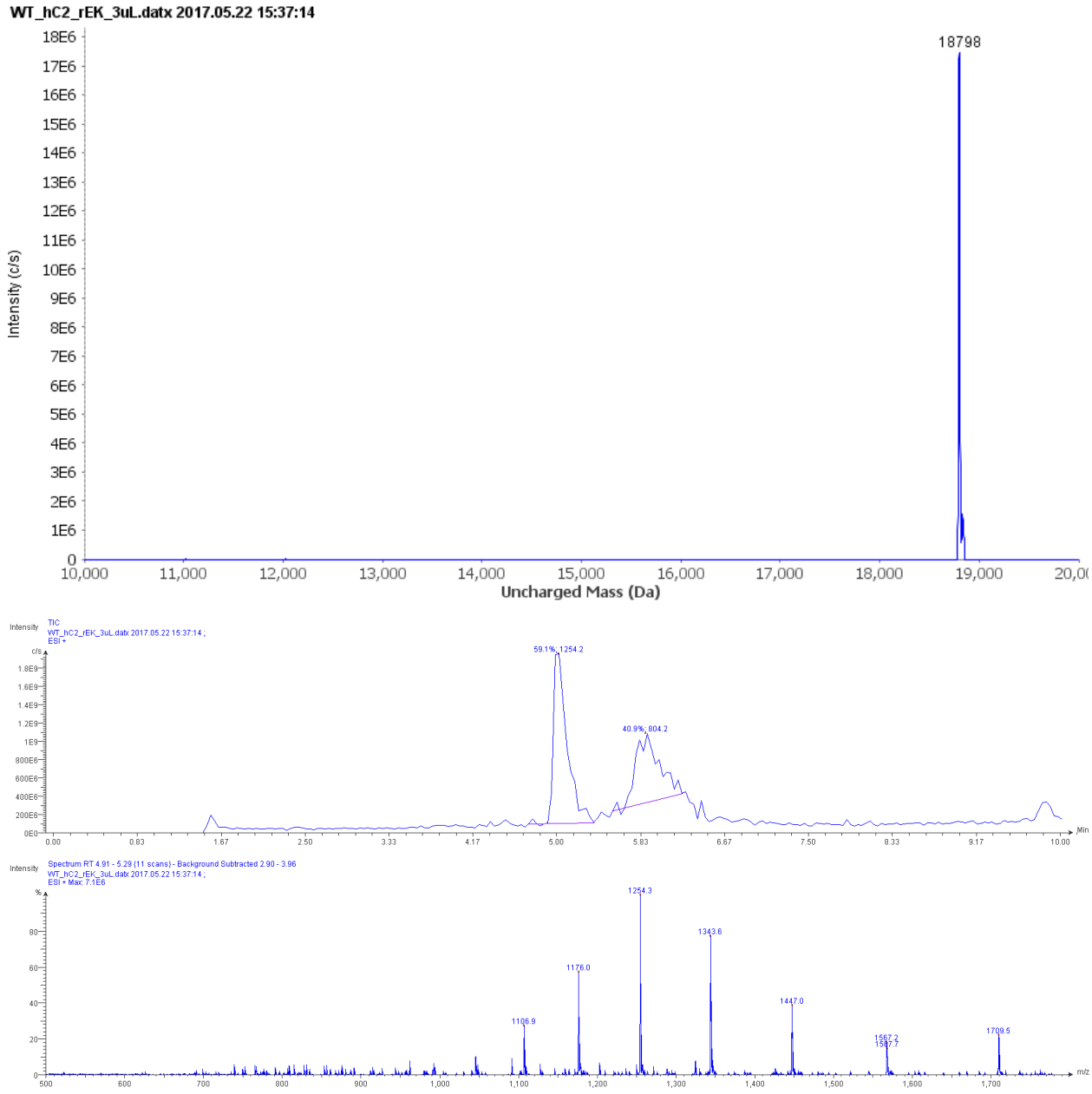

Appendix Figure 5. Human C2 wild type recombinant enterokinase cleaved mass spectrometry results.

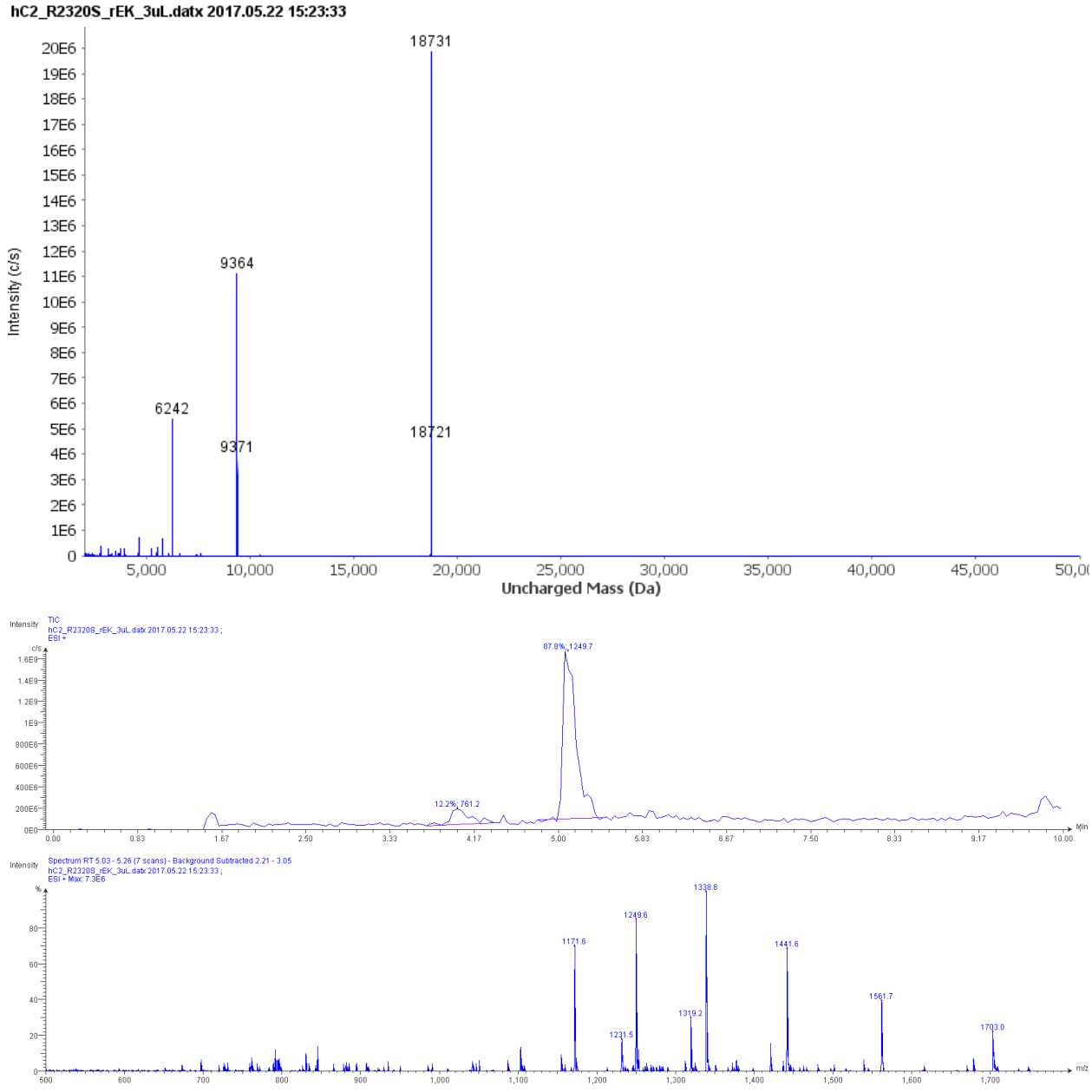

Appendix Figure 6. Human C2 R2320S recombinant enterokinase cleaved mass spectrometry results.

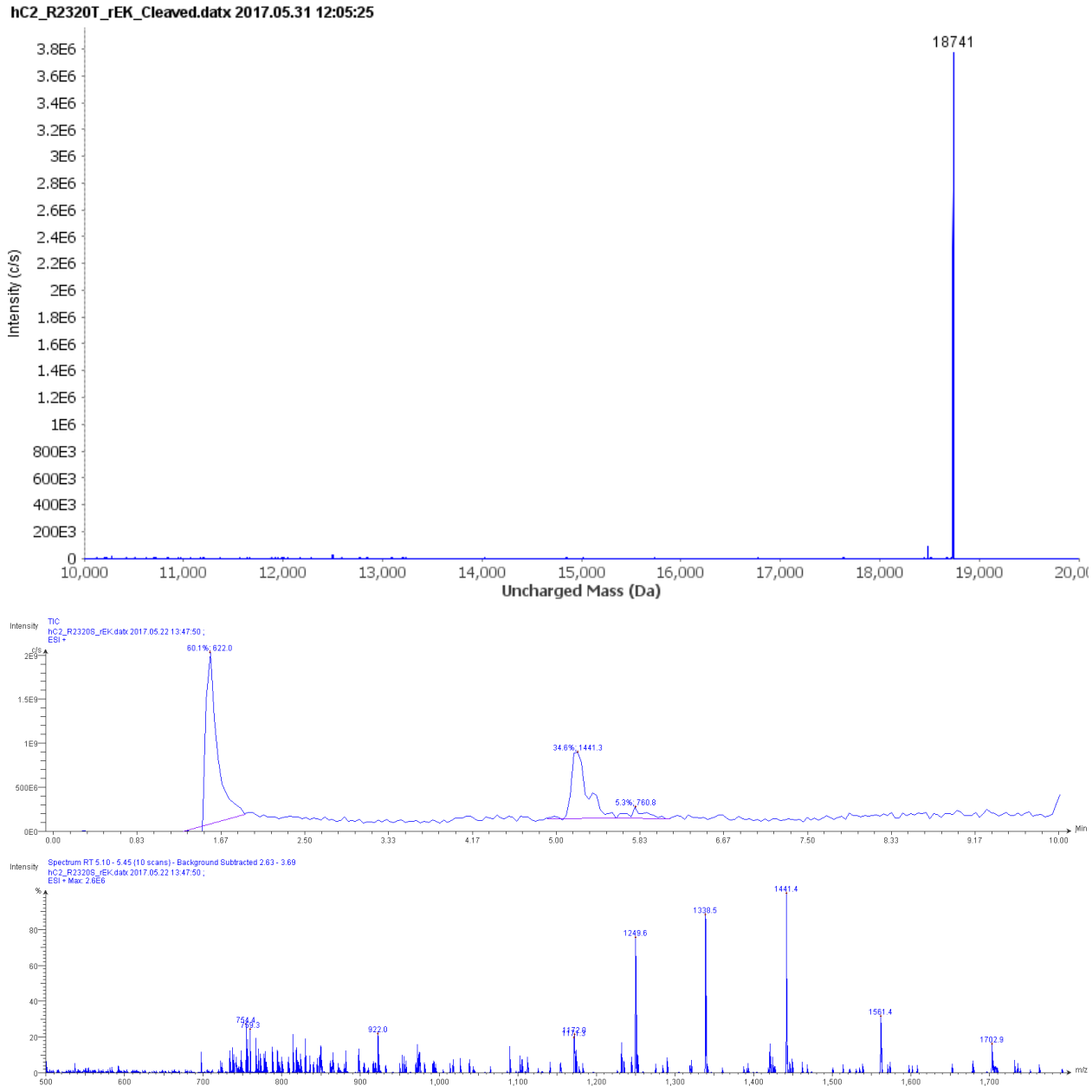

Appendix Figure 7. Human C2 R2320T recombinant enterokinase cleaved mass spectrometry results.